MONITORING THE PULSING BRAIN USING TRANSCRANIAL TISSUE DOPPLER ULTRASOUND

Poppy Turner

Thesis submitted for the degree of
Doctor of Philosophy

Department of Engineering
University of Leicester
April 2021

Abstract

Poppy Turner - Monitoring the Pulsing Brain Using Transcranial Tissue Doppler Ultrasound

It is well established that the brain pulsates with each cardiac cycle, yet relatively little is known about how these brain tissue pulsations (BTPs) are influenced by different physiological factors. Previous research suggests that measurement of BTPs could be used as a potential marker for brain pathology and impaired cerebral haemodynamics, however, existing methods used for BTP measurement are often costly, require an expert user, and are not suitable for continuous neuromonitoring.

The aim of this thesis is to use transcranial tissue Doppler ultrasound to investigate factors that affect healthy brain tissue pulsations, and to aid the development of a prototype device developed at University of Leicester, in collaboration with Nihon Kohden (Japan), for clinical measurement of BTPs.

An ultrasound phantom is used to investigate the impact of blood pressure on BTPs, along with a systemic state-space model of intracranial pressure dynamics. Numerous healthy volunteer studies are carried out to characterise healthy BTPs, and determine which factors influence BTP amplitude.

The system used was capable of obtaining quality data from numerous positions on the head, including the forehead. BTP signals were successfully detected in all volunteers studied, and the system was well tolerated. BTP amplitude was found to vary greatly between individuals, and with probe position, and increases with depth into the brain. A strong association between BTP amplitude and pulse pressure was observed in all studies.

This thesis introduces a new technique for measuring BTPs which has the potential to be used clinically to give real-time information on brain motion at the patient's bedside. BTP amplitude is strongly influenced by pulse pressure, which is a variable that can be greatly affected in critically unwell patients. Reference data from healthy subjects has also been generated, which can be compared to pathological cases in future work.

Acknowledgements

Firstly, I would like to thank Dr Emma Chung for helping me source funding for this project, and for her continuous support and advice throughout my time at the university and through my PhD. I would also like to thank Dr Andrea Lecchini-Visintini for all of his help and supervision throughout the PhD.

I want to thank Dr Caroline Banahan for her support and supervision at the start of the project, and Kelechi for all of his work and guidance on the development of the Brain TV GUI. Thank you to the Cerebral Haemodynamics in Ageing and Stroke Medicine (CHiASM) group. I would also like to thank Meshal and Jonathan for making the time working on the project so enjoyable, along with my friends Soheb and Charlie.

Finally, I would like to thank my parents, Carole and Neal, for their continued support and encouragement through the years.

Publications Arising from this Thesis

Work published in peer reviewed journals

P. Turner, C. Banahan, M. Alharbi, J. Ince, S. Venturini, S. Berger, I. Bnini, J. Campbell, KW. Beach, M. Horsfield, M. Oura, A. Lecchini-Visintini, EML. Chung. Brain tissue pulsation in healthy volunteers. Ultrasound in Medicine & Biology, 46(12):3268-3278, 2020.

M. Alharbi, **P. Turner**, J. Ince, M. Oura, KU. Ebirim, A. Almudayni, A. Lecchini-Visintini, JS. Minhas, EML. Chung. The effects of hypocapnia on brain tissue pulsations. Brain Sciences, 10(9):614, 2020.

J. Ince, C. Banahan, S. Venturini, M. Alharbi, **P. Turner**, M. Oura, KW. Beach, RG. Thompson, AK. Mistri, JS. Minhas, EML. Chung. Acute ischemic stroke diagnosis using brain tissue pulsations. J Neurol Sci, 419:117164, 2020.

Published conference abstracts

P. Turner, A. Lecchini-Visintini, C. Banahan, J. Ince, M. Alharbi, K.W. Beach, M. Oura, M.A. Moehring, E.M.L. Chung. Brain tissue pulsation in healthy subjects using transcranial tissue doppler (TCTD) ultrasound. Journal of Cerebral Blood Flow & Metabolism, 39(1S):p478-479, 2019. Brain & Brain PET 2019, Yokohama, Japan.

J. Ince, S. Venturini, C. Banahan, **P. Turner**, M. Alharbi, M. Oura, AK. Mistri, TG. Robinson, and EML. Chung. Brain tissue pulsation measurements for diagnosing acute ischaemic stroke: a pilot study. Journal of Cerebral Blood Flow & Metabolism, 39(1S):p268, 2019. Brain & Brain PET 2019, Yokohama, Japan.

ME. Alharbi, C. Banahan, J. Ince, J. Minhas, **P. Turner**, M. Oura, T. Coats, T. Robinson, E. Chung. Clinical evaluation of a prototype 'Brain TV' (tissue velocimetry) ultrasound system for emergency assessment of suspected acquired brain injury. Journal of Cerebral Blood Flow & Metabolism, 39(1S):p417-418, 2019. Brain & Brain PET 2019, Yokohama, Japan.

Contents

List of Figures

List of Tables

List of Abbreviations

ACA	Anterior cerebral artery
AIC	Akaike information criterion
aMRI	Amplified magnetic resonance imaging
BIC	Bayesian information criterion
BMF	Blood-mimicking fluid
BP	Blood pressure
Brain TV	Brain tissue velocimetry
BTP	Brain tissue pulsation
CBF	Cerebral blood flow
CBFV	Cerebral blood flow velocity
CO_2	Carbon dioxide
CSF	Cerebrospinal fluid
CT	Computed tomography
ECG	Electrocardiogram
$EtCO_2$	End-tidal carbon dioxide
FWHM	Full width at half maximum
GUI	Graphical user interface
HR	Heart rate
IC	Intracranial
ICC	Intraclass correlation coefficient
ICP	Intracranial pressure
IQ	In-phase and quadrature-phase
MAP	Mean arterial pressure
MCA	Middle cerebral artery
MRE	Magnetic resonance elastography
MRI	Magnetic resonance imaging
OH	Orthostatic hypotension
$PaCO_2$	Partial pressure of carbon dioxide
PCA	Posterior cerebral artery
PP	Pulse pressure
PRF	Pulse repetition frequency
PVAc	Polyvinyl alcohol cryogel
TCD	Transcranial Doppler
TCTD	Transcranial tissue Doppler
TDI	Tissue Doppler imaging
TMM	Tissue-mimicking material
TPI	Tissue pulsatility imaging
VIF	Variance inflation factor
WMH	White-matter hyperintensities

1 Introduction

1.1 Brain Tissue Pulsatility

As can be seen through the fontanelle of newborn infants, and in patients undergoing neurosurgery, the brain visibly pulsates over the cardiac cycle. It is thought that these pulsations occur due to blood entering the brain during systole faster than it leaves through the veins, causing the brain tissue to swell over part of the cardiac cycle, Wagshul *et al.* [1]. This is accompanied by an inward and downward motion of the brain that occurs with each heartbeat, Zhong *et al.* [2]. As blood drains from the intracranial region during diastole, the brain returns to its original volume and position. Therefore, the brain tangibly pulsates over the cardiac cycle, with regional pulsations thought to be strongly influenced by propagation of arterial pulsations into surrounding tissue and variations in brain tissue compliance. The characteristics of these pulsations are also influenced by damping, due to the brain being confined within the skull, and tethering of the brain to other structures. The balance between tissue, vasculature, and cerebrospinal fluid (CSF) compartmental volumes in the intracranial region also influence pulsations over the cardiac cycle, Greitz *et al.* [3], with venting of CSF through the foramen magnum thought to be a compensatory mechanism resulting from brain expansion due to arterial inflow, Balédent *et al.* [4].

Pulsation of tissue is also observed in other regions of the body, using a well-known technique, called plethysmography. In 1975, Strandness and Sumner [5] first used plethysmography to measure tissue pulsations in limbs, also suggesting that the expansion in tissue is due to arterial inflow occurring more rapidly than venous drainage. Plethysmography is a well established technique that has been used clinically since the 1960s for numerous diagnostic purposes, such as assessing arterial and venous disease, and determining lung capacity. It works by enclosing the patient, or part of the patient in a sealed chamber, and measuring the pressure change within the chamber, which can then be related to the volume change within the region of interest. Although the measurement of tissue pulsations using plethysmography has been widely researched and used clinically, brain tissue pulsations (BTPs) and measurement techniques remains relatively unexplored.

1.2 Previous Research into Brain Tissue Pulsations

1.2.1 Magnetic Resonance Imaging Studies

Our current knowledge of brain tissue motion comes predominantly from magnetic resonance imaging (MRI) studies, most of which focus on determining the magnitude and direction of tissue motion. Since 1992, the motion of brain tissue has been investigated using MRI. Greitz *et al.* [3] studied 15 healthy volunteers, and found that the brain moves inwards and downwards towards the foramen magnum in a 'funnel shaped fashion' when the heart contracts, before returning to its original position. This has been observed in more recent MRI studies, for example by Zhong *et al.* [2], who investigated tissue motion over the cardiac cycle in 3 healthy volunteers, which also suggested an inwards and downwards motion with each heart beat.

Both Zhong *et al.* and Greitz *et al.* found that tissue motion is stronger in the central basal region of the brain, and the brainstem, compared to peripheral brain tissue [2], [3]. Similarly, Weaver *et al.* [6] measured and modelled tissue strain over the cardiac cycle to estimate brain tissue elasticity. Weaver quantified intrinsic pulsations of brain tissue relative to their proximity to the circle of Willis. Pulsation amplitude was estimated for 4 regions of the brain in 6 volunteers. Pulsations were found to be strongest in tissue surrounding the circle of Willis ($\sim$150 μm) and weakest at the brain's periphery ($\sim$10 μm). These findings are supported by more recent work by Kiviniemi *et al.* [7], who determined the magnitude of tissue pulsations by measuring the change in magnetic resonance encephalography signal throughout the brain, finding a 13% signal change surrounding the circle of Willis which decreases to a $<$4% signal change in the cortex. Similarly, Atwi *et al.* used functional MRI to measure pulsatility in the insula in 55 participants, and found that the pulsatility index measured in the MCA was significantly related to pulsatility in the insula [8].

MRI studies have also looked into using BTP measurement to distinguish between healthy and pathological brain tissue motion. In 2018, Terem *et al.* [9] used a method of amplifying brain motion from a gated cine MRI scan, called amplified MRI (aMRI). This aMRI technique revealed clear differences in brain tissue motion between a healthy volunteer and a patient with a Chiari

I malformation, suggesting that measurement of brain tissue motion may be used clinically to study changes in brain tissue displacement associated with pathology.

1.2.2 Ultrasound Studies: Tissue Pulsatility Imaging

Tissue Doppler Imaging (TDI) is a well established echocardiography technique used clinically to measure the velocity of the cardiac tissue as it moves over the cardiac cycle, Ommen *et al.* [10]. This uses a phased-array ultrasound probe which consists of an array of piezoelectric elements that can be activated in sequence in order to direct the ultrasound beam. Doppler ultrasound is able to determine the velocity of structures by measuring the Doppler shifted frequency of received ultrasound echoes. It is a modality that is often used clinically in echocardiography, yet the application of tissue Doppler imaging to measurement of brain tissue motion is a relatively new concept.

In 2007, Tissue Pulsatility Imaging (TPI) was introduced by Kucewicz *et al.* [11], and has been used in the majority of ultrasound studies investigating BTPs. TPI uses a phased-array transducer, as used within echocardiography techniques, to measure brain tissue motion. TPI is able to obtain information on brain tissue motion from a 2D region of interest, however, as the transducer used is primarily used for cardiac imaging, it is not optimised for continuous monitoring. The measurements are also limited to the temporal and occipital windows, due to lack of penetration of the ultrasound beam through the skull.

After the development of TPI, Kucewicz *et al.* used this technique to determine how BTPs are altered when 2 healthy volunteers were presented with a visual stimulus. The results suggested an increase in BTP amplitude associated with the visual stimulus [11]. Kucewicz *et al.* also investigated the effects of hypocapnia on BTPs in 4 healthy volunteers, with a statistically significant decrease in BTP amplitude observed during hypocapnia [12].

In a study of 9 healthy volunteers, Ternifi *et al.* used TPI ultrasound measurements of BTPs along with MR imaging, with results suggesting a strong negative correlation between white-matter hyperintensities (WMH) and BTP amplitude [13]. In 2018, Angel *et al.* investigated the affect of ageing on

BTPs in 39 healthy volunteers, with results suggesting that BTPs decrease with increasing age [14]. In the same year, Desmidt *et al.* studied 25 healthy volunteers to investigate the relationship between the volume of 6 subcortical regions of the brain, determined using MRI, and BTP measurements obtained using TPI, finding a positive correlation between the two [15]. Most recently, in 2020, Siragusa *et al.* investigated the impact of music on BTPs in 25 healthy volunteers, with a significant decrease in BTP amplitude associated with listening to relaxing music [16].

Numerous TPI studies have also investigated BTPs in patients with diagnosed pathology. For instance, it was found that elderly patients diagnosed with both depression and diabetes experienced significantly weaker pulsations than those only diagnosed with diabetes, Desmidt *et al.* [17]. However, a later study investigating mid-life females with depression observed contradictory results, suggesting a significant increase in pulsations of those with depression compared to control subjects and those in remission, Desmidt *et al.* [18]. One study investigating BTP changes in 22 elderly subjects with orthostatic hypotension (OH), found that mean brain tissue pulsatility (representing global intracranial pulsatility) was significantly weaker in patients with OH compared to control subjects without OH, Biogeau *et al.* [19]. The differences observed between patients and control groups suggest that BTPs could be used as a potential marker for brain pathology and impaired cerebral haemodynamics.

A recent study introduced an alternative method to TPI, using transcranial sonography with a phased-array probe to quantify BTPs in a 2D region of interest. The technique was validated using a phantom, an elderly subject, and a patient with Alzheimer's disease, Jurkonis *et al.* [20]. This technique has also been used to investigate differences in BTPs between patients with Alzheimer's disease and healthy controls, Baranauskas *et al.* [21]. This study found that BTP amplitude did not differ between the two groups, however, the AD patients could be differentiated by a sharper BTP displacement morphology in some structures. A systematic review of ultrasound studies investigating BTPs gives details of all studies prior to 2020, Ince *et al.* [22]. All previous studies involve measuring BTPs with devices not optimised for continuous monitoring of brain motion, resulting in limitations regarding data acquisition.

1.2.3 Aims of this Thesis

Previous research into BTPs suggests that measurement of BTPs is of great clinical significance. With findings, using both MRI and ultrasound techniques, suggesting differences between patients with diagnosed pathology and control subjects. However, currently there is no reliable method for monitoring BTPs that is suitable for clinical use. MRI is time consuming and non-portable, while TPI is not optimised for continuous transcranial monitoring.

In this thesis, I introduce a novel ultrasound technique used for estimating brain tissue motion, called Transcranial Tissue Doppler (TCTD). This technique uses a small, single-element, transcranial Doppler probe traditionally used for measurement of cerebral blood flow. The probe is light and wearable, making it ideal for measurement of BTPs. The aim of this thesis is to use TCTD to investigate factors that affect healthy BTPs, and to aid the development of a prototype device developed at University of Leicester, in collaboration with Nihon Kohden (Japan), for clinical measurement of BTPs. This Brain Tissue Velocimetry (Brain TV) system is made specifically for measurement of BTPs, is portable, inexpensive, does not require a skilled operator, and can be used to take continuous measurements of BTPs through any position on the skull at the patients bedside. The Brain TV system can also take inputs from additional physiological measurement equipment, allowing for transient relationships between BTPs and physiological measurements to be explored.

Chapter 2 gives a technical description of the Brain TV system. This is followed by a study on 107 healthy volunteers, using TCTD to determine the variability of BTPs in the healthy population, and to determine physiological and demographical factors that may impact BTP amplitude. Chapter 4 focuses on the impact that a change in blood pressure (BP) has on BTPs, using the Brain TV system to carry out continuous measurements of all variables, this includes a healthy volunteer and ultrasound phantom study. Chapter 5 investigates the impact of CO_2 levels on BTPs in healthy volunteers. Chapter 6 further investigates the impact of BP on BTPs, with the implementation of a mathematical model describing pressure dynamics in the body. Finally, all results will be discussed in chapter 7.

2 Brain Tissue Velocimetry (Brain TV)

2.1 Introduction

There is increasing interest in brain tissue pulsation (BTP) measurement using both tissue pulsatility imaging (TPI) and magnetic resonance imaging (MRI), [1]. TPI is a Doppler ultrasound technique developed by Kucewicz *et al.* [11], which is based on the principle of plethysmography [5], as described in chapter 1. TPI uses a linear phased-array ultrasound transducer to sample the Doppler shift from specific 2D brain regions, [11] - [19]. Phased-array ultrasound transducers are more commonly used for echocardiography applications. TPI measurement of BTPs is limited to the temporal and occipital acoustic windows, and is unsuitable for continuous monitoring of brain motion as it is difficult to hold the probe in place and acquire data over long periods. Figure 1, taken from Kucewicz *et al* [11], shows the positioning of a phased-array ultrasound probe, used to insonate a 2D region of interest through the occipital acoustic bone window.

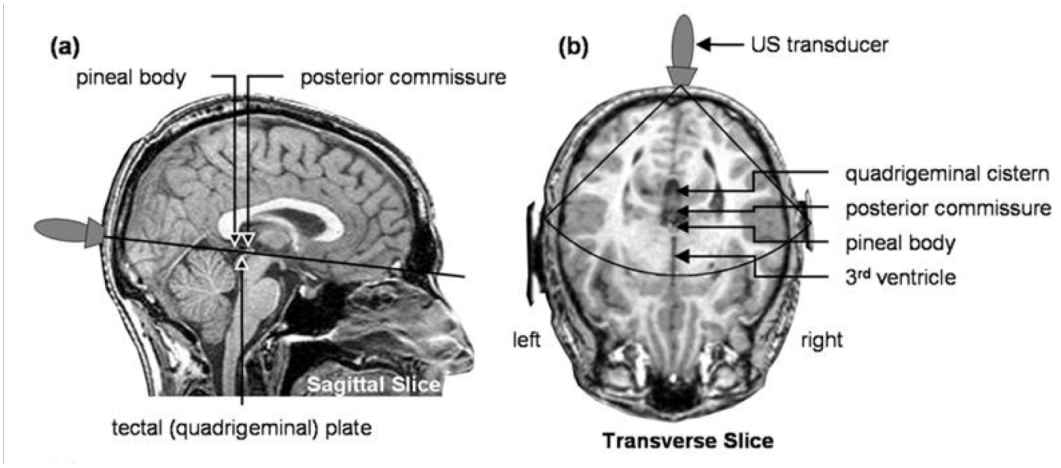

Figure 1: Kucewicz *et al.* [8] shows a 2D region of interest to be imaged using a phased-array ultrasound transducer using tissue pulsatility imaging (TPI). The footprint of the beam is superimposed over an MR image. Permission to use this image was granted by Elsevier (RELX, The Netherlands).

Doppler ultrasound is a technique that has been used clinically for a number of decades, and is used for measuring motion in the body, such as blood flow, and tissue motion. It works by emitting pulses of ultrasound with a known frequency distribution with a range of sample depths from which signals are

analysed. When the ultrasound waves pass through media with differing acoustic properties (i.e. different density, elasticity, and speed of sound), part of the beam will be reflected from sub-resolution scatterers, such as red blood cells. This reflected signal is then received at the ultrasound transducer. As the scatterers move in and out of the sample volume, the ultrasound wave will be reflected with a different frequency, as the signal will have been Doppler shifted. The change in frequency of the ultrasound signal, known as the Doppler frequency, can be related to the velocity of the scatterer, as shown in equation (1). Where f_D is Doppler frequency, f_t is the transmitted frequency, v is velocity of the scatterer, θ is the angle that the probe is oriented relative to the direction of motion of the scatterer (Doppler angle), and c is the speed of sound in tissue.

$$f_D = \frac{2 f_t v cos\theta}{c} \tag{1}$$

Phase-contrast MRI has also been used to measure BTPs by quantifying the velocity of different regions of brain tissue [2] - [9]. However, MRI is time consuming and non-portable, and requires an expert user and specialist equipment. Here we describe the acquisition and analysis of BTPs using an alternative wearable single-element TCD ultrasound probe designed for use as a continuous neuromonitoring device. This Brain TV technique is capable of providing real-time information about tissue motion along a single beam line, but does not provide imaging data.

2.2 Methods

2.2.1 Brain TV System Specification

Brain TV is a novel physiological measurement device, developed at the University of Leicester, in collaboration with an industry partner, Nihon Kohden (Japan). The purpose of the Brain TV system is to generate preliminary TCTD ultrasound data for the development of software to estimate and analyse BTPs. By recording TCTD data alongside other physiological measurements and comparing BTPs in patients and healthy subjects we hope to provide a better understanding of factors affecting BTPs and investigate the potential uses of Brain TV for investigating pathology.

The Brain TV system is made up of a small prototype device which emits pulses of ultrasound using a piezoelectric single-element transducer. The transducer is coupled to the participants head using an elasticated headband and custom probe holder. The transducer converts ultrasound echoes to an electrical signal, by generating a voltage when force (in the form of US echoes) is applied to the piezoelectric elements. This electrical signal is then converted to a digital signal using an analog-to-digital converter.

The Brain TV unit is connected to a Windows PC tablet (HP Elite x2 1012) which stores the recording and acts as a user interface for the operator. This user interface provides a real-time display of the digital signal (Figure 2), and allows the operator to adjust the ultrasound output, freeze the acquisition of data, and begin and end recordings. The ability to visualise the data allows the user to ensure that measurements are of good quality and free of artefacts prior to commencing a recording.

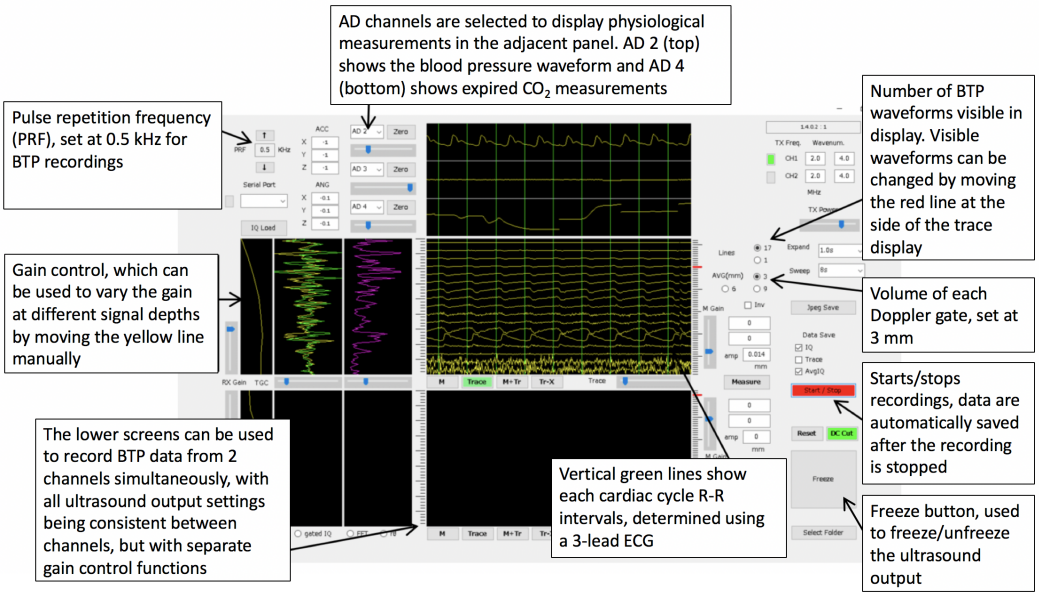

Figure 2: The Brain TV unit user interface with labelled controls.

2.2.2 Data Acquisition

The Brain TV system can simultaneously acquire data from two 2 MHz TCD probes, allowing synchronous BTP measurements from two positions on the cranium. The design of the headband and probe holders mean that recordings can be taken from most positions on the head, with the forehead being a preferred position due to ease of access. The TCD probes used with this technique contain a single piezoelectric element which generates the ultrasound pulses and receives the reflected echoes. This results in the probe being much smaller than the phased-array probes used in TPI, which contain an array of piezoelectric elements that can be fired in sequence to build up a larger image.

The Brain TV device can also be connected to an external ECG, accelerometer and gyroscope, as well as other physiological measurement devices, to acquire synchronous physiological measurements. In our current set-up continuous blood pressure measurements are obtained using a finger-cuff Finometer system (Finapres Medical Systems, The Netherlands), timing of ECG wave R-R intervals are recorded using a 3-lead ECG Lifescope monitor (Nihon Kohden, Japan), and capnography measurements are obtained using an LG-3800 CO_2 monitor (Nihon Kohden, Japan). An accelerometer can be fixed to the ultrasound transducer to record probe motion. Accelerometer and gyroscope data are displayed on the Brain TV user interface. An illustration of the equipment set-up is shown in Figure 3.

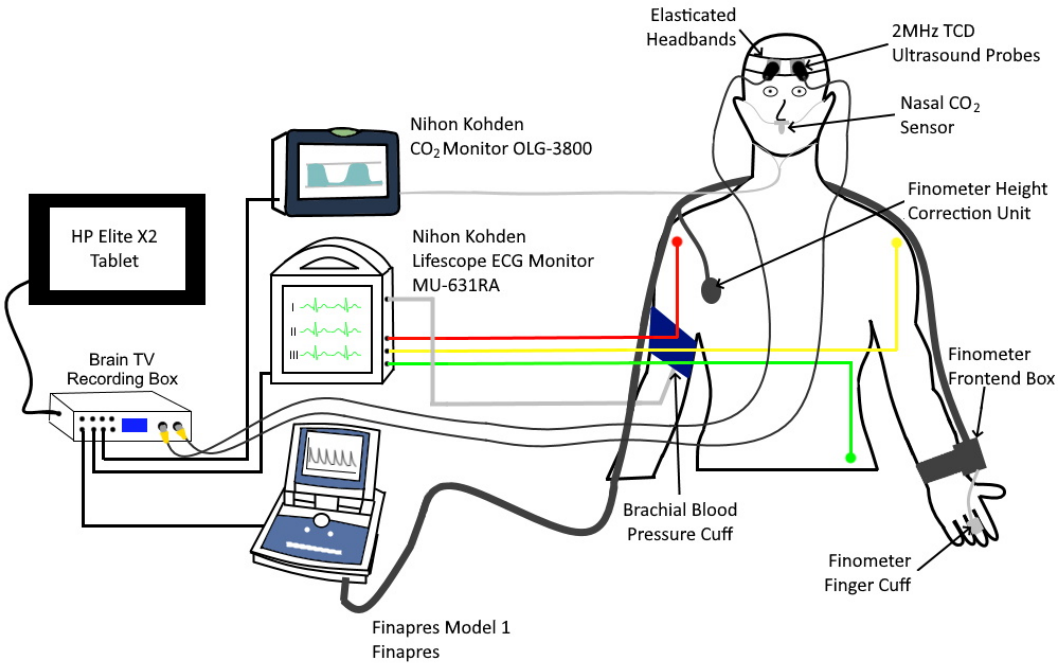

Figure 3: An illustration showing the Brain TV system equipment set-up, including additional physiological measurements equipment. Illustration credit: J. Ince, University of Leicester.

2.2.3 Characterisation of the Ultrasound Beam

Ultrasound recordings contain signals from 30 overlapping Doppler gates. These gates determine the volume of tissue that will be measured in the recording, with the sample volumes in TCTD chosen to be 3 mm, and gates positioned along the beam line with the centre of each gate spaced 2 mm apart. This results in information on tissue motion being measured from a depth range of 22 - 80 mm. The dimensions of the ultrasound beam were investigated using an in-house beam plotting system, comprising a hydrophone needle (Precision Acoustics Ltd., UK) submerged in a water tank. The needle was moved across the x, y, and z directions of the ultrasound beam using a mechanical stage, and was used to measure the intensity of the beam at a number of specified locations. The ultrasound beam was found to have a consistent narrow width along the length of the beam, with a Full Width at Half Maximum (FWHM) ranging from 2.7 mm at a depth of 5 cm, to a maximum width of 3.6 mm at a depth of 7 cm. The approximate path of the ultrasound beam within the brain for the temporal probe position can be found in Figure 4, along with informa-

tion on beam dimensions. It should be noted that the shape and direction of the beam profile is likely to be modified during TCTD recordings due to the beam passing through the skull, therefore, the beam plot shown in Figure 4 is only indicative and may not represent the exact path of the ultrasound beam within the brain.

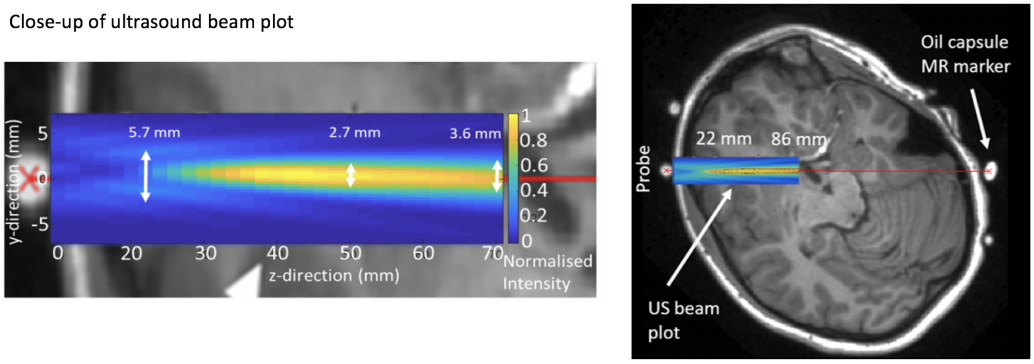

Figure 4: Close-up of a free-field beam plot displaying normalised intensity along the direction of the beam. The Full Width Half Maximum (FWHM) is provided for 3 depths, showing how beam width varies along the ultrasound beam path. The path of the free-field ultrasound beam has been superimposed on a resampled MR image showing brain anatomy on the right. N.B. It should be noticed that in reality the beam will be distorted somewhat by the skull.

2.2.4 Data Transfer

Ultrasound recordings comprise in-phase and quadrature-phase (IQ) demodulation data. IQ modulation is often used when transmitting RF signals. It is a simple method to achieve any form of wave modulation, such as amplitude, frequency, or phase modulation. This is achieved by summing in-phase and quadrature-phase waves, such as sine and cosine waves, and altering the amplitude of the 2 waves with time. The amplitude of the cosine wave is denoted as $I(t)$, and the amplitude of the sine wave is denoted as $Q(t)$. By changing the $I(t)$ and $Q(t)$ values appropriately, the RF signal received at the ultrasound transducer can be replicated. Therefore, if the frequency of the carrier signal (in this case the received ultrasound signal) is known, then the entire signal can be transmitted just using the values for $I(t)$ and $Q(t)$.

IQ modulation is carried out within the Brain TV system, the $I(t)$ and $Q(t)$ values are then transferred to a desktop PC or laptop for demodulation and

analysis of BTP signals in MATLAB (The MathWorks, Inc., USA). IQ demodulation is the process of forming the original RF signal using the $I(t)$ and $Q(t)$ values, along with the known carrier frequency. This is achieved simply by multiplying the $I(t)$ values by $\cos(2\pi ft)$, multiplying the $Q(t)$ values by $\sin(2\pi ft)$, and summing the resulting waves, where f is the carrier frequency. Therefore, information from the original ultrasound RF signal can be extracted using this carrier wave.

Continuous recordings of all measured variables are synchronised to ECG data before being transferred from the Brain TV tablet and stored to the hard-drive of a laptop, to be analysed using software developed in MATLAB (The MathWorks, Inc., USA). Each data file contains up to 3 minutes of data, with recordings longer than three minutes being divided into separate files to aid signal processing and analysis.

2.2.5 Signal Processing

IQ data from each recording are down-sampled from 8 kHz to 160 Hz to reduce the size of the files. This was achieved by removing samples at regular intervals, resulting in one sample every 6.25 ms, rather than every 0.1 ms. Tissue velocity at each depth is estimated using an autocorrelator, Hoeks *et al.* [24]. Autocorrelation involves determining the correlation between a signal and a delayed version of the same signal, which in this case has differing phase properties due to the interaction of reflected ultrasound signal with the moving tissue. The process of autocorrelation is used as it allows the change in phase experienced by the returning echo to be analysed, and the time lag between the two waves to be determined. From this, the mean Doppler frequency can be estimated and used to determine the velocity of the tissue using the relationship shown in equation (1). As velocity is equal to the rate of change of displacement, estimates of tissue velocity can be integrated over a specific time period to obtain a BTP signal representing real-time tissue displacement at each depth. In this case, integration is the process of determining the change in displacement represented by velocity at different points in time, these displacements can be summed to estimate the total displacement over a specified period. The BTP signals are then filtered to remove the effects of respiration using a high pass filter with cut-off at 75% of the mean cardiac cycle frequency.

This filter is chosen as the frequency of respiration is much lower than heart rate, therefore, the effects of respiration can be removed from the signal by ensuring that these low frequency signals are not included in the data. Heart rate is estimated by calculating the mean cardiac frequency using each subject's ECG R-wave interval.

2.2.6 Brain TV Graphical User Interface for Analysis of BTP Data

A Brain TV Graphical User Interface (GUI) was developed in-house using MATLAB to analyse data recorded using the Brain TV system. The Brain TV GUI displays BTP signals for each recording, along with corresponding physiological data, such as BP and CO_2. The BTP signals can then be manually inspected, with the R-R intervals overlaid, to allow the user to remove any cardiac cycles containing artefacts. Artefacts were defined as any noticeable perturbations not regularly repeating with the cardiac cycle, these are generally caused either by probe motion or sudden motion of the patient, e.g. due to blinking or coughing. Examples of waveforms including artefacts are provided in section 2.3.2, including a discussion into the effects of artefacts on BTP estimates. Once artefacts have been removed, these clean (artefact-free) data can be saved and used for further analysis.

The Brain TV data analysis GUI has been designed to extract numerous features from BTP signals. Beat-to-beat values for each feature are calculated for individual cardiac cycles and then averaged over the duration of the recording, giving one value per depth. Information from additional physiological measurements can also be calculated on a beat-to-beat basis, such as mean arterial pressure, pulse pressure, and maximum exhaled CO_2. These features are output into a separate file in MATLAB, which can then be used for further statistical analysis. The Brain TV data analysis GUI is shown in Figure 5. The instruction manual for the data analysis GUI, written by myself and K. Ebirim (University of Leicester, PhD student), is given in Appendix A. The instruction manual also describes the features that are calculated within the GUI.

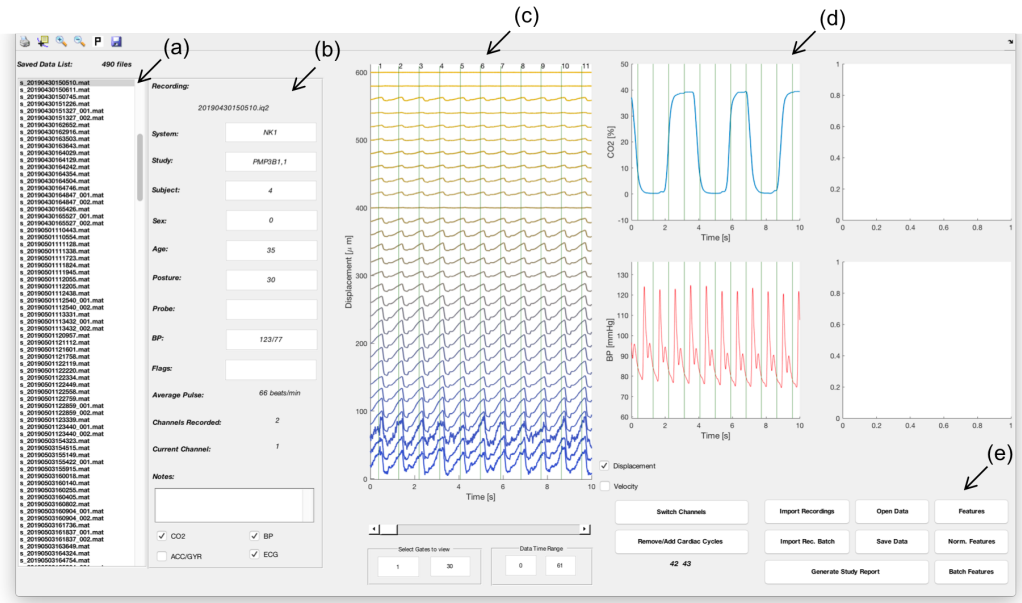

Figure 5: The Brain TV data analysis GUI. (a) Saved data list, (b) recording information (c) waterfall plot displaying BTP signals, (d) physiological measurements waveforms, (e) push buttons for data handling.

2.3 Results and Discussion

2.3.1 System Validation

Nihon Kohden carried out several in-house validation studies to determine the resolution and measurement error of the Brain TV system. The accuracy of displacement estimates was investigated using an ultrasound phantom made of tissue-mimicking material, developed to have the same acoustic properties as biological tissue. The Brain TV system took measurements of the ultrasound phantom, with the probe being moved from $\sim$ 10 - 70 μm, and measurements taken approximately every 10 μm. The probe was moved using a high-resolution XY stage, with resolution 0.25 μm, and repeated positioning precision of $<$ 0.3 μm (Kohzu Precision Co., Ltd., Japan). The equipment set-up is illustrated in Figure 6. The distance measured by the Brain TV system was compared with the known value for distance displayed on a dial gauge. This validation study suggested that the resolution of the system was approximately 1.6 μm. Results from the study are given in Table 1.

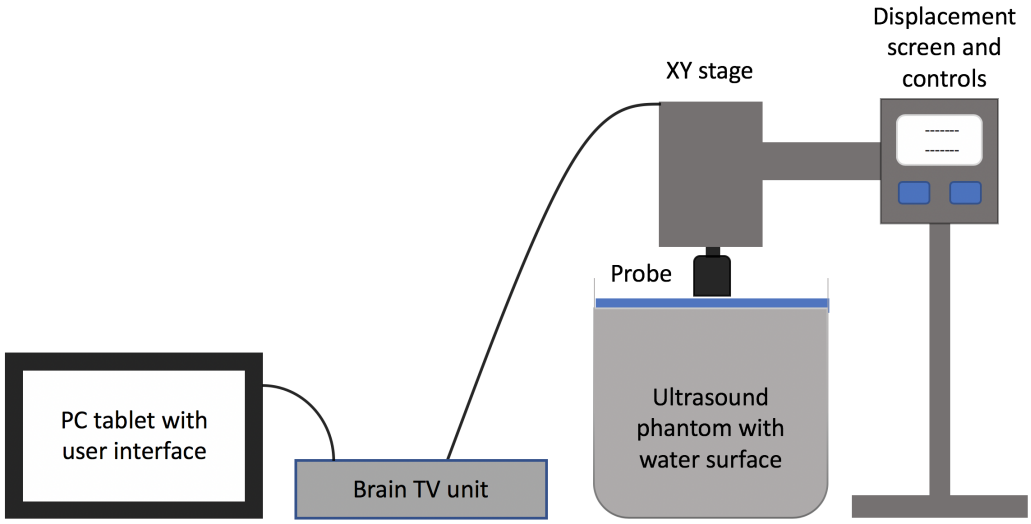

Figure 6: Equipment set-up for the validation experiments carried out on the Brain TV system using an ultrasound phantom.

Distance moved (μm)	**Measurement error (μm)**
12	0.64
23	0.94
42	1.34
53	1.88
63	1.33
73	1.60

Table 1: Results showing the distance the ultrasound probe was moved, and the corresponding Brain TV measurement error. These experiments estimated the resolution of the Brain TV unit to be approximately 1.6 μm.

2.3.2 Data Quality

The Brain TV system has been used for a number of research studies, and it has been confirmed that good quality BTP data can be obtained from a wide range of participants through any part of the skull, which is an advantage over conventional TCD measurements which require the presence of acoustic windows in the skull. TCTD measurements do not require the presence of acoustic windows as the signal from tissue is much stronger than the signal from blood flow, due to the greater density of scatterers in tissue. Therefore, the signal is strong enough to be detected following attenuation through thicker parts of the skull. Studies investigating the impact of artefacts on BTP estimates have

been carried out and it was found most artefacts are caused by participant movement (such as blinking or coughing). Probe motion produced the largest artefacts, causing BTP values to appear larger than their true values if cardiac cycles containing artefacts are not discarded. Therefore, removal of such artefacts prior to further analysis, as described in section 2.2.6, is important for obtaining accurate estimates. Figure 7(b) and (c) give examples of the appearance of different types of artefacts, along with an artefact-free recording for reference, Figure 7(a).

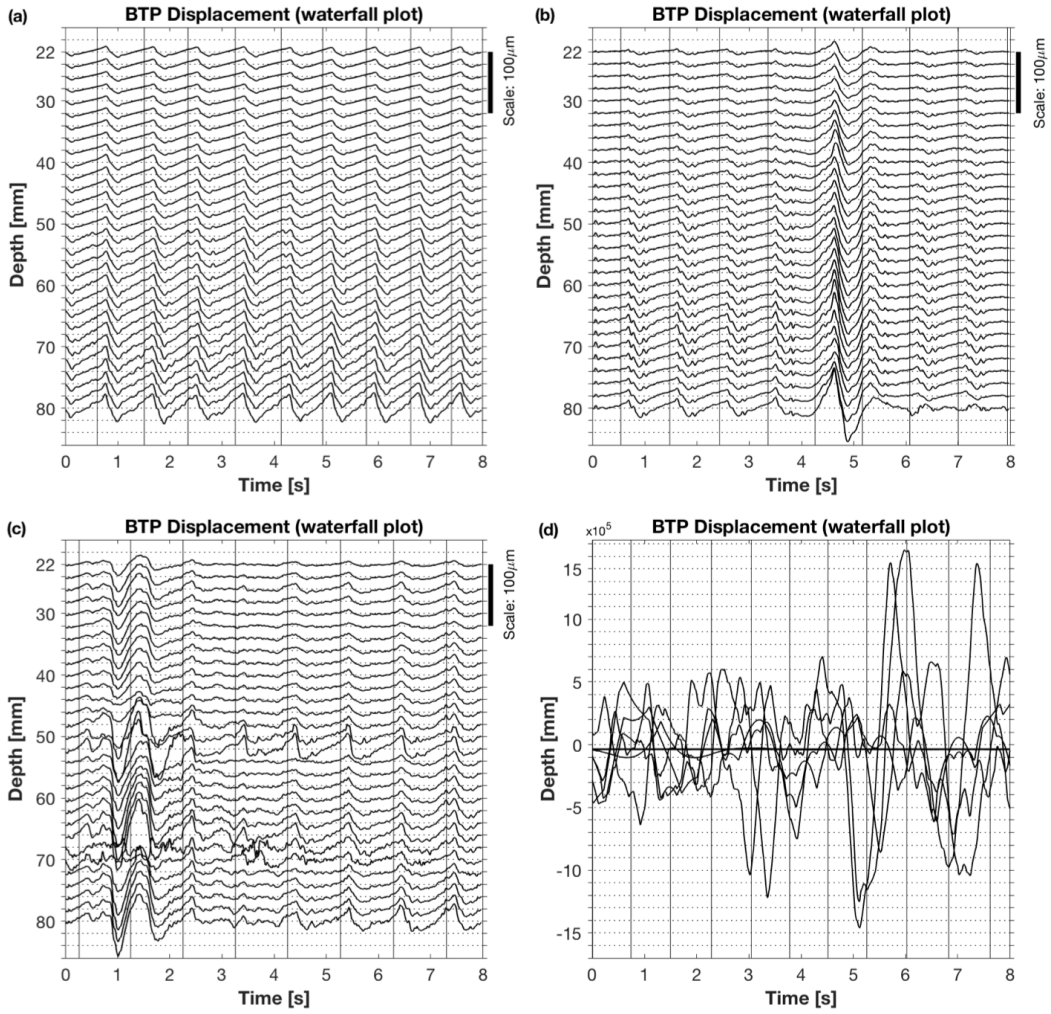

Figure 7: Examples of BTP data, including (a) a typical artefact-free recording, (b), and (c), common examples of motion artefacts, and (d) a recording in which the deeper gates give unphysiological values, with magnitudes much higher (10^5) than expected from brain tissue.

As mentioned previously, the Brain TV system is able to obtain data from 30 depths (or gates) within the brain. However, not all 30 gates provide usable BTP signals for all subjects, with deeper gates sometimes exhibiting much larger values (up to 10^5 times larger) that do not follow expected repetitive patterns of brain tissue motion, Figure 7(d). This could be due to the ultrasound beam passing through other brain structures, such as the ventricles. Or, could be due to limited penetration of the ultrasound beam, leading to greater noise in the deeper gates. For depths where the visualisation of BTPs appears to be limited, gates can be removed from analysis, ensuring only reliable tissue motion is quantified.

2.3.3 Use within a Clinical Environment

The Brain TV data acquisition prototype was developed with the aim of acquiring BTP measurements from both healthy volunteers and patients. The system has been used to acquire measurements from over 100 healthy volunteers, and over 50 patients with suspected brain injury. Measurements were successfully obtained from all participants, with the equipment and protocol being well tolerated by all. The Brain TV unit and all other components within the Brain TV system are stored on a single trolley, making the system portable, and easy to use at a patient's bedside, without interrupting routine care. Therefore, the Brain TV system meets all of the original user specifications listed in section 2.2.1.

2.4 Conclusions

Brain TV has several advantages over both echocardiography-based ultrasound and MRI approaches, including being cost effective, suitable for continuous neuromonitoring, and portable. The Brain TV system uses a small, wearable probe, which is well tolerated by patients in a clinical environment. It is capable of providing continuous real-time measurements of BTPs at the patient's bedside.

3 Characterising and Quantifying Brain Tissue Pulsations in Healthy Volunteers

3.1 Introduction

Previous research into healthy brain tissue pulsations (BTPs) has been conducted using both MRI and ultrasound using echocardiography-based techniques. MRI studies have been used to look at how tissue motion varies in magnitude and direction throughout the brain, with a study on 15 healthy volunteers by Greitz *et al.* suggesting that the brain moves inwards and downwards in a 'funnel-shaped' fashion each time the heart contracts, with the highest tissue velocities reported in the basal ganglia and brainstem [3]. Similarly, Weaver *et al.* used magnetic resonance elastography (MRE) on 6 volunteers to determine how tissue displacement varied in different regions of the brain, finding that tissue displacement increased with proximity to the circle of Willis [6]. Figure 8 illustrates the location of the basal ganglia, brainstem, and circle of Willis, which are all regions with increased pulsation amplitude [3], [6].

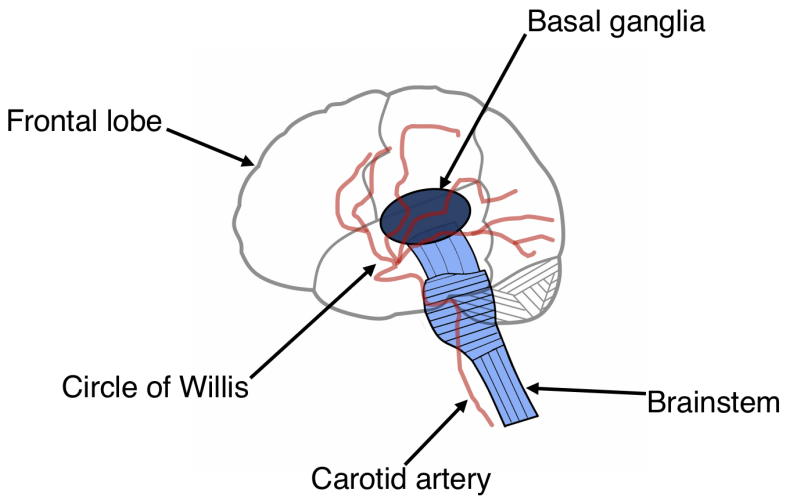

Figure 8: Previous research has suggested that the basal ganglia (dark blue) and brainstem (light blue) were the regions of the brain found to pulsate with the highest velocities in a study by Greitz *et al.* [3]. While tissue in the proximity of the circle of Willis (red) was found to show the greatest pulsation amplitude in a study by Weaver *et al.* [5]. All of these regions are situated near the centre of the brain. This illustration is intended for visualisation purposes, and was created with the assistance of J. Ince (University of Leicester).

Studies using ultrasound (mainly Tissue Pulsatility Imaging) as a means of measuring BTPs have also looked into brain tissue motion in healthy volunteers. Kucewicz *et al.* studied 2 healthy volunteers and found that BTPs in the visual cortex increased when volunteers were presented with a visual stimulus [11]. Kucewicz *et al.* also investigated how BTPs in 4 healthy volunteers were affected by induced hypocapnia, suggesting BTP amplitude decreased during hypocapnia [12]. Ternifi *et al.* studied 9 healthy volunteers and suggested a strong negative correlation between BTP amplitude and white-matter hyperintensity volume (imaged using MRI) [13]. The affects of ageing on healthy BTPs has also been investigated, reporting an increase in age corresponding to a decrease in BTP amplitude, Angel *et al.* [14]. Desmidt *et al.* investigated 25 healthy volunteers and found a positive correlation between subcortical volumes and BTP measurements [15]. The impact of music on healthy BTPs has also been investigated, with Siragusa *et al.* finding a significant decrease in BTP amplitude when listening to relaxing music [16]. Additional research into brain tissue motion focuses on comparing BTPs of patients with pathology to control subjects, or validating measurement techniques [20].

All previous research into healthy BTPs has been carried out on populations with relatively small sample sizes, with the largest healthy sample size being n = 39 [14]. Therefore, results should be interpreted with caution. It is important to establish the true extent of variability in BTPs amongst the healthy population so that any differences can be confidently identified. The aim of the study presented in this chapter is to provide normative data characterising variations in tissue displacement across a wide cross-section of healthy adults. An exploratory statistical analysis is performed to summarise the range of pulsations seen in healthy subjects, and a linear regression model is developed to characterise BTPs measured through the forehead and temporal position as a function of Age, Sex, HR, MAP, and PP. The comparison of ultrasound measurements with MR images in five volunteers is included for illustrative purposes to aid the interpretation of pulsation waveforms in relation to brain anatomy.

This study introduces Transcranial Tissue Doppler (TCTD) as an alternative method of measuring BTPs. TCTD uses a small single-element transcranial Doppler ultrasound probe, to provide real-time information about tissue

motion in the absence of imaging data. An advantage of TCTD measurement of BTPs is that measurements can be obtained from any position on the head; the probe is light enough to wear, and measurements do not require a skilled operator.

This study was conducted prior to the development of the Brain TV system (described in chapter 2), therefore, the ultrasound data is obtained using a commercially available TCD system and probes (Spencer Technologies, Seattle, WA). The system was modified to extract BTP signals, rather than signals from cerebral blood flow, by removing the filter that would usually discard the signal from tissue in TCD recordings. However, the software and principles used within the Brain TV system are also used in the acquisition and analysis of the data in this study. This study aided the development of the Brain TV system by highlighting issues that needed to be addressed specifically for measurement of BTPs.

I conducted the data collection and analysis of BTP measurements. The collection and analysis of ultrasound and MRI data in 5 volunteers was conducted by C. Banahan (University of Leicester, Medical Physics). Results from this study, including MRI results, are included in an article on which I am joint first author with Dr. Banahan, Turner *et al.* [25].

3.2 Methods

3.2.1 Subjects

Adults with no previous history of brain injury were recruited to the study following a protocol approved by the University of Leicester, Medicine and Biological Sciences Research Ethics Committee. Participants were recruited through online and email advertising to staff and student groups within the University of Leicester. To provide a good spread of ages, working age participants were also recruited with the co-operation of a local business (Cloudcall Ltd., UK) who advertised the study to their employees and allowed interested staff to take part during working hours. Volunteers aged over 65 years were recruited with the assistance of our local branch of the University of the Third Age (an international network of learning groups aimed towards older people), who included an advert for our study in their newsletter. All participants pro-

vided written informed consent. The participant information sheet and ethics approval letter can be found in Appendix B.

3.2.2 MRI Protocol and Analysis

In order to better understand the impact of brain anatomy on BTP signals, an additional 5 participants underwent magnetic resonance imaging (MRI). The transducer was attached to a head frame so that the path of the beam through the head could be estimated and fiducials (oil filled capsules) were attached to the head to act as landmarks that would be visible on the MRI scan. Participants then underwent brain imaging using a 3T MR scanner (Magnetom Skyra; Siemens Medical, Erlangen, Germany). The scans included a 3-plane localizer, 3D T1-weighted sagittal and time-of-flight magnetic resonance angiography (MRA). The T1-weighted slices were resampled using a 3D multi-planar reconstruction tool (Jim, Xinapse Systems, UK) to visualise a plane through the dataset containing the ultrasound beam path, using the oil capsule fiducials as a guide.

3.2.3 TCTD Protocol and Data Acquisition

Participants completed a health questionnaire recording prescribed medications and current health conditions. Participants reporting any acute or chronic medical conditions were excluded. Participants had their brachial blood pressure measured using a standard arm-cuff device. Blood pressure measurements were repeated at the start and end of each recording session to provide an average value for statistical analysis. Participants were asked to wear a 3-lead ECG monitor (Nihon Kohden, Japan) to record the timing of the pulsations relative to the QRS of each cardiac cycle. Participants were seated in an upright position, and were asked to close their eyes and remain still during each measurement to avoid generating motion artefacts.

Ultrasound recordings were obtained using a modified Spencer Technologies (Seattle, WA) Transcranial Doppler (TCD) system (8 kHz PRF, M-mode, 33 Doppler gates), equipped with a 2 MHz transducer. The transducer was held in place using an elasticated headband and custom probe holder. For each participant, TCTD data were separately recorded from 4 probe positions: through the temporal window, and through the forehead above the centre of the eye-

brow, from both the left and right hemispheres.

Each ultrasound recording was 8 seconds long, providing tissue motion data from 33 overlapping 3 mm sample depths (or gates) spaced 2 mm apart. Sample depths ranged from 22 to 86 mm, however, data from the last 3 gates (82 - 86 mm) were discarded due to increased signal noise. Two measurements were recorded from each probe position, and the recording least affected by artefacts was taken forward for further analysis. Artefacts were typically caused by movement of the head (e.g. coughing, blinking, or probe motion). Ultrasound recordings were synchronised to ECG data and analysed using software developed in MATLAB (The Mathworks, Inc., United States).

3.2.4 TCTD Signal Processing

The signal processing for this study is described in chapter 2, as the signal processing remains the same regardless of the equipment used for recording the ultrasound measurements. The BTP signals were displayed in MATLAB, and manually inspected, with the R-R intervals overlaid, to allow the user to remove any cardiac cycles containing artefacts. Further analysis was based on these cleaned (artefact free) data. Artefacts were defined as any noticeable perturbations not regularly repeating with the cardiac cycle. Example BTP signals are shown in Figures 9(a) and (b).

In general, over each R-R interval, the tissue is initially moving outwards towards the transducer. The tissue then moves sharply inward, away from the transducer for approximately 25% of the cardiac cycle, and then relaxes by moving outward again for the remainder, and for the initial part of the next cardiac cycle. For most brain regions the peak consistently preceded the trough, however, for some recordings, BTP signals at different depths moved in opposite directions (see Figure 10) and the timing of the peak and trough were reversed.

The analyses presented in this work focus on quantifying typical amplitudes of BTP signals. For each recording, the BTP Amplitude at each depth was calculated as the average of the maximum displacement (i.e. the absolute difference between the peak and trough of each cardiac cycle – as illustrated in Figure

9c). For each recording, a Bulk BTP signal was also calculated as the average of the BTP signals across all 30 depths, representing collective displacement of the brain over the cardiac cycle. For each Bulk BTP signal the Bulk BTP Amplitude was then calculated.

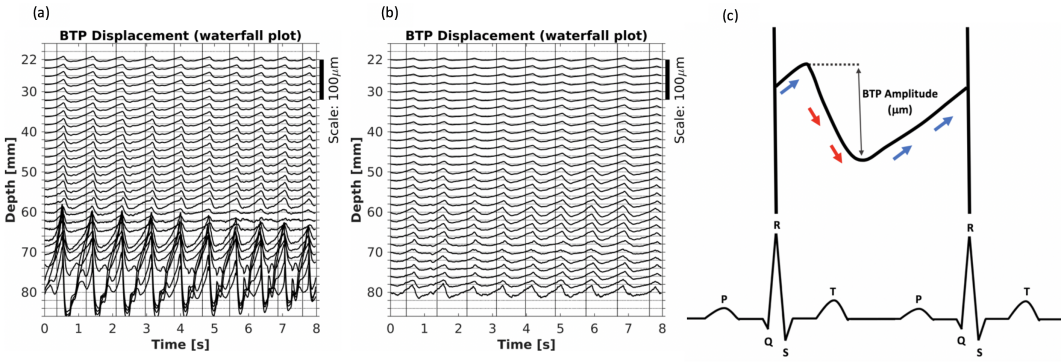

Figure 9: Signals showing brain tissue motion for each 8 second recording presented as a waterfall plot; the shallowest depth of 22 mm is at the top of the figure, signals from successive depths are offset by 20 μm. (a) Shows an example of the largest pulsations of 156 μm, observed from a 23 year old male, (b) provides a more typical example of a 15 μm pulsation from 46 year old female. BTP Amplitude was defined as shown schematically in (c) illustrating the direction of tissue motion, with upward blue arrows indicating outward tissue motion (toward the transducer), and downward red arrows indicating inward tissue motion (away from the transducer). The timing of BTPs, relative to the ECG waveform R-R interval, is indicated by the vertical lines in (a) and (b).

3.2.5 Statistical Analysis

Statistical analysis of demographic and BTP features were performed in MATLAB. As the BTP Amplitude distribution was skewed toward lower values (i.e. non-normally distributed), and since variances were observed to increase with amplitude, data were log-transformed prior to modelling. The resulting log-transformed distribution was confirmed to be normally distributed. Paired t-tests were then carried out on log-transformed Bulk BTP Amplitude data to assess whether pulsations differed with probe position. Statistical tests resulted in a p-value, all of which are reported in the results section where appropriate. P-values show the probability of rejecting a hypothesis when it is actually true, therefore, a low p-value suggests that a hypothesis can be rejected with greater confidence. Conventionally, a p-value of less than 0.05

gives enough confidence in a result to reject the hypothesis, therefore, a significance level of $p<0.05$ is used throughout the studies in this thesis.

Stata v.15 (StataCorp LLC) was used to develop a multivariate regression model to explore the effects of Age, Sex, PP, MAP, and HR on Bulk BTP Amplitude, see section 3.4.2. A multivariate regression model was used as it allows variability in the outcome variables (in this case Bulk BTP Amplitude for both positions) to be explained using the remaining measured variables. The output of the results for the model includes a coefficient for each explanatory variable, along with a corresponding p-value, and an R^2 value for the whole model. The coefficient is the value that the explanatory variable is multiplied by to give the value of Bulk BTP Amplitude. Therefore, a positive value indicates that an increase in the explanatory variable results in an increase in Bulk BTP Amplitude, whereas a negative coefficient suggests that a decrease in the explanatory variable results in an increase in Bulk BTP Amplitude. Similarly, a large coefficient indicates a greater change in Bulk BTP Amplitude per unit change, whereas a smaller coefficient indicates a smaller change in Bulk BTP Amplitude. As previously described, the p-value describes how likely it is that a significant relationship is observed in error. For example, a commonly adopted p-value of 0.05 suggests that if the data were sampled 20 times, 1 in 20 would show an erroneous significant relationship between parameters. The R^2 value shows how much of the variability in Bulk BTP Amplitude is described by the explanatory variables in the model.

The multivariate nature of the model allows for numerous outcome variables to be described separately using the same explanatory data. In this case, the two outcome variables were Bulk BTP Amplitude for the forehead and temporal positions separately, as the data could not be combined due to the significant difference between amplitudes measured through the forehead and the temporal positions. Univariable analysis was first carried out to determine how each variable affected Bulk BTP Amplitude separately, with each variable found to significantly affect Bulk BTP Amplitude ($p<0.05$) taken for further analysis. Each of the significant variables was considered for the final model to determine the relationship between each of the variables and Bulk BTP Amplitude. A linear model was used, meaning that the effects corresponding to each significant explanatory variable were summed to give the outcome variable. The

final model was determined using a method introduced by Peixoto *et al.* [26].

3.3 MRI Results

In the 5 subjects who underwent MRI, BTPs were studied alongside the corresponding brain structure visualised using T1-weighted MRI. From these data, variations in BTP waveform features with depth were related to regional variations in brain anatomy.

Two examples, from a 22 year old male and 20 year old female, are provided in Figure 10. In the case of the 22 year old male volunteer - Figure 10(a) - the associated T1-weighted MRI shows the ultrasound beam entering the frontal cortex within the frontal lobe, passing from white to grey matter at 36 mm, moving from the frontal cortex to the corpus callosum at 40 mm and from the corpus callosum into the ventricles at 68 mm. In the case of the 20 year old female volunteer - Figure 10(b) - the MRI shows the beam passing through a region of white matter to grey matter in the inferior frontal lobe at 30 mm, before entering the anterior cingulate cortex at 40 mm and to the corpus callosum at 62 mm. In both cases, BTP signals were well correlated in homogenous brain regions, while changes of waveform were associated with differing motion in adjacent tissue structures.

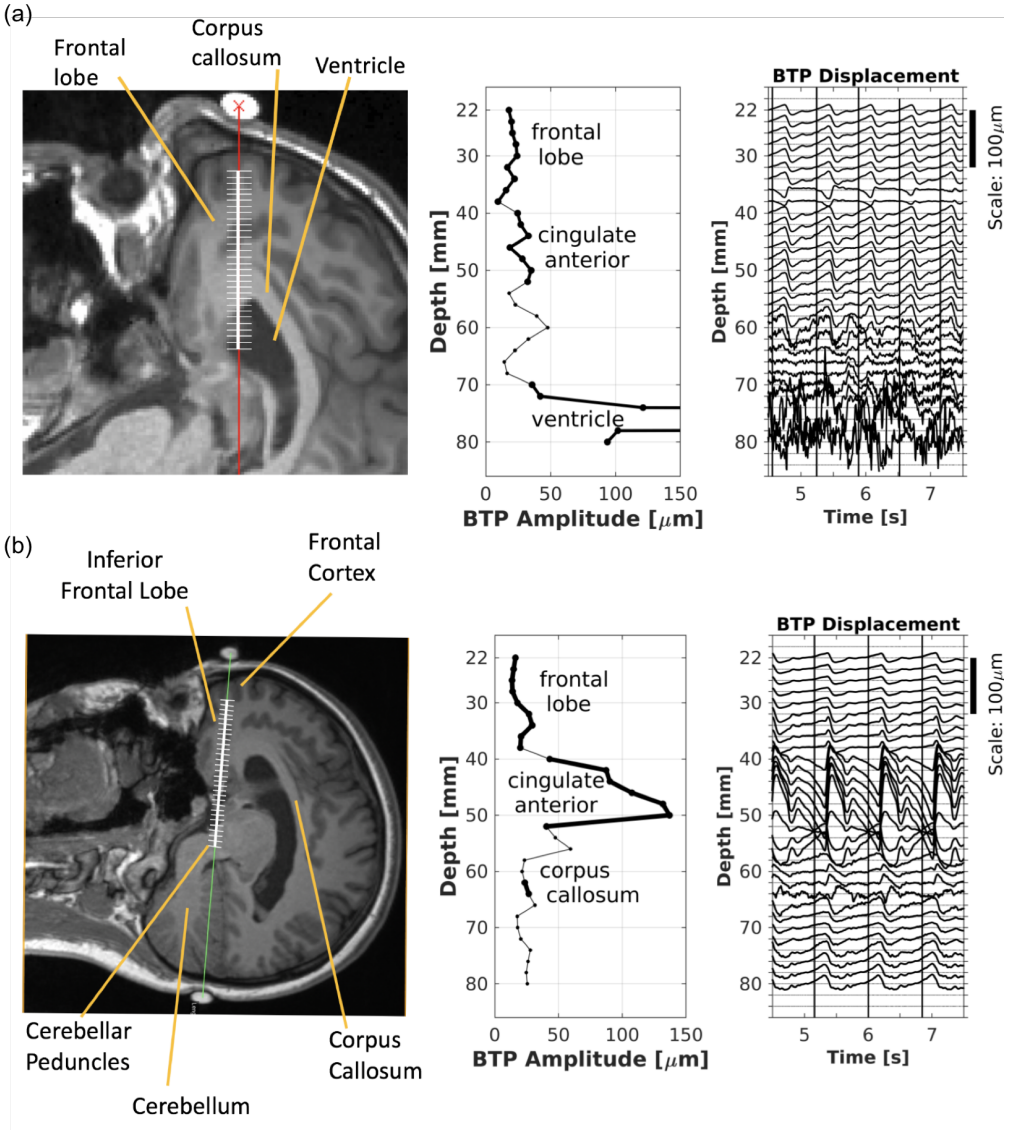

Figure 10: Example of BTP waveform changes with brain anatomy. T1-weighted MR image from (a) a 22 year old male volunteer and (b) a 20 year old female volunteer. Doppler gates are superimposed as white lines from 22 to 80 mm in depth. BTP Amplitude is displayed for each of the 30 depths in the middle panels. The right side panel shows BTP signals as a waterfall plot, with signals from adjacent depths offset by 20 μm.

3.4 TCTD Results

A total of 107 healthy volunteers were recruited to this study, comprising 56 men and 51 women. Volunteers ranged from 20 to 81 years of age (mean age: 41 years). Out of a total of 428 independent recordings, 405 recordings were suitable for further analysis; 23 recordings were rejected due to a large number of artefacts. For the forehead position, 96 subjects provided acceptable recordings for analysis from both the left and right hemispheres, and 105 subjects provided at least one acceptable recording. For the temporal position, 97 subjects provided acceptable recordings from both the left and right hemispheres, and all 107 subjects provided at least one acceptable recording.

3.4.1 Amplitude of Tissue Displacement

Median forehead Bulk BTP Amplitude was 16.1 μm [IQR: 10.5, 22.9] for the left hemisphere and 18.4 μm [IQR: 11.6, 27.3] for the right. The median Bulk BTP Amplitude measured from the temporal position was 8.8 μm [IQR: 5.9, 12.6] for the left hemisphere, and 9.3 μm [IQR: 6.4, 13.6] for the right hemisphere. To further investigate the nature of any potential differences in pulsation amplitude between hemispheres, the difference in Bulk BTP Amplitude (Δ Bulk BTP Amplitude) for each pair of BTP measurements was estimated by subtracting the left from the right side, see Figure 11.

A noticeable difference between hemispheres was a common occurrence. The median absolute magnitude of Δ Bulk BTP Amplitude was 8.7 μm [IQR: 3.9, 15.2] in the forehead positions and 3.8 μm [IQR: 1.6, 7.4] in the temporal positions. For the forehead position, 59% of participants experienced stronger right brain pulsations. The median Δ Bulk BTP Amplitude at the forehead was 2.6 μm [IQR: -5.1, 12.0]. This difference between hemispheres at the forehead was of borderline significance, based on a paired t-test using log-transformed values ($p = 0.05$). For the temporal position, 57% of participants experienced stronger pulsations in their right hemisphere. The median Δ Bulk BTP Amplitude at the temporal positions was 0.9 μm [IQR: -3.1, 4.0]. This small difference in pulsation amplitude at the temporal positions was not found to be statistically significant, $p = 0.73$. It may be of interest in future to examine whether inter-hemispheric differences are impacted by brain dominance or cognitive tasks, but this was not the focus of this initial study.

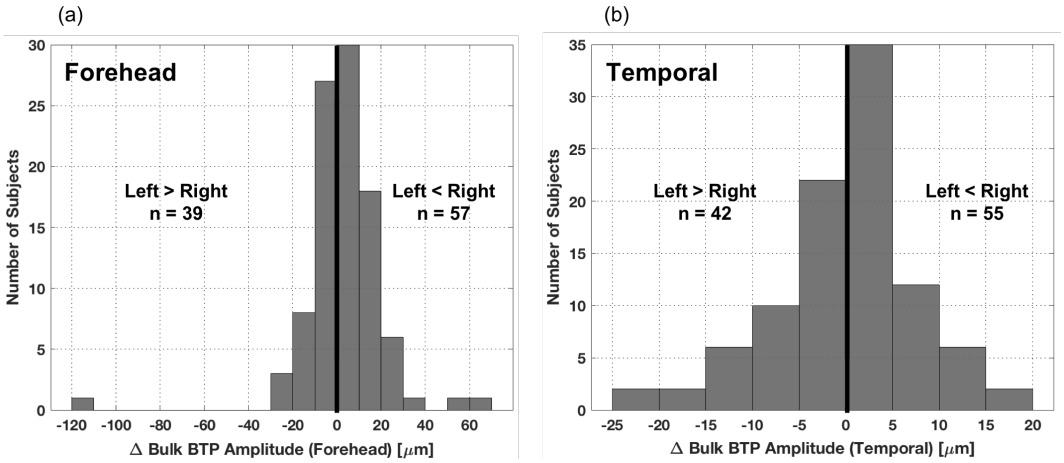

Figure 11: Difference in Bulk BTP Amplitude between the right and left sides (right amplitudes minus left amplitudes), for (a) forehead positions (96 subjects) and (b) temporal positions (97 subjects). The majority of subjects had higher right side pulsations.

Bulk BTP Amplitude was found to be significantly higher for measurements obtained from the forehead position than through the temporal window, Figure 12. The median Bulk BTP Amplitude for the forehead position was 17.0 μm [IQR: 11.3, 25.4], compared to 9.2 μm [IQR: 6.0, 12.9] from the temporal position ($p < 0.001$ using a paired t-test on log transformed data).

BTP Amplitude increased approximately linearly with depth; weakest pulsations were typically observed from the shallower gates with strongest pulsations from the deepest gates. Median BTP Amplitude for the forehead position increased from 10.4 μm [IQR: 7.2, 14.6], at a depth of 22 mm, to 32.4 μm [IQR: 23.1, 46.5] at 80 mm. Median BTP Amplitude for the temporal position increased from 5.2 μm [IQR: 3.4, 7.6] at 22 mm to 17.6 μm [IQR: 11.5, 27.4] at 80 mm. Variations in BTP Amplitudes with depth, when observed through the forehead and temporal positions, are presented in Figure 13.

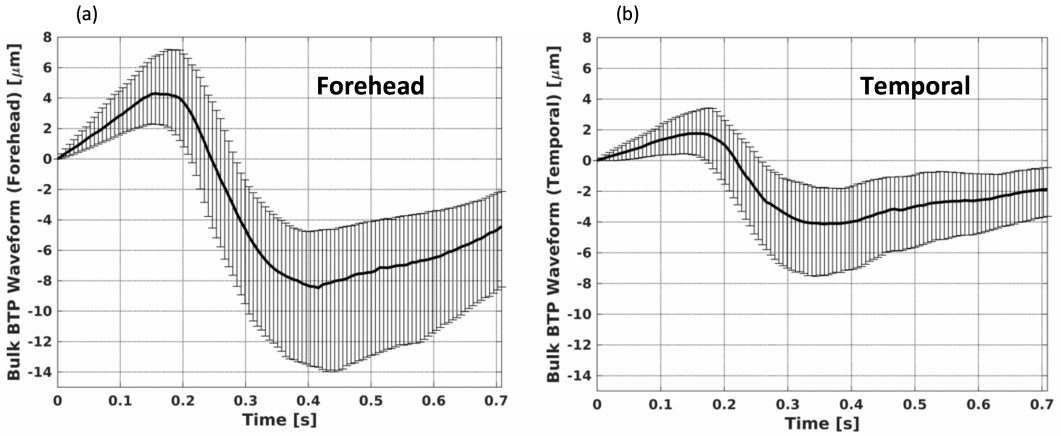

Figure 12: Representative Bulk BTP waveforms over the cardiac cycle for (a) forehead positions (201 recordings) and (b) temporal positions (204 recordings). The line shows the median TCTD waveform, with error bars to indicate the IQR. This representative waveform has been obtained by averaging the BTP signal over 30 gates and multiple cardiac cycles.

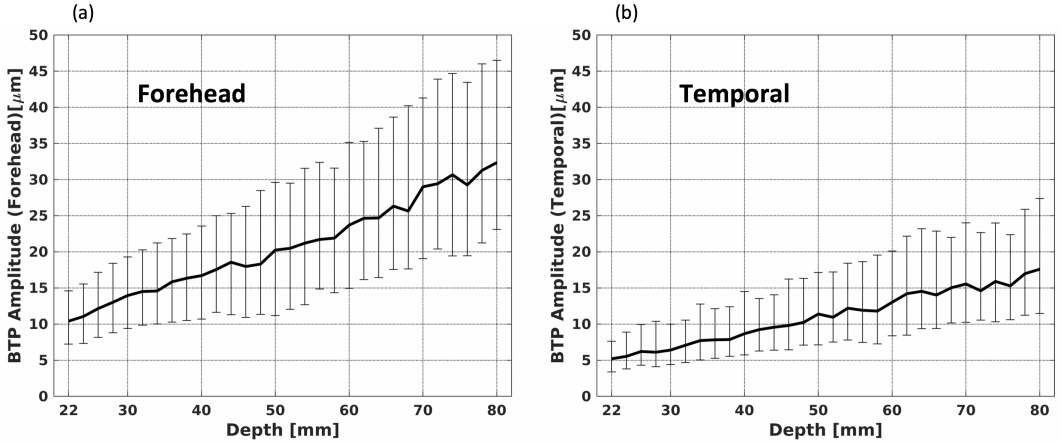

Figure 13: Median BTP Amplitude and IQR (error bars), observed from (a) the forehead position (201 recordings) and (b) the temporal position (204 recordings). BTP Amplitudes were significantly larger and more varied when measured through the forehead. The IQR also increased with depth, suggesting greater variability in measurements at depth.

3.4.2 Multivariate Regression Model

A multivariate regression model was constructed to investigate how much of the variability seen in Bulk BTP Amplitude measurements could be explained by continuous variables, such as Age, Pulse Pressure (PP), Mean Arterial Pressure (MAP), and Heart Rate (HR). This model was also used to explore whether there were any significant differences in Bulk BTP Amplitude between men

and women. Recordings from 105 subjects, with at least one valid forehead recording and one valid temporal recording, were included in the regression analysis. For each subject, Bulk BTP Amplitude measured from equivalent probe positions on the left and ride sides were averaged if both recordings were present.

Data relating to Age, Sex, PP, MAP and HR were available for all subjects. To assess the potential for multicollinearity between variables, the variance inflation factor (VIF) for each parameter was estimated and found to be < 2.5 in all cases (Mean VIF = 1.34), suggesting collinearity was unlikely to be an issue for our model. Pearson's correlation coefficients were also calculated for all explanatory variables within the model, and only weak/moderate correlations were observed (Pearson's correlation coefficient <0.5). Prior to inclusion in the model, PP, MAP, HR, and Bulk BTP Amplitude values were log-transformed to improve adherence to underlying statistical assumptions of normality.

As a first step, a univariable analysis was carried out to explore associations between individual explanatory variables and log(Bulk BTP Amp. Fore.) and log(Bulk BTP Amp. Temp.) as outcomes. Parameters where $p > 0.1$ on univariable analysis were not modelled further. This analysis suggested that log(MAP) and log(HR) ($p = 0.50$ and $p = 0.55$ respectively) were not significant predictors of Bulk BTP Amplitude.

For the remaining explanatory variables (Age, Sex, and log(PP)), multivariable regression models featuring polynomial terms up to order 2 were considered. In order to select significant combinations of terms, 36 hierarchically well-formulated models (out of 127 possible models) were assessed following the procedure suggested by Peixoto [26]. Criteria for identifying the best model included: (1) all variables in the model had to be statistically significant for at least one of the outcome variables (log(Bulk BTP Amp. Fore.) or log(Bulk BTP Amp. Temp.)), (2) the overall model should significantly explain both outcome variables, and (3) the variability in outcome parameters explained by the model (R^2 value) should be the highest after considering steps (1) and (2).

Following this plan, our preferred model included only linear terms; log(PP), Age, and Sex, with an overall level of significance of $p < 0.001$ across both

outcome variables. A Doornik-Hansen test suggested the residuals of this reduced model did not significantly deviate from a normal distribution ($p = 0.07$). Final preferred model coefficients, and p-values values are summarised in Table 2.

Outcomes	**Variable**	**Coefficient (95% CI)**	***p*-value**
log(Bulk BTP Amp. Fore.)	Constant	0.198 (-0.527, 0.923)	0.589
	log(PP)	0.753 (0.277, 1.229)	$< 10^{-3}$
	Age	-0.004 (-0.006, -0.001)	$< 10^{-3}$
	Sex	-0.045 (-0.129, 0.040)	0.297
log(Bulk BTP Amp. Temp.)	Constant	-0.090 (-0.793, 0.612)	0.799
	log(PP)	0.597 (0.136, 1.058)	0.01
	Age	0.001 (-0.002, 0.003)	0.44
	Sex	0.110 (0.028, 0.192)	0.01

Table 2: Model coefficients, 95% confidence intervals, and p-values for each of the variables included in our preferred final regression model. The R^2 values for each outcome variable were calculated, suggesting that the model accounts for 11% of the variability in log(Bulk BTP Amp. Fore.), and 21% of the variability in log(Bulk BTP Amp. Temp.). The overall p-value for the model was $p < 0.001$.

The final model is summarised below:

$$\begin{bmatrix} \log(\text{Bulk BTP Amp. Fore.}) \\ \log(\text{Bulk BTP Amp. Temp.}) \end{bmatrix} = \begin{bmatrix} 0.198 \\ -0.090 \end{bmatrix} + \begin{bmatrix} 0.753 \\ 0.597 \end{bmatrix} \log(\text{PP}) + \begin{bmatrix} -0.004 \\ 0.001 \end{bmatrix} \text{Age} + \begin{bmatrix} -0.045 \\ 0.110 \end{bmatrix} \text{Sex}$$

The influence of each continuous variable on Bulk BTP Amplitude can be explained in terms of small percentage increments. A 1% increase in PP is associated with a 0.8% increase in Bulk BTP Amplitude for the forehead and a 0.6% increase for the temporal position. For example, holding Age at a constant value of 41 years (the average value), an increase in PP from 40 mmHg to 50 mmHg is predicted to be associated with an increase in Bulk BTP Amplitude from 17.4 μm to 20.6 μm when measured through the forehead, and an increase from 8.1 μm to 9.2 μm when measured from the temporal position.

Age was found to be a significant predictor of Bulk BTP Amplitude for measurements made through the forehead. A 1 year increase in Age, above the

age of 20, corresponded to a decrease in Bulk BTP Amplitude of 0.9% for forehead BTP measurements. As an example, if PP is held at the median value of 43 mmHg, an increase in Age from 20 to 80 years would be associated with a decrease in Bulk BTP Amplitude from 22.3 μm to 12.8 μm. For measurements made from the temporal position the effect of Age was smaller, with a non-significant p-value and 95% confidence intervals that included zero.

Sex was found to be a significant factor for temporal position measurements ($p = 0.01$), with Bulk BTP Amplitude being 29% higher in men than in women. For example, adopting average values for all terms in the model, Bulk BTP Amplitude measured through the temporal position for a man would be 10.9 μm, compared to 8.4 μm for a woman. This small difference between the sexes was not confirmed in the forehead BTP measurements, where no significant difference between men and women was identified. This difference in Bulk BTP Amplitude between the sexes might be attributed to PP as a confounding variable, as men were found to have significantly higher PP than women across all ages ($p < 0.001$), see Figure 14.

The final model was able to account for 11% of the variability in log(Bulk BTP Amp. Fore.), and 21% of the variability in log(Bulk BTP Amp. Temp.). These relatively small percentages suggest that there are other factors determining the variability of Bulk BTP Amplitude which have not been considered in this model. Relationships between Bulk BTP Amplitude, PP, Age, and Sex are presented graphically in Figure 14.

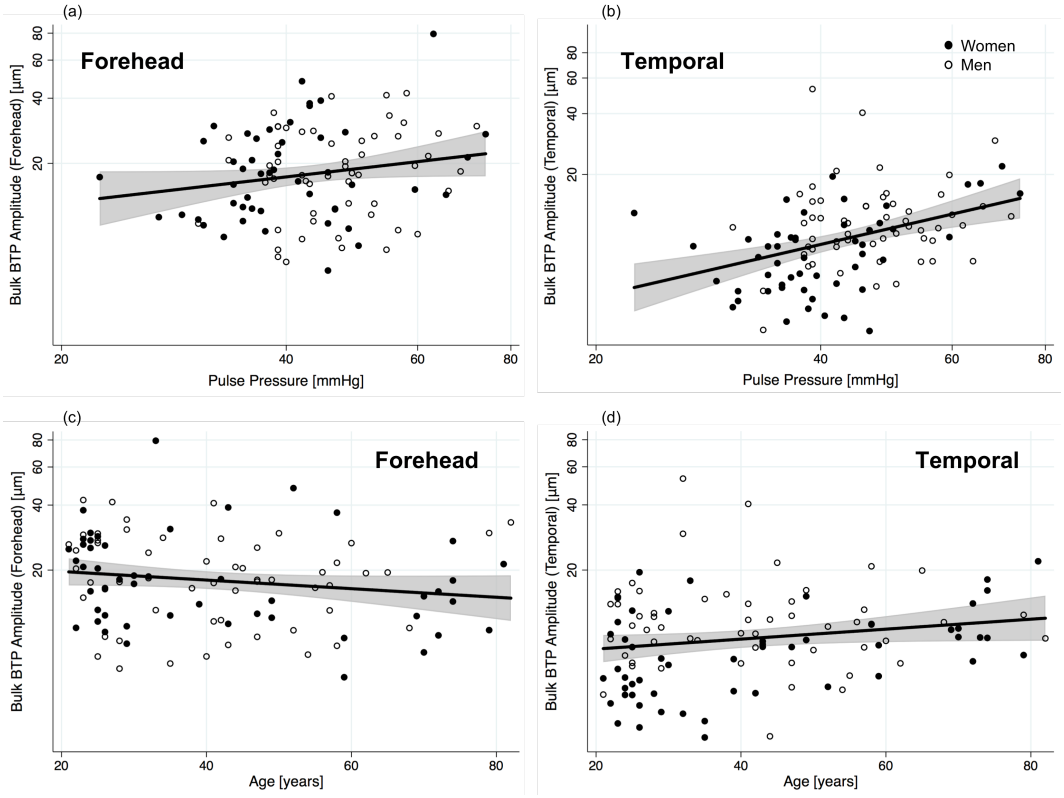

Figure 14: Shows how Bulk BTP Amplitude varies with PP, Sex, and Age for the forehead and temporal position, with both Bulk BTP Amplitude and PP displayed using a logarithmic scale. Graphs (a) and (b) show variations with PP, and (c) and (d) show how Bulk BTP Amplitude varies with Age. Men and women are indicated by hollow and filled markers, respectively.

3.5 Discussion

Transcranial Doppler (TCD) ultrasound has been used for many years for measuring blood flow through the major arteries, Aaslid *et al.* [27]. However, TCD for measurements of blood flow requires the skill and experience of a trained operator and is unsuitable for a high proportion of patients due to difficulty in obtaining measurements through the skull, Naqvi *et al.* [28]. As TCTD measures ultrasound backscatter from dense tissue rather than echoes from red blood cells suspended in an anechoic plasma, the received ultrasound signal from tissue is stronger than from blood, due to the higher density of scatterers available. TCTD measurements are also much easier to obtain than conventional TCD, as there is no need to orient the beam to coincide with a particular vessel location. BTP signals have been successfully obtained in all participants we have studied to date. Therefore, TCTD may prove to be

a clinically useful addition to TCD by providing complementary tissue motion estimates. This initial study investigated BTPs in a large cross-section of healthy subjects. Our findings show that BTP Amplitude varies considerably between hemispheres and between subjects in healthy participants, and is skewed towards lower values.

Insights into the characteristics of healthy BTPs gained using TCTD may help to improve our understanding of factors affecting brain tissue pulsatility. In this study we provide reference data from healthy volunteers, to be used for comparison with patient data in future research. The aim of this study was to better understand factors affecting Bulk BTP Amplitude in healthy subjects. Importantly, we confirm that good quality BTP data can be obtained from all participants from both the temporal and forehead positions. A small number of recordings were excluded from analysis due to the presence of artefacts rather than the absence of a signal. BTP amplitude was found to depend on probe position and sample depth, and to differ between hemispheres. A correlation between Bulk BTP Amplitude and PP was confirmed, and potential for a weaker influence of Age and Sex on Bulk BTP Amplitude was also indicated.

Our study concurs with previous MRI measurements by Weaver *et al.* [6], describing increases in pulsation amplitude with proximity to the circle of Willis. BTP Amplitude measured through the skull increased with sample depth. Weaver *et al.* examined 6 subjects and found that the tissue surrounding the circle of Willis pulsates with an amplitude of approximately 150 μm. In our study, the highest reading obtained was 156 μm from a depth of 76 mm. Superficial brain tissue was found to pulsate at an amplitude of 10 μm in Weaver's study, which is similar to the median BTP Amplitude found in our study of 10.4 μm [IQR: 7.2, 14.6] for the forehead position and 5.2 μm [IQR: 3.4, 7.6] for the temporal position at the shallowest depth of 22 mm. However, the expected gate depths displayed in Figure 10 may be different, due to the ultrasound beam being distorted and attenuated in the presence of real skull, as shown by Evans and Gittins [29]. The extent of this distortion will vary between individuals, therefore, we were unable to determine which brain structures are truly being measured. As our measurements were not corrected for Doppler angle, it should also be remembered that our V.cos(θ) estimates provide an estimate of the component of tissue motion in the direction of the

beam, which is likely to underestimate the true velocities and displacement of brain tissue depending on the angle of the beam with the direction of tissue motion.

The TCD system used to acquire BTP data for this study was designed for blood flow measurements and not optimised for BTP measurement. For example, our recordings were limited to 8 seconds of data, and there was no user display for BTP visualisation. A system capable of making continuous BTP recordings would be useful for future investigation of the effects of PP, MAP, cerebral blood flow, CO_2, and inter-hemispheric differences on BTP waveform shape and amplitude in physiological measurement studies. It may also be beneficial to extend the age range and other characteristics of our healthy cohort to octogenarians and to perform a subgroup analysis investigating participants with specific risk factors, e.g. hypertension and diabetes. Although we aimed to attract healthy participants, some of the subjects recruited to our study may have had undiagnosed underlying health conditions.

There is also an opportunity to advance understanding of brain tissue motion using new Doppler capabilities offered by high framerate ultrasound imaging. Echocardiography studies have shown that high framerate ultrasound provides additional information on cardiac tissue motion during early and late systole, Brekke *et al.* [30]. This could be applied to future studies into brain tissue motion to achieve a greater temporal resolution, and therefore, a more in-depth understanding of how brain tissue moves over the cardiac cycle. This study is limited by the assumption that tissue strain is in one dimension (in the direction of the beam), whereas previous MRI studies suggest that brain tissue moves in an inward and downward motion with each heartbeat, Greitz *et al.* [3]. It would be of interest to improve this technique by using vector Doppler ultrasound to estimate both the magnitude and direction of tissue motion. Another technique that could be considered is time reversal transcranial ultrasound, which is a method that could be used to avoid aberration of the skull, as mentioned previously.

MRI results from this study suggest that BTP signals may experience regional variations due to differing tissue structures. It is important that the probe position is standardised in all measurements to account for this. In this study,

the probe was placed 1 cm above the centre of the eyebrow for the forehead position, and in the centre of the temporal acoustic window for the temporal position. It is ensured that the probe is placed flat against the surface of the skull for each participant. However, due to differences in skull shapes, this may cause inconsistencies between participants, regarding the angle of the ultrasound beam. Therefore, it would be beneficial to attempt to standardise the probe position in such a way that enables measurement of similar tissue structures in all participants. It is also possible that the presence of blood vessels may result in larger BTP amplitudes, however, as this study did not involve the measurement of blood flow or the localisation of vessels, this remains unclear. It would be useful to address this in future research when investigating the impact of CBF on BTPs with the Brain TV system. It may also be useful to acquire simultaneous B-mode transcranial colour-coded duplex images alongside TCTD measurements to more easily locate different structures in the brain, however, it would only be possible to obtain these images through the temporal bone window.

Overall, this study has confirmed that transcranial tissue Doppler ultrasound is capable of measuring brain tissue pulsations in human subjects. Overall, 5% of 8 second recordings were excluded due to artefacts. Our results provide insights into how BTPs vary amongst individuals, and have allowed us to develop a preliminary model of healthy Bulk BTP Amplitude as a function of PP, Age, and Sex. If BTPs are sensitive to pathophysiology, TCTD may be useful for distinguishing between healthy and pathological brain tissue motion.

3.6 Conclusions

Brain tissue pulsations are synchronous with the cardiac cycle, and can be measured and quantified using transcranial tissue Doppler (TCTD) ultrasound. Our analysis reveals that BTPs depend on sample depth, probe position, PP, and potentially age and sex. This dataset provides a useful model of healthy brain tissue pulsations for comparison with future clinical studies. Based on the promising results of this study the brain tissue measurement prototype described in chapter 2 was developed and used in all of the remaining studies described in this thesis.

4 Investigating the Impact of Blood Pressure on Brain Tissue Pulsations

4.1 Introduction

Our initial healthy volunteer study (presented in chapter 3) aimed to characterise and quantify healthy brain tissue pulsations (BTPs), and the results suggested a relationship between BTPs and blood pressure (BP), with a significant impact of pulse pressure (PP) on Bulk BTP Amplitude. However, this study had limitations regarding data acquisition, as the data were obtained using a conventional TCD machine which was not optimised for visualisation or measurement of BTPs. Limitations of the device include the length of the recordings, as only 8 seconds of ultrasound data could be recorded at a time, and the BP results were based on a single value measured using a standard arm cuff BP monitor, as the TCD device used for data acquisition was not capable of synchronous physiological measurements. Since this study, there have been a number of hardware, software, and headset developments, and data acquisition has been greatly improved. The new Brain Tissue Velocimetry (Brain TV) system, introduced in chapter 2, is capable of taking continuous measurements for numerous variables (including BP and expired CO_2). This makes it possible to observe beat-to-beat fluctuations in each measured variable and investigate any possible relationships more thoroughly.

This chapter details the methods and results of a healthy volunteer, and ultrasound phantom study, investigating the impact of BP on Bulk BTP Amplitude. The healthy volunteer data was gathered by G. deVries (University Hospitals of Leicester NHS Trust) as part of her MSc project. I analysed her data and completed the phantom experiment.

4.2 Healthy Volunteer Experiment

Previous research into BTPs has mainly focused on characterising BTPs in particular subsets of patients, compared to healthy controls. For example, Desmidt *et al.* studied patients with depression [17], [18], and more recently, Terem *et al.* observed differences in BTPs between a healthy volunteer and a patient with a Chiari I malformation [9]. Only one study has looked into the

impact of blood pressure on BTPs, investigating BTP changes in 22 elderly subjects with orthostatic hypotension (OH), a condition in which a person's blood pressure decreases significantly after moving from a sitting/supine position to standing. Results suggested that BTPs were significantly weaker in patients with OH compared to those without OH, Biogeau *et al.* [19]. There is no current research focusing on the impact of BP on brain tissue motion in healthy volunteers. This study uses Transcranial Tissue Doppler (TCTD) ultrasound to estimate BTPs in 20 volunteers at rest, and during a leg raise manoeuvre used to increase BP. The repeated measures study design enables the subjects to act as their own controls, therefore the impact of raised BP is investigated directly in each individual.

4.2.1 Methods

Subjects

Healthy adults were recruited to this study through the University of Leicester. Exclusion criteria included participants under the age of 18 years, those with a known brain injury, and those with history of cardiovascular or respiratory illnesses. All participants provided written informed consent prior to data acquisition.

Equipment

TCTD measurements were taken using the Brain TV system, described in chapter 2, an ultrasound prototype designed by Nihon Kohden (Japan) for research purposes at the University of Leicester. Ultrasound measurements were taken from the forehead and temporal window on the participants right side, with the ultrasound transducer attached using a custom probe holder and an elasticated headband. TCTD recordings were taken alongside continuous BP and CO_2 measurements, using equipment described in chapter 2.

Protocol

Physiological measurements were carried out by G. DeVries (University Hospitals of Leicester NHS Trust). Recordings were 3 minutes in length, consisting of a 1 minute baseline, 1 minute of repeated leg raise manoeuvres, and ending with a 1 minute rest period. The leg raise manoeuvre involved the participant

extending both legs directly in front of them with their feet raised above the floor, this position was held for 10 seconds, before returning to the rest position with feet placed fully on the floor. The manoeuvre is carried out 3 times with a 10 second rest between repetitions. Participants were sat upright, and asked to remain still, with their eyes closed during recordings, to reduce the occurrence of motion artefacts. Two recordings were taken for each participant, one for the forehead position, and one for the temporal position. Data from the forehead position were taken forward for further analysis.

Data Analysis

Signal processing of TCTD recordings was carried out using the method described in chapter 2. BTP signals were displayed in MATLAB with the R-R intervals overlaid and traces manually inspected to allow the user to remove any cardiac cycles containing artefacts. Artefacts were defined as any noticeable perturbations not regularly repeating with the cardiac cycle. Similarly to artefacts in TCD measurements of cerebral blood flow, TCTD artefacts result from motion of the probe or participant during recordings. Further analysis was based on these cleaned (artefact free) data.

Inspection of the quality of the recordings showed that good quality signals were obtained through the forehead for the first 20 gates, corresponding to depths within the brain ranging from 22 to 60 mm. Signal quality weakened beyond this depth for the majority of participants, therefore, only data from the first 20 gates were analysed. One additional gate was removed for 3 participants during the analysis of recordings due to limited penetration of the ultrasound beam in specific subjects.

For each recording, a Bulk BTP signal was calculated by averaging signals across all available depths. The Bulk BTP signal shows collective displacement of brain tissue in the direction of the beam over time (corresponding to the instantaneous bulk movement of tissue located at a depth of 20-60 mm from the face of the probe). A further quantity describing the magnitude of each pulsation, beat-to-beat Bulk BTP Amplitude, was estimated by calculating the absolute difference between the peak and the trough of the Bulk BTP signal for each cardiac cycle.

The remaining physiological measurements (BP, ECG, and $EtCO_2$) were analysed to provide beat-to-beat estimates of pulse pressure (PP), mean arterial pressure (MAP), heart rate (HR) and $EtCO_2$. HR was calculated by measuring the length of the subject's R-R interval and determining the frequency per minute, this gives an instantaneous HR for each cardiac cycle. Beat-to-beat estimates of PP and MAP can both be calculated using the systolic and diastolic pressure values measured during each cardiac cycle. Time series of an entire recording for one participant can be seen in Figure 15, with the leg raise periods highlighted.

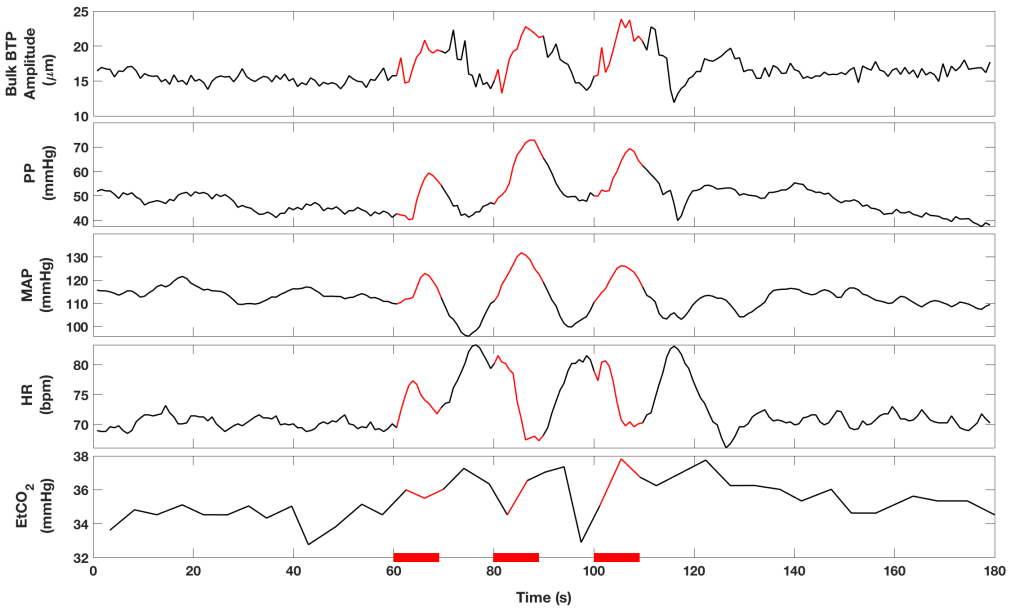

Figure 15: Time series for each variable are shown for an entire recording in which a 47 year old male performs the 3 leg raise manoeuvres at times 60, 80, and 100 seconds, each of 10 seconds duration. Leg raise time periods are shown in red, with red bars also given across the x-axis. Peaks in PP, MAP, and Bulk BTP Amplitude can be seen during the leg raise periods. HR can be seen to increase and then decrease during the leg raise manoeuvres, and $EtCO_2$ appears to increase slightly for the duration of the leg raise section of the protocol compared to the baseline values.

Statistical Analysis

Time intervals were selected for each recording to ensure that data taken forward for further analysis were high quality and artefact free. For each recording 30 seconds of baseline data and approximately 6 seconds during each leg raise manoeuvre were selected for further analysis, resulting in $\sim$ 18 seconds of leg raise data for each participant.

Beat-to-beat values for the duration of the selected baseline and leg raise periods were compared for each participant individually. The distribution of the beat-to-beat values for each variable was visually inspected. For each variable, the mean and standard deviation of the beat-to-beat values were calculated, giving one value per participant. These mean values were used to investigate the response of the entire cohort.

The distribution of the cohort data was investigated using a Shapiro-Wilk test for normality. Any non-normally distributed variables (Bulk BTP Amplitude) were log-transformed to ensure a normal distribution. Paired t-tests were carried out on normally distributed data (including the log-transformed variables) to compare baseline and leg raise values. The median and IQR were calculated for non-normally distributed variables (Bulk BTP Amplitude), and the mean and standard deviation were calculated for variables that were normally distributed between subjects (PP, MAP, HR, and $EtCO_2$).

4.2.2 Results

Twenty healthy volunteers (10 men, 10 women) of ages 20 - 51 years were recruited to this study. Ages were skewed towards younger participants, with median age being 29 years [IQR: 24, 41].

BTP Variations in the Population

Blood pressure was successfully increased during the leg raise manoeuvre compared to baseline, this is reflected in both PP and MAP values. PP significantly increased from a baseline value of 42.4 (6.4) mmHg to 48.7 (11.0) mmHg during the leg raise manoeuvres, showing an estimated increase of 6.3 mmHg [95% CI: 3.5, 9.1, p = 0.0002]. Similarly, MAP increased from a baseline value of 89.1 (12.5) mmHg to 93.2 (14.4) mmHg, corresponding to an increase of 4.1

mmHg [95% CI: 1.5, 6.7, p = 0.004].

Remaining variables, HR and $EtCO_2$, also displayed an increase during the leg raise manoeuvres. HR showed an increase of 6.9 bpm [95% CI: 4.7, 9.1, p < 0.0001], increasing from a baseline value of 71.5 (10.0) bpm to 78.4 (8.9) bpm during the leg raises. $EtCO_2$ showed a slight increase of 1.0 mmHg [95% CI: 0.4, 1.6, p = 0.004], from 35.5 (3.1) mmHg to 36.4 (3.2) mmHg.

Median Bulk BTP Amplitude began at a baseline value of 12.5 μm [IQR: 10.0, 18.1] and increased to 15.5 μm [IQR: 13.3, 20.3] during the leg raise manoeuvres, this corresponds to an increase of 3.0 μm (p = 0.004 using a paired t-test on log-transformed values). Due to the repeated significance testing, an adjusted p-value was calculated using the Bonferroni correction, giving an adjusted significance level of 0.01. As the results from the significance tests resulted in p-values lower than 0.01, it is clear that the results are significant. Changes in all variables between baseline and leg raise periods for the entire cohort can be seen in Table 3, and Figure 16.

Variable	**Baseline**	**Leg Raise**
Med. Bulk BTP Amp. (μm)	12.5 (10.0, 18.1)	15.5 (13.3, 20.3)
Mean PP (mmHg)	42.4 (6.4)	48.7 (11.0)
Mean MAP (mmHg)	89.1 (12.5)	93.2 (14.4)
Mean HR (bpm)	71.5 (10.0)	78.4 (8.9)
Mean $EtCO_2$ (mmHg)	35.5 (3.1)	36.4 (3.2)

Table 3: Median and mean values for all volunteers are displayed for baseline and leg raise data, with IQR shown in brackets for the median values, and standard deviation shown in brackets for the mean values. A statistically significant increase is observed in all variables during the leg raise period. The estimated differences between phases and the associated p-values are displayed in Figure 16.

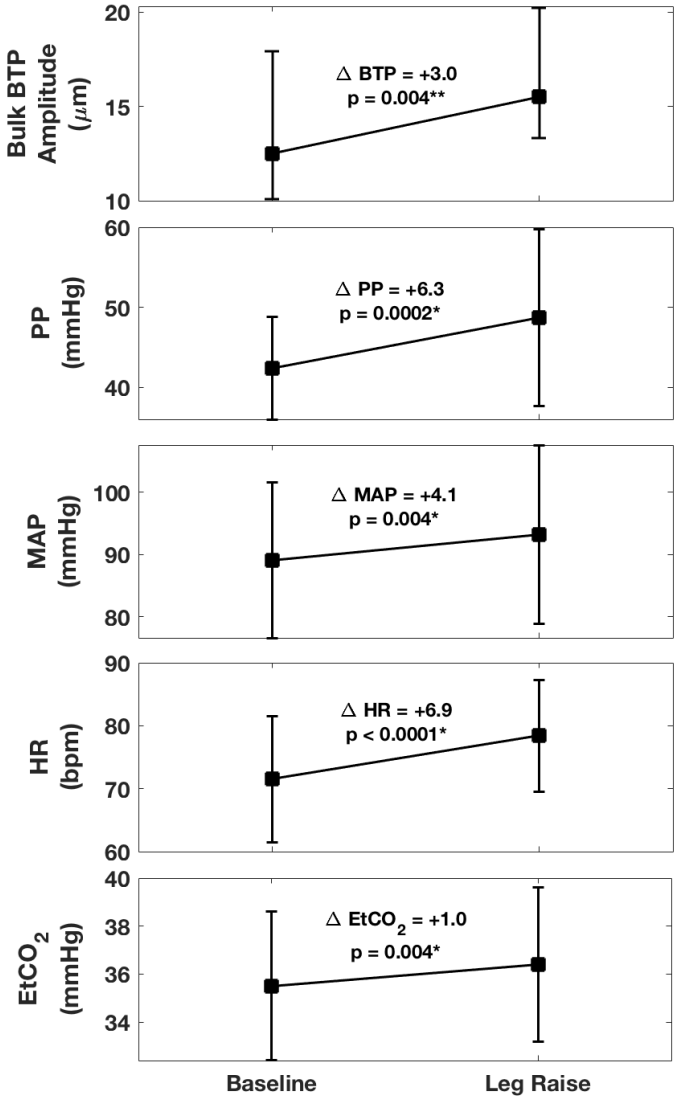

Figure 16: Changes between baseline and leg raise data averaged across the entire population of volunteers. The median and IQR are shown for the Bulk BTP Amplitude values, and the mean and standard deviation are shown for all other variables. Estimated differences between baseline and the leg raise manoeuvre are labelled, with differences for median Bulk BTP Amplitude calculated on log-transformed data, results have been back-transformed to μm for ease of understanding. Paired t-tests were carried out on normally distributed variables* and on log-transformed data** to determine whether changes were statistically significant at an adjusted p-value of p=0.01.

BTP Variations in Individuals

Individual changes were investigated, with differences in Bulk BTP Amplitude between baseline and leg raise periods varying from $< 0.5\mu$m to $\sim$10 μm. It was observed that 15 subjects experienced an increase in Bulk BTP Amplitude, with 11 of these instances being statistically significant, and the greatest increase being 9.6 μm. In the 5 subjects that experienced a decrease in Bulk BTP Amplitude, 2 of these instances were statistically significant, with the greatest decrease corresponding to a value of 3.5 μm. Fifteen participants experienced a statistically significant increase in PP, and only 1 participant experienced a significant decrease. Thirteen participants experienced an increase in both PP and Bulk BTP Amplitude, 6 participants experienced an increase in one and a decrease in the other, and 1 participant experienced a decrease in both PP and Bulk BTP Amplitude. Figure 17 shows changes in each variable for each participant.

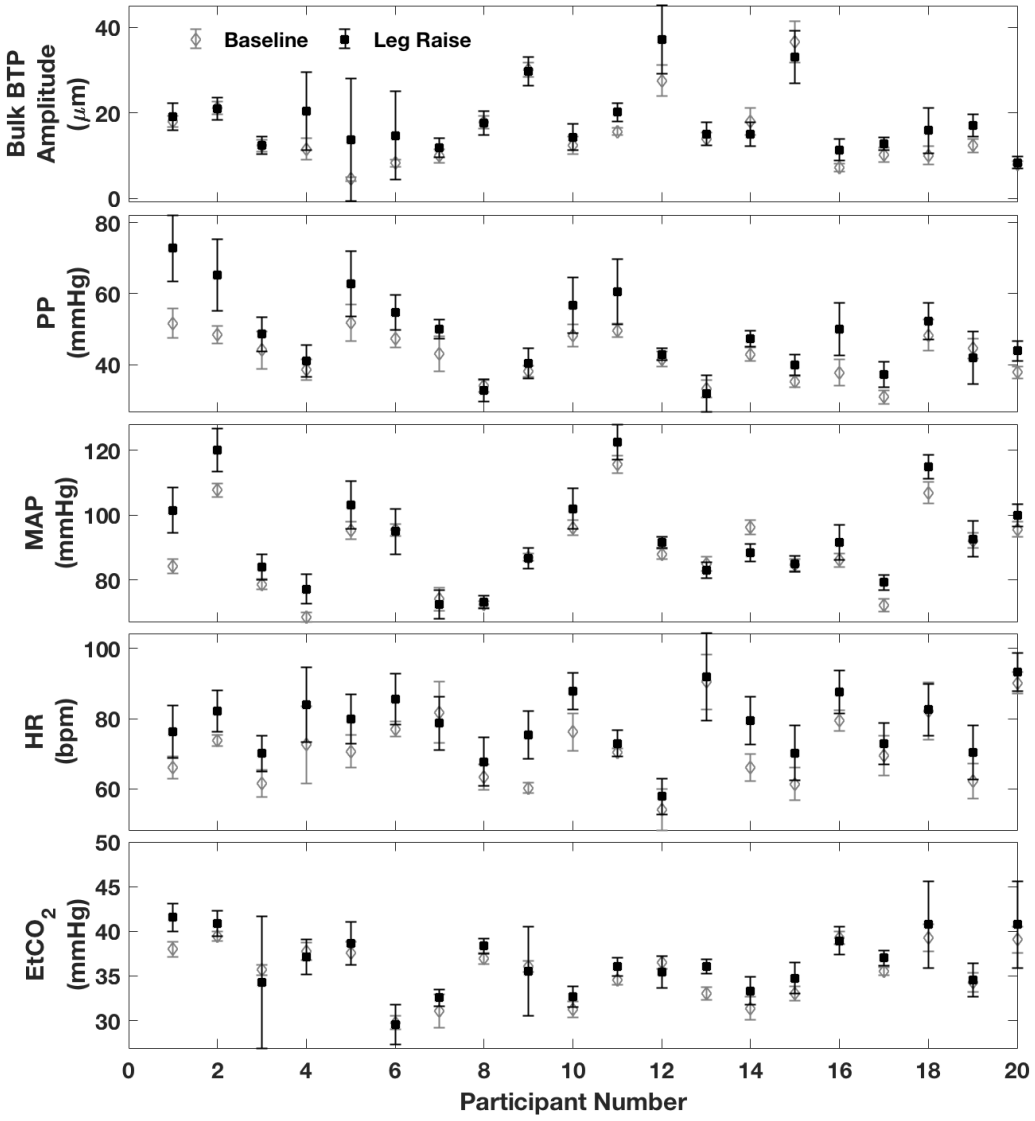

Figure 17: Summary of changes in variables between the baseline and leg raise manoeuvre for each participant. Graphs for all variables show the mean beat-to-beat value, with the SD indicated by error bars. The majority of participants experienced a significant increase in PP and MAP, with only 4 participants not responding to the leg raise manoeuvres for PP, and 6 not responding for MAP.

4.3 Phantom experiment

Research involving human subjects can have limitations, for instance it can be difficult to get ethical approval to test new clinical ideas on patients without prior evidence suggesting that there will be a beneficial outcome. Additionally, certain variables in an experiment may need to be controlled, which may be difficult to achieve *in vivo*. In cases such as these, phantom studies may be useful. A phantom is an object that has similar anatomical or physiological properties as the tissue that is to be imaged, meaning that the imaging device can be tested on the phantom rather than a human subject.

Phantoms are often used for device development and validation, teaching, and hospital Quality Control tests. Tissue phantoms have been used clinically since the 1960s, and many forms of tissue-mimicking materials (TMM) have been developed, with the most commonly used TMM being prepared using agar based solutions, Culjat *et al.* [31].

Brain tissue motion has previously been investigated using brain tissue phantoms. In 2006 a phantom developed using polyvinyl-alcohol cryogel (PVAc) TMM was used to validate brain shift correction techniques for use in neurosurgery. Deformation of brain tissue was simulated by inflating a balloon catheter placed within the phantom, this deformation was then imaged using MRI and ultrasound, Reinertsen and Collins [32]. More recently, in 2020, a dynamical agarose gel phantom was developed to validate a technique for measuring BTPs using transcranial sonography, Jurkonis *et al.* [20]. The TMM developed in this study was held in a plastic container, and BTPs were simulated using a moving wooden rod, embedded in the TMM, driven by a linear solenoid actuator.

In this study a PVAc brain tissue phantom is used to investigate the relationship between BP and BTPs. BTPs will be generated using a pulsatile flow of blood-mimicking fluid (BMF) through a silicone replica of the major cerebral arteries embedded within the TMM. PVAc tissue substitutes require fewer ingredients than agar based solutions, Surry *et al.* [33], and also have the benefits of structural rigidity, and longevity, Culjat *et al.* [31]. A phantom is used to enable the blood pressure to be altered rapidly and easily in a con-

trolled environment. Data obtained from the parallel study of the effect of BP on BTPs in healthy volunteers (presented in section 4.2), will be compared to the phantom work. The arterial brain tissue phantom featuring only arteries and brain tissue is heavily simplified compared to the human, and may not capture all relevant behaviours. However, this makes it easier to conclude which variables affect BTP amplitude, while also giving an understanding on the impact of the major cerebral arteries on brain tissue motion.

4.3.1 Methods

Phantom Development

The phantom contained a silicone replica of the cerebral arteries (2 anterior [ACA], 2 posterior [PCA], and 2 middle cerebral arteries [MCA]) surrounded by a polyvinyl-alcohol (PVA) material, designed to mimic the acoustic and elastic properties of brain tissue (speed of sound 1630 ms^{-1}, density 1.06 kgm^{-3}, Young's Modulus 8 kPa). This anatomical artery replica was then encased within a 3D-printed skull based on a computed tomography (CT) scan of a human skull, as shown in Figure 18.

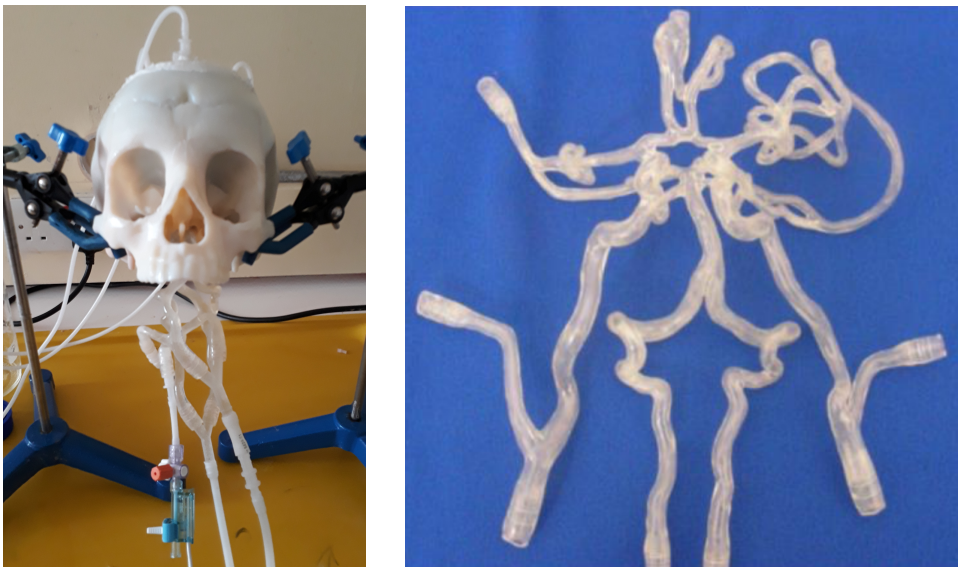

Figure 18: The image on the left shows the finished phantom set up for the experiment, with the pressure catheter inserted into the external carotid artery. The image on the right shows an example of the silicone replica of the cerebral arteries (Elastrat, Geneva) which is then surrounded by tissue-mimicking material and encased within the 3D-printed skull.

The properties of the 3D-printed skull and a human skull were compared using a beam plotting system to investigate how the characteristics of the ultrasound beam differ between skulls. When taking ultrasound measurements, the phantom had blood mimicking fluid (BMF) flowing through the arteries, consisting of 60% water and 40% glycerol in weight, giving the fluid a viscosity comparable to that of blood (∼3 mPa.s).

The vascular replica contained 4 inlet pipes (2 carotid and 2 vertebral arteries) for blood flow to the brain and 3 outlets. The first outlet combines the flow from both ACAs, the second outlet combines the left MCA and PCA, and the final outlet combines the right MCA and PCA.

Implementation of Physiological Conditions within the Phantom

To mimic physiological blood flow, there were a number of factors to consider. Firstly, the correct flow rate had to be achieved using a programmable pump which generated pulsatile flow within the phantom. It was calculated that ∼ 650 ml of blood flows through the arteries in the brain every minute, Scheel *et al.* [34], (∼150 ml from the vertebral artery, and 250 ml from each internal carotid artery). Therefore, the settings on the pump had to be adjusted so that the flow rate was 650 ml/min without exceeding physiological values of blood pressure. The pump had 4 inbuilt waveform options which determine the shape of the flow waveform, and the one which most represented a physiological pulsatile flow was chosen. The 'heart rate' was set to be 60 BPM.

It also had to be ensured that the correct amount of liquid was passing through each artery. This was achieved by varying the resistance of the tubing for the inlets and outlets - in line with electric circuit analogue theory. Firstly, the inlet tubing had to be altered to ensure that the anterior circulation acquired 75% of the total flow, and the posterior circulation obtained the remaining 25%. This was achieved by altering the length and the radius of the tubing as a means of changing the resistance. To ensure that the 75:25 split was accurate, the pump was started and the tubes for the anterior and posterior inlets were placed into separate beakers. After 1 minute the pump was stopped and the fluid collected in the respective beakers was measured, this was repeated 3 times to ensure that the results were reliable. This procedure was repeated

when attempting to acquire the correct flow rate from each outlet tube. The flow rates for each MCA + PCA outlet were equal and received the majority of the flow, with only 11% of the BMF flowing through the ACA outlet, these ratios were found in previous work on CBF volume, Alastruey *et al.* [35].

Data Acquisition

TCTD measurements were obtained using the Brain TV system described in chapter 2. Ultrasound recordings were taken from the right forehead position, and the probe was not moved between recordings. Continuous blood pressure measurements were obtained using a pressure transducer attached to the right external carotid artery, and viewed using an ECG Lifescope monitor (Nihon Kohden, Japan).

For the first experiment, MAP was changed by increasing the height at which the BMF reservoir was placed, whilst the rest of the equipment remained at a constant height. This has the effect of increasing MAP by increasing the pressure within the tubing while the flow remains constant. The reservoir was moved vertically by approximately 20 cm every 20 seconds for the duration of the 3 minute recording, this resulted in 8 different values of MAP contained in one recording, see Figure 19.

The second experiment involved altering PP within the phantom, this was achieved by increasing the amplitude of the waveform output using the pump. This has the impact of changing the flow waveform to increase the difference between systolic and diastolic flow velocities and make the flow generated by the pump more pulsatile. The amplitude was increased from 0.2 V to 1.8 V in steps of 0.4 V until an amplitude of 1.0 V was reached, then the step size was reduced to 0.2 V. A recording of approximately 10 seconds was taken for each amplitude setting, resulting in 7 recordings. The changes induced in PP can be seen in Figure 20.

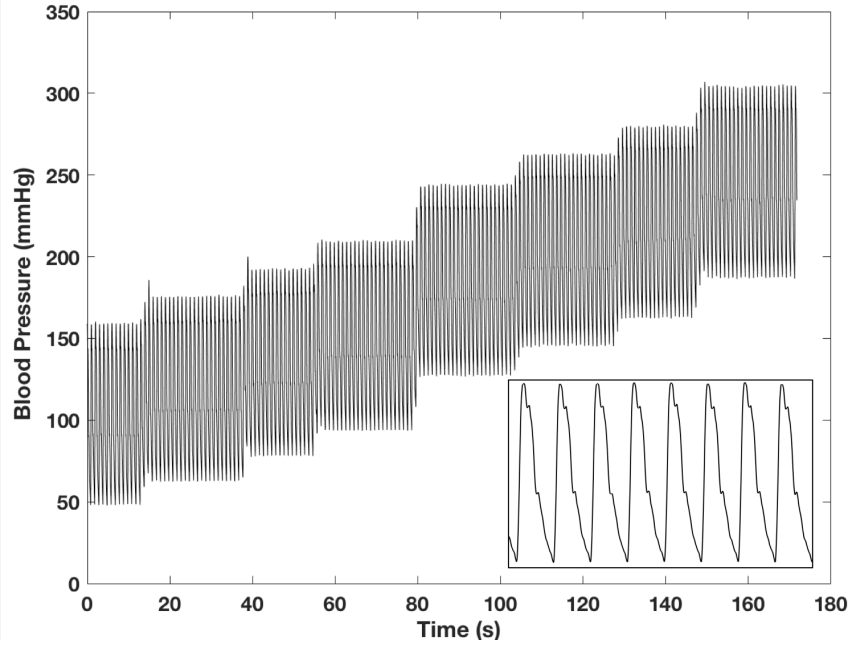

Figure 19: Changes in MAP induced by altering the height of the reservoir. A close up of the BP waveform can be seen in the bottom right corner.

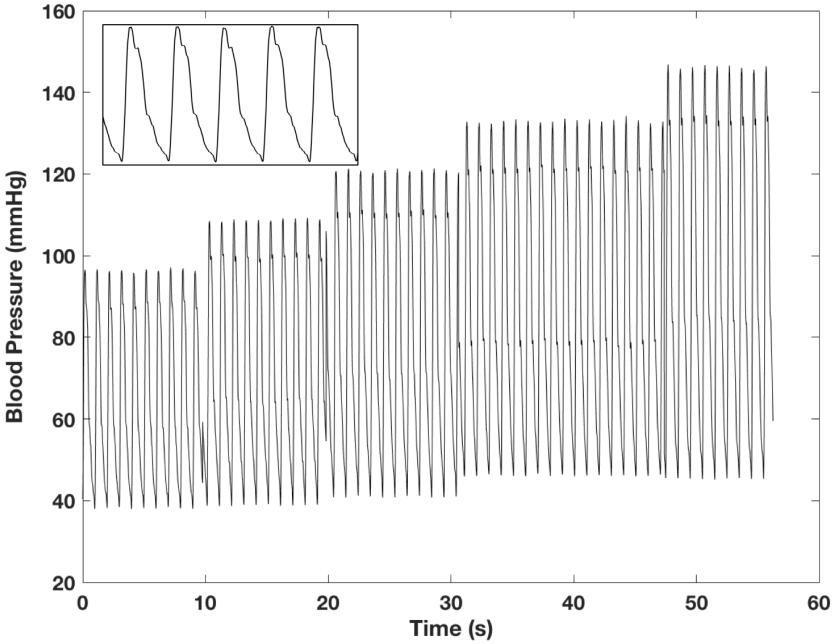

Figure 20: Changes in PP induced by altering the amplitude of the waveform output using the pump. A close up of the BP waveform is shown in the top left corner.The first two readings did not include continuous BP measurements, and are therefore not included in this graph. All readings were included in statistical analysis and are shown in Figure 21.

Data Analysis

Data were viewed using MATLAB (R2018b), which allowed the user to determine the quality of the data. Any gates not exhibiting good quality data were omitted. A total of 27 gates were used in the analysis of the first experiment, and all 30 gates were used in the second experiment.

Beat-to-beat values were calculated for PP, MAP, and Bulk BTP Amplitude using MATLAB (R2018b). For both experiments, the beat-to-beat values from ten second time intervals for each change in BP were analysed. These beat-to-beat values were visually inspected to confirm a normal distribution. Values for each variable were then averaged and their standard deviation was calculated. Paired t-tests were used to compare data from the recording with lowest BP to the recording with highest BP. For the second experiment the continuous BP measurements were not available for the first 2 recordings, therefore the BP value observed on the ECG Lifescope monitor was used in these cases, hence a standard deviation cannot be provided for the lowest measured value of PP.

4.3.2 Results

Bulk BTP Amplitude Variations with MAP

MAP was successfully increased using the protocol, from the lowest value of 85.2 (0.3) mmHg to the highest value of 227.8 (0.3) mmHg, see Figure 19. This gives an increase of 142.6 mmHg [95% CI: 142.4, 142.9, $p < 0.0001$]. PP was also found to increase slightly, from 112.1 (0.5) mmHg to 118.5 (0.4) mmHg, an increase of just 6.4 mmHg [95% CI: 6.0, 6.7, $p < 0.0001$]. These changes in blood pressure corresponded to a slight decrease in Bulk BTP Amplitude, from 19.5 (0.8) μm to 18.9 (0.6) μm, giving a decrease of 0.6 μm [95% CI: 0.0, 1.1, $p = 0.05$]. However, as the measurement accuracy of the Brain TV system was calculated to be $\sim$1.6 μm (see chapter 2), this is unlikely to be a significant difference.

Bulk BTP Amplitude Variations with PP

PP was successfully increased using the protocol for the second experiment, from a value of 12.0 mmHg, to a value of 100.9 (0.4) mmHg. MAP was also found to increase during this protocol, from a value of 38.0 mmHg, to a value

of 79.0 (0.2) mmHg. Unfortunately, with our current pump, we were unable to alter PP while maintaining constant MAP, however, total flow was constant throughout these experiments. These changes in blood pressure correspond to a significant increase in Bulk BTP Amplitude of 30.2 μm [95% CI: 28.3, 32.1, $p < 0.0001$], from a value of 5.2 (1.7) μm at the lowest PP, to 35.4 (0.8) μm at the highest PP. Changes in all variables for both of these experiments are summarised in Figure 21.

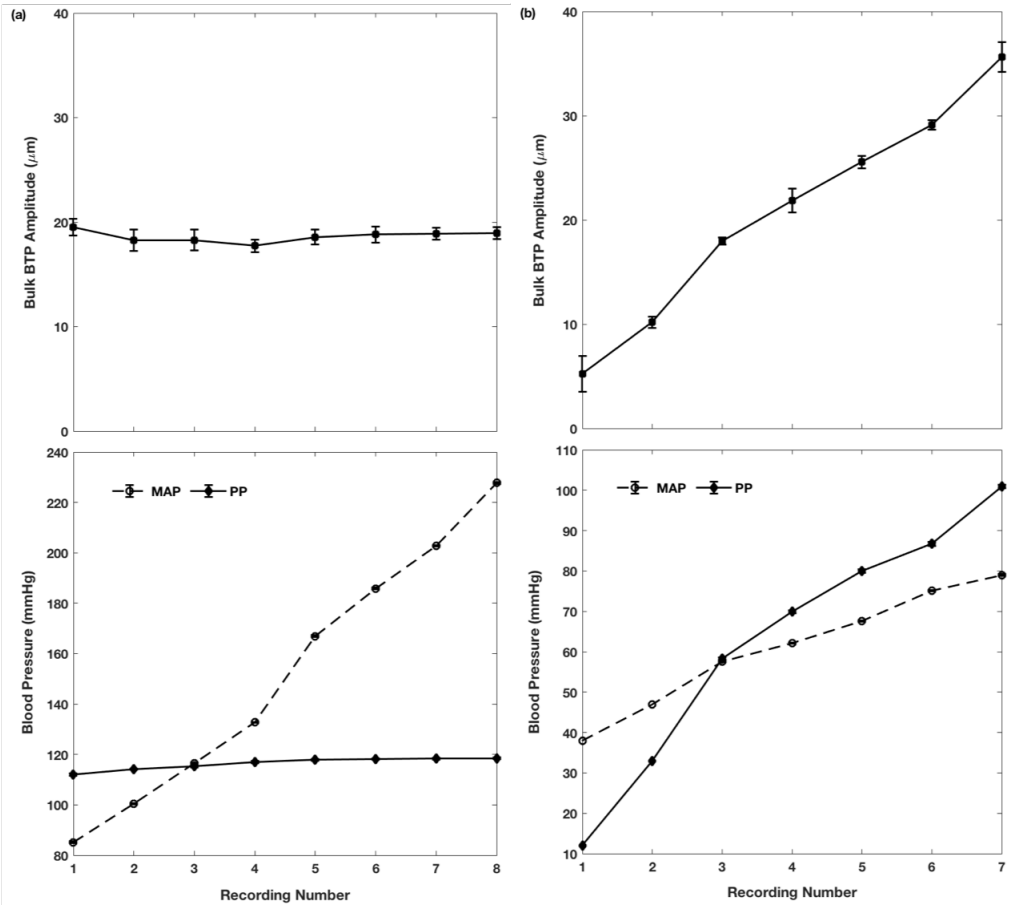

Figure 21: The relationship between BP and Bulk BTP Amplitude is shown, with Bulk BTP Amplitude displayed in the top graphs and BP displayed in the bottom graphs. (a) shows the results of the first experiment, exploring the impact of an increase in MAP. (b) shows the results of the second experiment, with PP increasing along with MAP and Bulk BTP Amplitude.

The relationship between Bulk BTP Amplitude and PP is shown in Figure 22. A linear equation describes the data, as displayed in Figure 22, with the gradient being 0.34, and the intercept being -0.41. This suggests that for an increase in PP of 1 mmHg, Bulk BTP Amplitude increases by 0.34 μm.

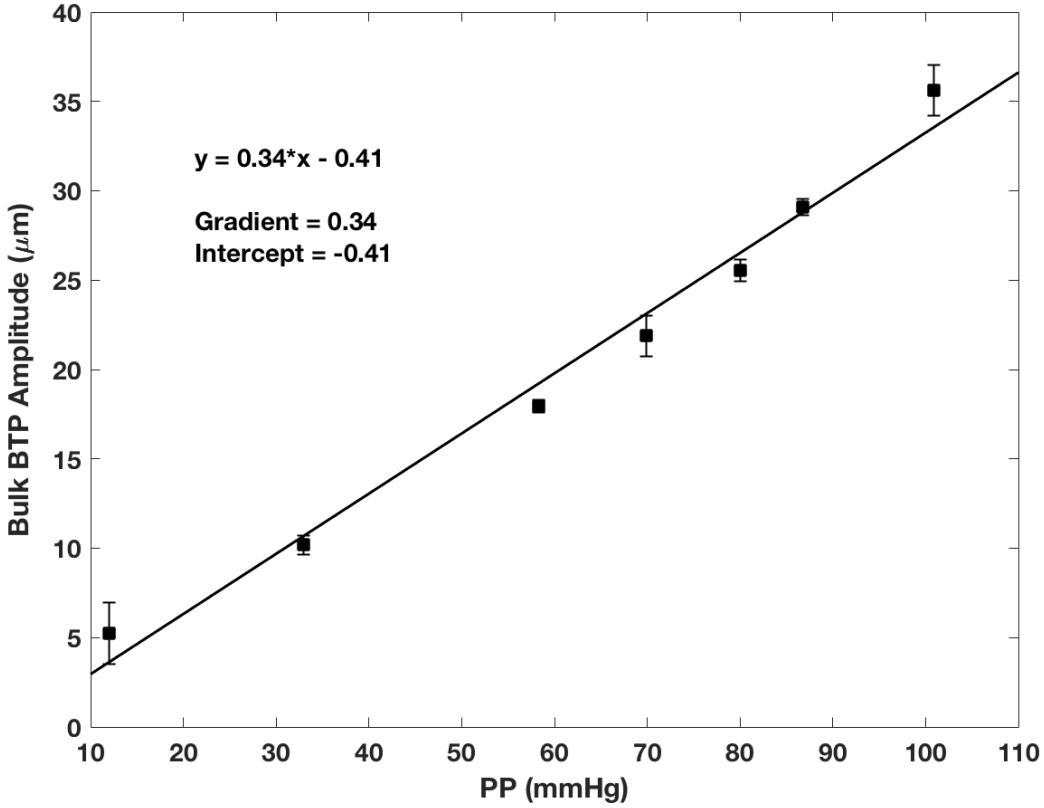

Figure 22: The relationship between Bulk BTP Amplitude and PP is linear and has a positive correlation. The equation of the fitted line is also displayed, quantifying the relationship between Bulk BTP Amplitude and PP.

Comparing Phantom and Healthy Volunteer BTPs

BTP waveforms from the phantom were visually compared with waveforms from healthy volunteers. It is clear in both instances that BTPs increase with depth into the brain. The general waveform shape described in chapter 3 is also exhibited by the healthy volunteers and the phantom, with a clear peak and trough with each cardiac cycle. Figure 23(a) shows the BTP waterfall plot from the phantom with a physiological PP value of 58.3 (0.3) mmHg. A participant with a comparable PP was selected to compare against the phantom results.

Figure 23(b) shows the BTP waterfall plot from a 29 year old male healthy volunteer, recruited to the study in section 4.2. The PP corresponding to this recording is 51.7 (4.1) mmHg. It can be seen that the waveform shapes and amplitudes in these waterfall plots appear somewhat similar, however, the BTP waveforms in the phantom appear to be reversed. This is due to the waveform output selected on the flow pump, however, this reversal can also be seen in some healthy participants, as discussed in chapter 3. The Bulk BTP Amplitudes from these 2 recordings are also similar, with the phantom Bulk BTP Amplitude being 18.0 (0.3) μm, and the healthy volunteer's Bulk BTP Amplitude being 18.1 (1.3) μm. Therefore, it is clear that while the phantom is heavily simplified compared to human physiology, the BTP results are comparable to that of healthy volunteers.

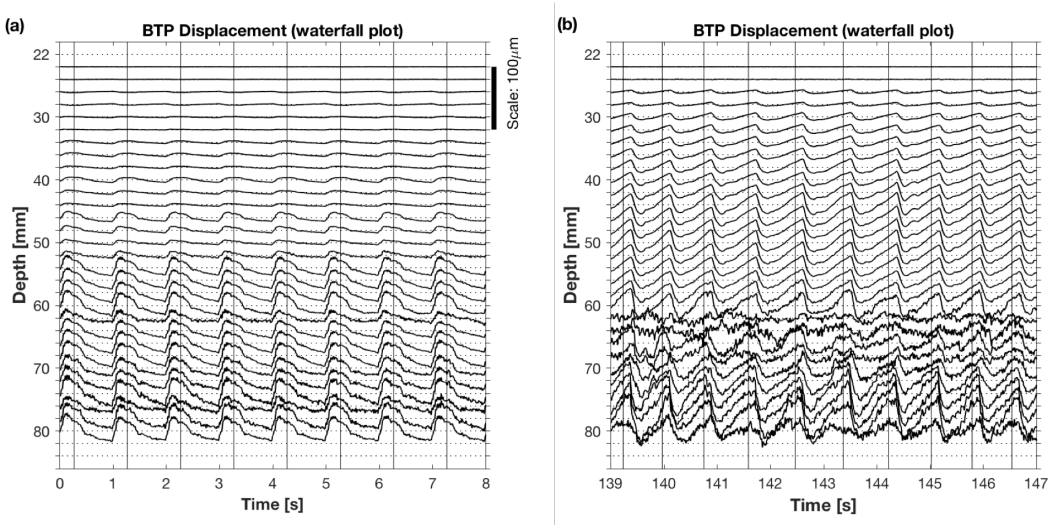

Figure 23: Waterfall plots for (a) the phantom operating with a physiological PP of 58.3 (0.3) mmHg, and (b) a 29 year old male healthy volunteer with a PP of 51.7 (4.1) mmHg. Both the general waveform shape and amplitude are similar between the phantom and healthy volunteer.

4.4 Discussion

The aims of the studies presented in this chapter were to further examine the relationship between BTPs and blood pressure. This was achieved firstly by inducing a change in blood pressure in 20 healthy volunteers through a leg raise manoeuvre. BP was successfully increased across the cohort, with an increase of 6.3 mmHg [95% CI: 3.5, 9.1, p = 0.0002] in PP and an increase of 4.1 mmHg [95% CI: 1.5, 6.7, p = 0.004] in MAP. This increase in BP was accompanied by an increase in Bulk BTP Amplitude of 3.0 μm (p = 0.004 using a paired t-test on log-transformed values). Although there has been very little research into the effect of BP on BTPs, the findings from this study support previous research by Biogeau *et al.* who found decreased BTP amplitude in patients with OH [19]. These results also support our previous findings from chapter 3, indicating that an increase in PP results in an increase in Bulk BTP Amplitude.

This study was the first to use the new Brain TV system to obtain physiological data. The system is portable, non-invasive, and has the potential to provide real-time data to the user. The current Brain TV system has improved on the prototype device used in previous studies due to the ability to obtain continuous recordings, rather than the previous limitation of 8 second recordings under blinded acquisition. The new system's ability to record synchronous measurements from a number of devices, facilitates the direct comparison between brain tissue motion and other physiological parameters. These improvements to the Brain TV system enabled analysis of transient changes in blood pressure.

Although it is clear that the leg raise manoeuvre did cause a significant increase in Bulk BTP Amplitude and BP, this was also accompanied by a significant increase in all other measured variables (HR and $EtCO_2$). Therefore, it is unclear from this study alone which factors are independent predictors of Bulk BTP Amplitude. Consequently, a phantom study was carried out to enable the investigation of the relationship between PP, MAP, and Bulk BTP Amplitude under a more controlled environment. Both MAP and PP could be altered in the phantom, MAP was increased by changing the height of the BMF reservoir, and therefore, changing the resistance in the tubing. PP was altered by changing the amplitude of the flow waveform using the pump.

The results from the phantom study show that MAP and PP were both successfully altered using the methods described. The first experiment resulted in large increases in MAP while PP remained constant at lower values, along with Bulk BTP Amplitude, suggesting that MAP alone had no impact on Bulk BTP Amplitude. The second experiment successfully resulted in an increase in PP, with an accompanying increase in MAP. It is clear from Figure 21(a) that Bulk BTP Amplitude seems to mirror the changes in PP, with both variables remaining at a relatively constant value in the first experiment with respect to the larger changes in MAP. This is also evident in Figure 21(b) where Bulk BTP Amplitude again seems to directly mirror changes in PP, with the significant increase in PP resulting in a significant increase in Bulk BTP Amplitude of 30.2 μm [95% CI: 28.3, 32.1, $p < 0.0001$]. This suggests that Bulk BTP Amplitude is greatly influenced by PP, with very little effect of MAP. These results agree with our previously developed linear regression model, presented in chapter 3, in which PP was found to be a significant factor in Bulk BTP Amplitude variability, whereas no significant changes were found with MAP.

Further investigation of the relationship between Bulk BTP Amplitude and PP in the phantom, shown in Figure 22, suggests that a 1 mmHg increase in PP results in an increase in Bulk BTP Amplitude of 0.34 μm. Results from the linear regression model presented in chapter 3 suggested that an increase in PP of 1% would result in a 0.8% increase in Bulk BTP Amplitude for the forehead position. Using the example described in chapter 3, an increase in PP from 40 mmHg to 50 mmHg is predicted to be associated with an increase in Bulk BTP Amplitude from 17.4 μm to 20.6 μm when measured through the forehead. This suggests that an increase in PP of 10 mmHg results in an increase of 3.2 μm, which can be directly compared to the results in this study, which similarly suggests that an increase in PP of 10 mmHg results in an increase in Bulk BTP Amplitude of 3.4 μm.

TCTD data was successfully obtained for all participants and for the phantom recordings. However, the visualisation depth for some recordings was limited, with deeper gates displaying atypical signals of much greater amplitude than expected from tissue motion, especially for human subjects. This meant that a number of gates were removed from analysis to ensure that only tissue motion

was quantified. Work is currently in place to determine the cause of decreased visualisation depth, including analysis of the ultrasound echo intensity for each recording, this will enable us to better understand the origins of erratic and high amplitude signals from the deeper gates.

For the healthy volunteer study the leg raise protocol was successful in significantly increasing BP in the majority of participants, and it was well tolerated by all. Due to the active movement of the participant during the manoeuvre, some motion artefacts were detected in the TCTD data, however, these were rare and easily excluded from our analysis. However, if the study were to be be repeated, it may be useful to induce changes in blood pressure through the use of a tilt table to raise the legs, therefore, reducing motion artefacts. Similarly, for the phantom study, the pump often generated large vibrations when set to higher amplitudes, which caused interference with the phantom. However, the effects of this were minimised by securing the phantom in place using clamp stands and ensuring that the pump was placed on a different surface to both the phantom and the Brain TV system. The ultrasound cable was also secured so that any vibrations would not cause the ultrasound probe to move. Interference from the equipment is easily identified and excluded as this results in high frequency vibrations in the BTP data.

Continuous blood pressure and expired CO_2 measurements were successfully recorded for all healthy volunteers using equipment that was well tolerated. For a number of participants the heart rate recordings exhibited some inaccurate readings, with numerous R waves being detected in a single cardiac cycle, visible on the ECG monitor. The equipment was investigated and it was found that the ECG leads were faulty and needed to be replaced. Therefore, for a small number of participants the HR data may not be accurate. The small sample size in this study means that removing these participants from the analysis would significantly reduce the power, therefore, the decision was made to keep these data, however, care was taken during the analysis to avoid including sections of the recording where these faulty readings had occurred.

Compared to the real brain, our phantom is heavily simplified and does not include a division of the brain into hemispheres, CSF, or ventricular spaces. The tissue mimic was also less soft than real brain and the ‘arteries’ are stiffer than

real arteries. Strengths of the phantom were that it approximated the dimensions of the human head and coupling of tissue pulsations with physiologically realistic major artery pulsatile blood flow. The flow of BMF was calculated to replicate blood flow within a human brain, with a pulsatile waveform chosen to represent the pulsatile flows generated by the heart. However, reproducing physiological blood pressure in the phantom proved to be difficult, with the systolic BP generally being higher than normal values, and the diastolic BP being lower than normal. When taking MAP and PP into account, some of the readings do represent physiological values, and the data can be extrapolated to determine BTP amplitudes at lower pressures. The apparent agreement between the phantom study and our previous research suggests that the phantom is able to reliably replicate this aspect of human physiology. BTP signals between a healthy volunteer and the phantom are compared in Figure 23 and were found to show similar amplitudes and waveform shape, suggesting that pulsations generated by the cerebral arteries are a significant factor in the origin of BTPs.

There are many other aspects of the data obtained in these study that could be analysed in future work. For the healthy volunteer study, TCTD data from both the forehead and temporal position were recorded, with only the forehead data being analysed in this chapter. Taking readings from the forehead is greatly preferred in a clinical environment due to ease of access, but analysis of temporal values may also be of interest. Our previous study, presented in chapter 3, investigated healthy brain tissue motion and involved the development of a linear regression model to determine which variables affected the tissue motion in the forehead and temporal positions independently. The regression model determined that physiological variables significantly affecting BTP in the forehead position also affected BTPs in the temporal position. Therefore, it was determined that any changes detected in the forehead position would be mirrored in the temporal position. However, this could be investigated more thoroughly using the temporal data obtained in this healthy volunteer study. Bulk BTP Amplitude was focused on in these studies, which is a representation of brain tissue averaged over all depths. However, many other features of the BTP signal are available for analysis which may provide further insight into the results of this study, such as waveform shape and timing.

4.5 Conclusions

The Brain TV system has provided an opportunity to further investigate the relationship between brain tissue pulsations and blood pressure, using continuous measurements of numerous physiological variables. The healthy volunteer study found that brain tissue motion, measured at the forehead position, increases during a leg raise manoeuvre, along with PP, MAP, HR, and $EtCO_2$. An increase in both PP and Bulk BTP Amplitude was evident in the majority of volunteers. It would be useful to repeat this study with a larger sample size to distinguish which variables have a significant effect on Bulk BTP Amplitude using a regression model. The phantom experiment allowed further analysis into this topic with the benefit of holding certain variables constant, and therefore, only taking blood pressure into account. It was found that Bulk BTP Amplitude appears to mirror changes in pulse pressure, with little effect of mean arterial pressure. The results of these studies agree with previous research into brain tissue motion.

5 Investigating the Impact of End-tidal CO_2 on Brain Tissue Pulsations

5.1 Introduction

Carbon dioxide (CO_2) levels play a vital role in cerebral autoregulation, as shown by Minhas *et al.* [36] - [38], yet the impact of CO_2 levels on brain tissue pulsations (BTPs) remains relatively unexplored. Cerebral autoregulation is a physiological mechanism, which maintains cerebral blood flow (CBF) by regulating numerous systems in the body, including the cardiovascular, respiratory, and nervous systems, Donnelly *et al.* 2016 [39]. CBF is predominantly maintained through vasoconstriction and vasodilation of particular blood vessels. Vasodilation is known to be associated with increased arterial pressure of CO_2 ($PaCO_2$), as shown by numerous studies using MRI to map cerebrovascular reactivity induced by CO_2 changes, Liu *et al.* [40]. A previous transcranial Doppler (TCD) ultrasound study investigating the relationship between $PaCO_2$ and cerebral blood flow velocity (CBFV) found a sigmoidal association between the two variables during hypercapnia [37]. As BTPs appear to rely primarily on CBF, it follows that physiological changes affecting cerebral haemodynamics are likely to also affect BTPs.

Kucewicz *et al.* [12] previously investigated the relationship between hypocapnia and BTPs in 4 healthy subjects. Both $EtCO_2$ and BTPs were found to significantly decrease during the 20 minute hyperventilation period, with a $\sim$ 20 mmHg drop in $EtCO_2$ resulting in BTP decreases ranging from 25% to 50%. We aim to investigate this relationship further, using a larger sample size to account for high variability between individuals.

This chapter gives details of a study carried out on 30 healthy volunteers, in which the Brain TV system is used to investigate the relationship of induced mild hypocapnia on Bulk BTP Amplitude. This will include an exploratory statistical analysis, and the development of a mixed effects linear regression model to determine which of the measured variables affect Bulk BTP Amplitude within this study. The results from the study will then be compared to results from previous research.

The data was collected by myself, M. Alharbi (University of Leicester, PhD student), and J. Ince (University of Leicester, MSc student). I conducted all data analysis presented in this chapter, and the results from the exploratory statistical analysis have been published as an article, on which I am listed as joint second author, Alharbi *et al.* [41].

5.2 Methods

5.2.1 Subjects

After advertising via email and word of mouth, healthy adults were recruited from university staff, students, and their relatives, in line with a protocol approved by the University of Leicester Medicine and Biological Sciences Ethics Committee. Participants with a history of cardiovascular, respiratory, or neurological illness were not recruited to the study. All participants provided written informed consent. The participant information sheet and ethics approval letter can be found in Appendix B.

5.2.2 Experimental Protocol

BTP, CO_2, BP, and HR measurements were taken using the Brain TV system described in chapter 2. Simultaneous TCTD measurements were obtained from two positions on the forehead, 1 cm above each eyebrow. The experimental protocol was developed based on a previous study exploring cerebral haemodynamic responses to CO_2 levels, using TCD measurement of CBF [37]. Participants were positioned lying supine on a couch with their legs horizontal and their heads and torso angled at 30°, and were asked to remain at rest with their eyes closed throughout the protocol to avoid the generation of motion artefacts. A 1 minute baseline recording was taken, in which the participant was asked to breathe at their normal rate. During this time, the participant's normal respiratory rate was determined and a metronome was set to increase the participants breathing rate by 5 breaths per minute. Participants were asked to breathe in time with the metronome for 90 seconds, resulting in hyperventilation, aiming to reduce $EtCO_2$ levels by 5 mmHg. This hyperventilation recording was followed by a 2 minute recovery period, in which the participants were asked to relax and return to their normal breathing rate.

5.2.3 Data Analysis

BTP signals were processed as described in chapter 2, and the signals were then displayed in MATLAB with the R-R intervals overlaid to enable the user to remove any cardiac cycles including artefacts. Further analysis was based on these artefact free data.

Recordings were inspected to investigate the quality of the data, and it was observed that the majority of recordings displayed good quality signals for the first 20 gates on both right and left sides, corresponding to depths within the brain ranging from 22 to 60 mm. As signal quality weakened beyond this depth, only data from the first 20 gates were analysed. Some additional gates (1 to 3 of the deepest gates) were removed during analysis of recordings from 5 out of 30 participants, this was due to penetration of the ultrasound being limited in specific participants.

For each recording, a Bulk BTP signal was calculated by averaging signals across all available depths, as described in previous chapters. From this signal, beat-to-beat Bulk BTP Amplitude was estimated as the absolute difference between the peak and trough of the Bulk BTP signal for each cardiac cycle. This gives a value for collective brain tissue motion and how it changes over time. Beat-to-beat estimates of pulse pressure (PP), mean arterial pressure (MAP), heart rate (HR), and $EtCO_2$ were also calculated using the remaining physiological measurements.

5.2.4 Statistical Analysis

For each phase of the protocol, 30 second intervals were selected to be used in statistical analysis. These intervals were chosen to be as close to the end of each phase as possible, while also avoiding sections including a large number of artefacts. Statistical analysis was carried out using Stata, version 15.1 (StataCorp, USA). For each 30 second interval, the corresponding beat-to-beat values for each variable were visually assessed to identify any non-normal distributions. Beat-to-beat values for all variables were averaged and a standard deviation was calculated for each. This results in a mean value for each variable at each stage of the protocol (baseline, hyperventilation, recovery).

Bulk BTP Amplitude for both the left and right hemispheres was non-normally distributed across the population of volunteers, being skewed towards lower values, and are therefore summarised by a median value and IQR. All other variables (PP, MAP, HR, and $EtCO_2$) were normally distributed, and are summarised by a mean and SD for each. Time series for the duration of the protocol for one participant are shown in Figure 24, with the 30 second intervals used in further analysis indicated on the x-axis.

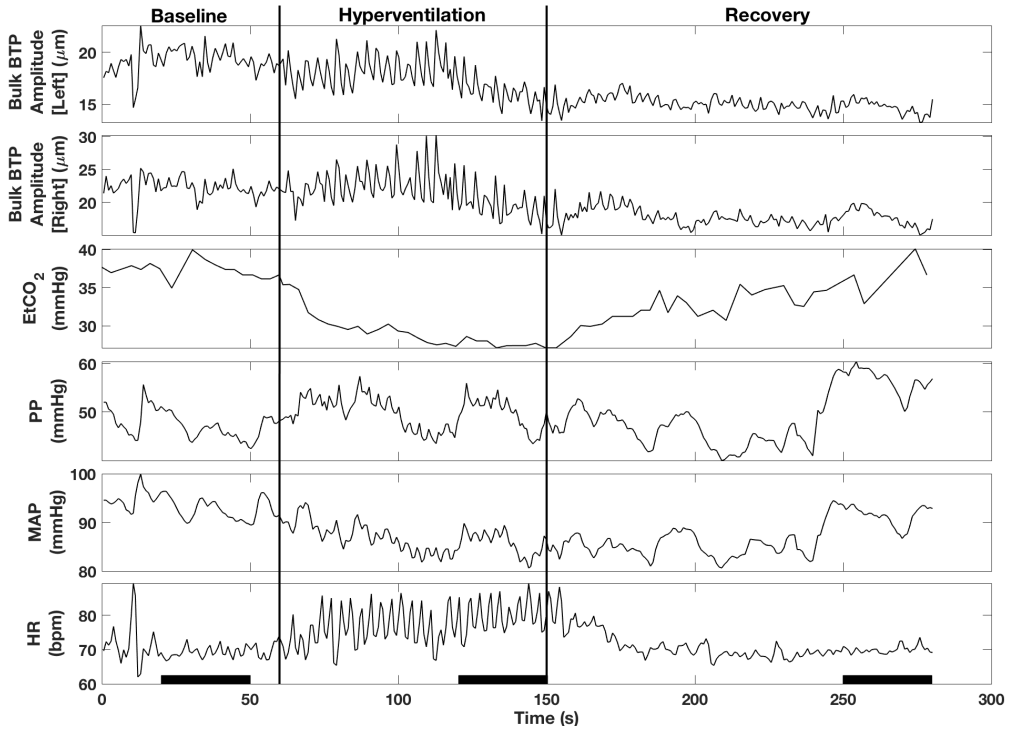

Figure 24: Time series for each variable are shown for the length of the protocol for one volunteer (a 26 year old male). During the hyperventilation period, a decrease in $EtCO_2$ can be observed, along with an increase in HR. Changes in PP and MAP appear to mirror each other, and Bulk BTP Amplitude shows similar trends for both hemispheres. It appears that HR and Bulk BTP Amplitude experience similar oscillations throughout the hyperventilation period, which may suggest a relationship between Bulk BTP Amplitude and cardiac cycle length. The variability in Bulk BTP Amplitude appears to increase during the hyperventilation phase, before decreasing in the recovery phase. The 30 second time intervals used in statistical analysis for this recording are indicated by the black bars on the x-axis. All 30 second intervals were chosen to be close to the end of each phase, while also avoiding the inclusion of artefacts.

Paired t-tests were used to compare values for each variable between baseline and hyperventilation, and between hyperventilation and recovery. As Bulk BTP Amplitude was found to be non-normally distributed for both hemispheres, a paired t-test was used to compare the log-transformed Bulk BTP Amplitude values for baseline and hyperventilation, and for hyperventilation and recovery. However, the median and IQR of Bulk BTP Amplitude in micrometres is reported in the results, along with the difference in micrometres between phases, to aid understanding.

A two-level mixed effects linear regression model was then used to determine which variables account for any changes in log(Bulk BTP Amplitude). A mixed effects model was used rather than a typical linear regression model to account for any intraclass correlation that may be present, due to each participant having a total of 3 measurements (one for each phase). Therefore, participant ID was selected as the level 2 variable, and PP, MAP, HR, $EtCO_2$, Age, and Sex were level 1 variables, see Figure 25.

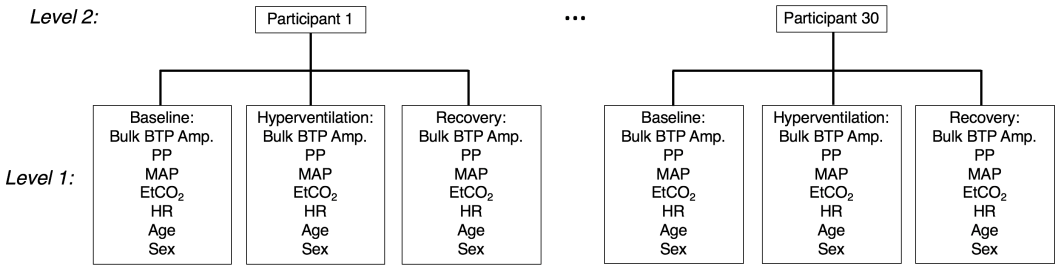

Figure 25: The structure of the data for the linear mixed effects model comprises two levels. The level 2 variable is participant ID, corresponding to the healthy volunteers (n = 30). The level 1 variables comprise the measured variables, with one for each phase in the protocol.

Initially, a univariable analysis was carried out to determine which variables should be investigated further, with any variables not showing a significant effect at a level of $p < 0.1$ being removed from further analysis. Using the method previously described in chapter 3 for model formation, introduced by Peixoto [26], all possible formations were tested. The best fitting model was determined by assessing the p-value of the entire model (and the p-values of individual variables within the model), the Akaike Information Criterion (AIC) and Bayesian Information Criterion (BIC), and by comparing different models

using a likelihood ratio test to determine whether the addition of a particular variable results in a significantly improved model.

5.3 Results

Thirty healthy volunteers (12 male, 18 female), with ages ranging from 19 to 46 years, took part in this study. Ages were skewed towards younger participants, with a median age of 25 years [IQR: 24, 30].

5.3.1 Effects of Hypocapnia on All Measured Variables

The protocol successfully decreased $EtCO_2$ by 4.7 mmHg [95% CI: 3.6, 5.8, $p < 0.0001$], from a baseline $EtCO_2$ value of 37.3 (2.6) mmHg. This was followed by an increase of 3.1 mmHg [95% CI: 2.2, 4.1, $p < 0.0001$] during the recovery period, as shown in Table 4 and Figures 26 and 27.

During the hyperventilation period, median Bulk BTP Amplitude increased slightly by $< 2\mu$m, from baseline values of $\sim$13 μm in both hemispheres. This was followed by a statistically significant decrease in Bulk BTP Amplitude of 4.3 μm ($p = 0.0004$, using a paired t-test on log-transformed values) in the right hemisphere, and a smaller decrease of 1.3 μm ($p = 0.01$, using a paired t-test on log-transformed values) in the left hemisphere. Due to the repeated significance testing, an adjusted p-value was calculated using the Bonferroni correction, giving an adjusted significance level of 0.004, suggesting that only the decrease in Bulk BTP Amplitude in the right hemisphere is statistically significant.

Hyperventilation resulted in reproducible physiological changes for all remaining variables, see Table 4. PP increased by 4.8 mmHg [95% CI: 0.7, 8.9, $p = 0.02$], and returned almost completely to baseline during the recovery period. MAP decreased significantly by 3.0 mmHg [95% CI: 1.3, 4.7, $p = 0.001$], and also returned to baseline almost completely. HR increased significantly by 4.3 bpm [95% CI: 1.7, 6.9, $p = 0.002$], and was overcompensated by a 5.7 bpm [95% CI: 3.1, 8.3, $p < 0.0001$] decrease during the recovery phase.

Variable	Baseline	Hyperventilation	Recovery
$EtCO_2$ (mmHg)	37.3 (2.6)	32.7 (3.9)	35.8 (3.9)
Left Bulk BTP Amp. (μm)	12.7 (8.0, 19.4)	13.7 (8.4, 17.3)	12.4 (8.7, 15.9)
Right Bulk BTP Amp. (μm)	12.9 (8.6, 20.1)	14.5 (8.5, 19.5)	10.2 (6.6, 18.2)
PP (mmHg)	45.8 (10.3)	50.6 (11.7)	46.8 (8.0)
MAP (mmHg)	89.3 (8.6)	86.4 (9.1)	89.2 (8.4)
HR (bpm)	75.0 (12.3)	79.2 (14.3)	73.6 (12.0)

Table 4: The 90 second hyperventilation period successfully reduced $EtCO_2$ by 4.7 mmHg and generated significant changes in PP, MAP and HR. A significant drop in Bulk BTP Amplitude was observed for both the left and right hemispheres during the recovery phase. The IQR is given in brackets for the median values and the standard deviation is given in brackets for the mean values.

When comparing baseline to recovery values, no statistically significant differences were observed in PP, MAP, or HR, suggesting that this hyperventilation protocol induces transient and reversible physiological changes. However, $EtCO_2$ values remained decreased by 1.5 mmHg [95% CI: 0.5, 2.6, $p = 0.007$] during the recovery phase compared to baseline values. Bulk BTP Amplitude in the right hemisphere was also found to be lower during the recovery period compared to the baseline ($p = 0.007$ using a paired t-test on log-transformed values). However, these decreases were not significant at an adjusted level of $p = 0.004$.

It was observed that 4 participants did not experience a change in $EtCO_2$, therefore, a sensitivity analysis was carried out by removing data from these participants. This did not induce a significant effect on the results. Changes calculated across the whole population of volunteers for each phase of the protocol can be seen in Figure 26. All measured variable responses during each phase of the protocol for each individual can be seen in Figure 27.

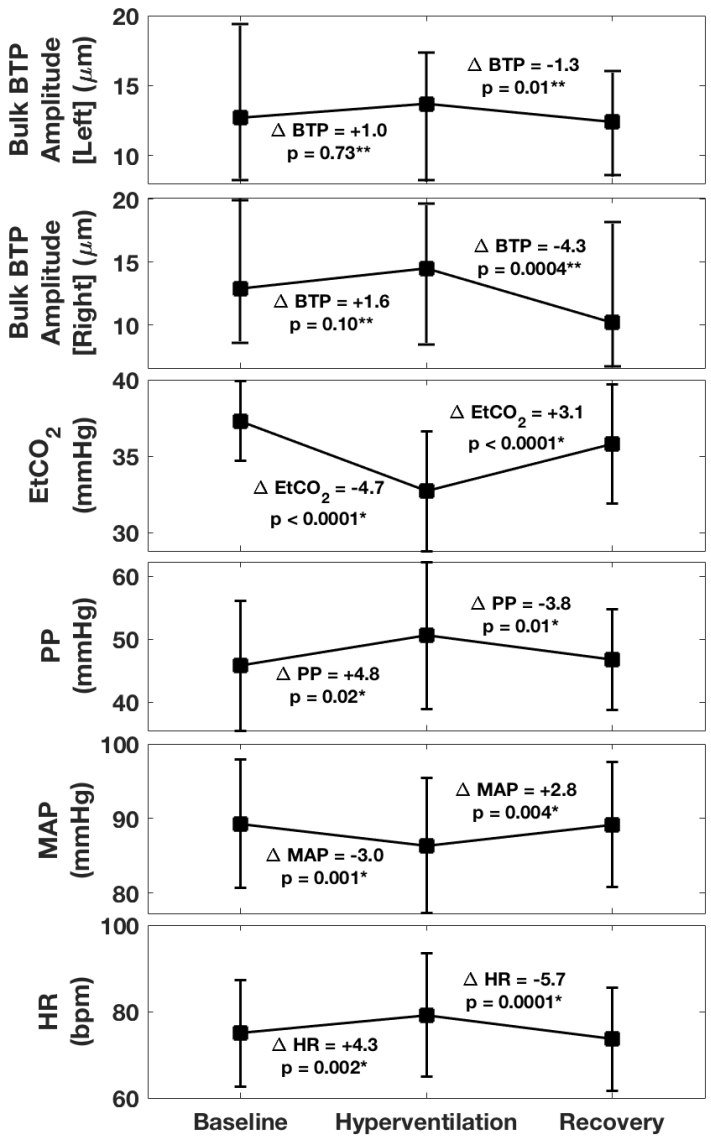

Figure 26: Changes between the baseline, hyperventilation, and recovery phases averaged across all participants. The median and IQR are shown for the Bulk BTP Amplitude values, while the mean and SD are shown for all remaining variables. Estimated differences between baseline and hyperventilation, and between hyperventilation and recovery, are labelled in the figure. Paired t-tests were carried out on normally distributed data* and log-transformed data** to determine whether changes between phases were statistically significant at a significance level of p = 0.004 (adjusted using the Bonferroni correction).

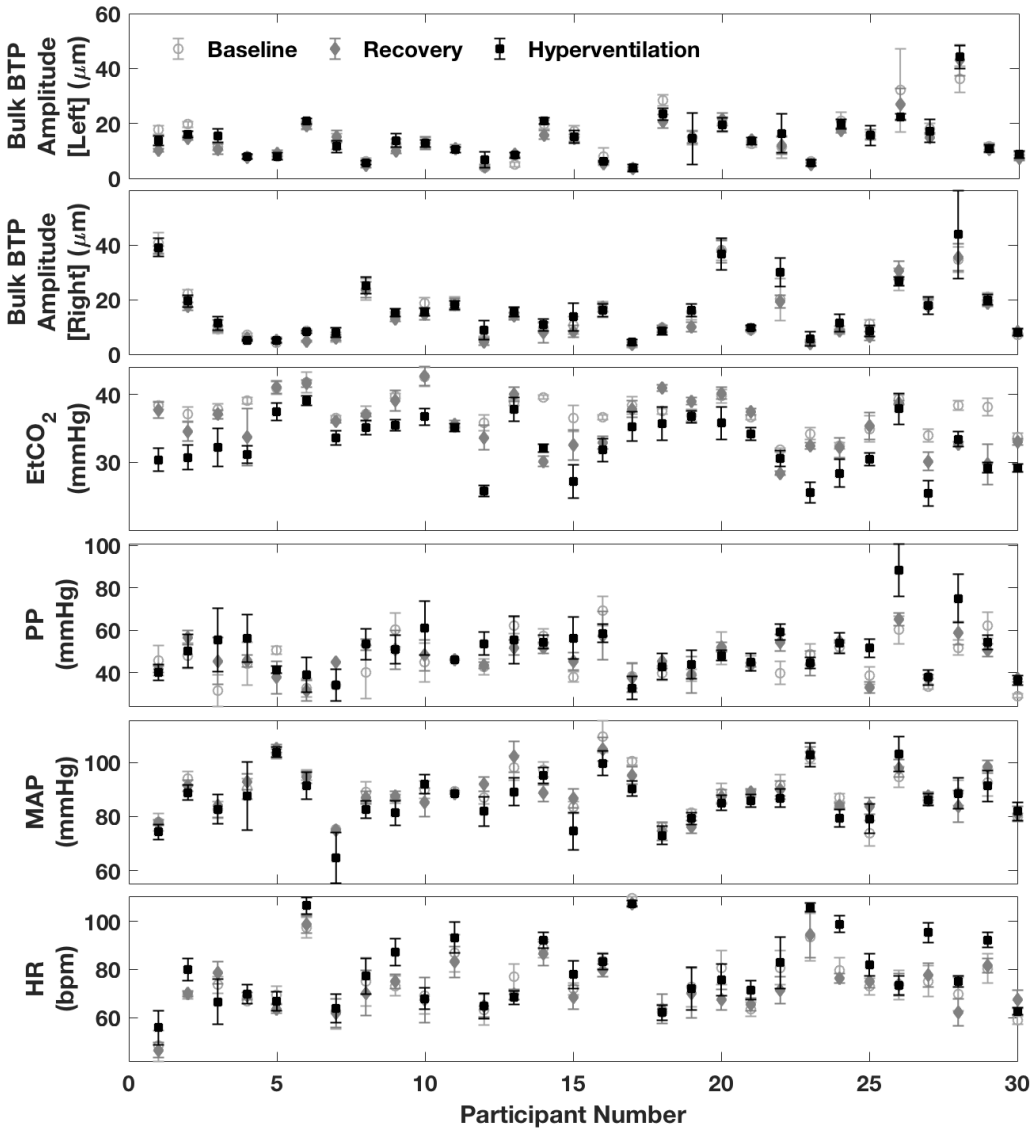

Figure 27: Changes in each variable between the baseline, hyperventilation, and recovery phases are shown for each participant. All graphs show the mean beat-to-beat value calculated over a 30 second interval, with the standard deviation (SD) indicated by error bars.

5.3.2 Mixed Effects Linear Regression Model

A mixed effects linear model differs from a typical linear regression model as there is an additional term to account for adjustments between different groups. Clustering of the data was investigated by calculating the intraclass correlation coefficient (ICC) for numerous groups. Grouping the data depending on the phase of the protocol (baseline, hyperventilation, recovery) showed no intraclass correlation, suggesting that a mixed effects model would not be needed. However, the ICC for repeated measurements within subjects was calculated to be high (ICC = 0.96), supporting the use of a mixed effects model with participant ID as the level-two variable. The structure of the model is shown in equation (2), where β_0 is the value of the intercept, and all additional β values correspond to the gradient of the regression line relating to the included explanatory variables. α_i is the additional term that accounts for differences between individuals (with i denoting the level 2 variables), and has a calculated variance σ_α^2. While ϵ_{ij} accounts for level 1 errors (with j denoting the level 1 variables), and has an associated variance of σ_ϵ^2. As the relationship between the explanatory variables and Bulk BTP Amplitude were sufficiently represented using a linear regression model in chapter 3, the same method was used, with slight adaptations to account for the repeated measurements for individuals in this study. This mixed effects model equation is a well-validated method for describing variables using non-independent measurements.

$$log(BulkBTPAmp.) = \beta_0 + \beta_1 x_1 + \beta_2 x_2 + ... + \alpha_i + \epsilon_{ij} \tag{2}$$

Bulk BTP Amplitude values suggested that the right hemisphere experienced a slightly stronger impact from the breathing manoeuvre, however, no significant differences between the left and right hemispheres were observed for any stage of the protocol. Therefore, these values were averaged to give one Bulk BTP Amplitude value as the dependent variable within the model. As the model assumes that all variables follow a normal distribution, Bulk BTP Amplitude was log-transformed prior to inclusion. A univariable analysis was carried out to determine which variables appear to have a significant effect on log(Bulk BTP Amplitude). It was found that PP (continuous, mmHg), MAP (continuous, mmHg), Age (continuous, years), and Phase (categorical, 0 = baseline, 1 = hyperventilation, 2 = recovery) each had a significant effect

when considered individually. Results from the univariable analysis are shown in Table 5.

Variable	**Coefficient** [95% CI]	**p-value**
$EtCO_2$ (mmHg)	-0.006 [-0.015, 0.003]	0.174
Age (years)	-0.027 [-0.052, -0.001]	0.042
Sex (M=1/F=0)	0.216 [-0.147, 0.579]	0.244
PP (mmHg)	0.004 [0.000, 0.008]	0.043
MAP (mmHg)	-0.009 [-0.017, -0.002]	0.013
HR (bpm)	0.002 [-0.003, 0.007]	0.496
Phase (H=1)	0.032 [-0.018, 0.083]	0.208
Phase (R=2)	-0.074 [-0.125, -0.024]	0.004

Table 5: Univariable analysis was carried out to determine how each measured variable impacts Bulk BTP Amplitude individually. Age, PP, MAP, and the Recovery Phase were found to have a significant effect on Bulk BTP Amplitude, and were therefore investigated further. All variables that did not appear to be significant at a significance level of $p = 0.1$ were removed from the analysis ($EtCO_2$, Sex, and HR).

All possible hierarchically valid models formed using the remaining variables were tested to determine which model had the best fit. This included terms up to an order of 2, for example, PP^2 and PP×Age. The models with the lowest AIC and BIC were tested using a likelihood ratio test to determine whether the addition of a particular variable resulted in a significantly improved model. From this it was apparent that the best fit model included variables PP, MAP, Age, Phase, and PP×Age. However, after investigating the correlations between the explanatory variables, it was clear that structural multicollinearity was present within the model due to the PP×Age term. All explanatory variables were standardised and the model was tested again, resulting in reduced multicollinearity, but also a significant increase in AIC and BIC values, suggesting that the model could be improved. The final model included the explanatory variables Age and Phase, and no multicollinearity was present. The AIC and BIC of the final model were calculated to be - 20.9 and - 5.9 respectively.

After determining the explanatory variables that should be included in the model, the inclusion of random slopes was investigated. This determines

whether the regression lines sufficiently fit the data for each group if they all have the same gradient. A model with random slopes for each participant was implemented and compared to the original random intercept model, using a likelihood ratio test. It was determined that random slopes did not significantly improve the model and therefore, they were not included. Therefore, the final model is structured as previously shown in equation (2), with a β coefficient for each of the 3 explanatory variables, and with β_0 as the constant intercept coefficient. The values for the coefficients in the final model are shown in Table 6, along with the 95% confidence intervals on the coefficients, and the variance of the random effects terms.

Variable	β **Coefficient [95% CI]**	**p-value**
Constant	3.309 [2.577, 4.040]	0.000
Phase (H=1)	0.032 [-0.018, 0.083]	0.208
Phase (R=2)	-0.074 [-0.125, -0.024]	0.004
Age	-0.027 [-0.052, -0.001]	0.042
Variance type	**Estimate [95% CI]**	
Level 2 (α_i)	0.224 [0.134, 0.374]	
Level 1 (ϵ_{ij})	0.010 [0.007, 0.014]	

Table 6: The model that was found to best fit the data included the variables Phase and Age. The β coefficients, along with the 95% confidence intervals and p-values are given for each included explanatory variable. The variance of the random effects on the model is given in the bottom section of the table. This model was found to give the lowest overall p-value, along with the lowest AIC and BIC values (-20.9 and -5.9 respectively).

The β coefficients displayed in Table 6 can be used to determine the change in Bulk BTP Amplitude associated with a unit change in each explanatory variable. This is done by reverse transforming the coefficients, for instance a 1 unit increase in x_1 is calculated as $e^{x_1\beta_1}$, whereas a 10 unit increase in x_1 is calculated as $e^{10x_1\beta_1}$. An increase of 1 year in Age results in a 2.7% decrease in Bulk BTP Amplitude, and an increase of 10 years results in a decrease of 31%. As determined in the initial analysis, there is a slight increase in Bulk BTP Amplitude from baseline to hyperventilation, followed by a significant decrease in the recovery phase, this is also shown in the model, with a slight increase of 3.3% in Bulk BTP Amplitude from baseline to hyperventilation, and a significant decrease of 16% during the recovery phase.

5.4 Discussion

In this study, it was found that a protocol consisting of 90 seconds of mild hyperventilation resulted in a changes in all recorded physiological measurements. During hyperventilation an increase in HR and PP was observed, along with a decrease in MAP. It was found that these changes were reversible, and values returned to their initial baseline within the recovery period, however, $EtCO_2$ took a longer time to return to baseline, and was still slightly decreased during the recovery phase when compared to baseline values, however, this was not significant at the adjusted level of $p = 0.004$. A slight increase in Bulk BTP Amplitude was observed during hyperventilation for both hemispheres, followed by a significant decrease in Bulk BTP Amplitude in the recovery phase in the right hemisphere. However, all changes observed in Bulk BTP Amplitude in this study were small, and in the order of magnitude that is similar to normal beat-to-beat variability within subjects ($\sim$1 - 4μm).

A reduction in BTP amplitude is expected during hypocapnia, as it causes vasoconstriction, reducing blood flow to the brain, and resulting in reduced expansion of brain tissue. Previously, Kucewicz *et al.* [12] observed a decrease in BTP amplitude ranging from 25 to 50% after reducing $EtCO_2$ from $\sim$ 40 mmHg to $\sim$ 20 mmHg, through a 20 minute period of hyperventilation. These results were based on TPI measurements from 4 healthy subjects, we aimed to further investigate the effect of hypocapnia on BTPs by studying a larger sample size of 30 participants. From our larger dataset, we observed an increase in Bulk BTP Amplitude during hyperventilation, followed by a decrease in the recovery phase. To compare our results to the previous study, the percentage change in Bulk BTP Amplitude was calculated for each volunteer and ranged from +71% to -31% from baseline to hyperventilation, and +77% to -42% from baseline to recovery. However, our study aimed to achieve a much smaller hypocapnic change (-5 mmHg) for a much shorter period of time (90 seconds). Therefore, it would be of interest to induce a more extreme change in $EtCO_2$ levels over a longer period of time to allow for direct comparison with previous work by Kucewicz *et al.* [12].

Our study on a larger sample size suggests that baseline values for Bulk BTP Amplitude vary greatly between volunteers, along with physiological responses

to the hyperventilation protocol. Although this study has a greater sample size than previous work, we are limited by the fact that ages of the participants are skewed towards lower values, with a median age of just 25 years. It has been documented that cerebral autoregulation varies with age [42], therefore, including a wider range of ages would be beneficial. It should also be noted that the Brain TV system is being developed as a diagnostic tool for brain injury, such as stroke, which is more commonly seen in elderly patients. Therefore, it would be beneficial to understand the impact that hypocapnia has on BTPs in the elderly population.

This study measured a number of additional physiological variables that have not previously been investigated when looking into the effect of hypocapnia on BTPs. However, it would be beneficial to also measure CBF using conventional transcranial Doppler ultrasound to further understand the relationship between cerebral haemodynamic changes and autoregulation. Measuring CBF simultaneously would also allow us to determine whether neurovascular coupling could be the reason for the slight increase in Bulk BTP Amplitude that was observed during the hyperventilation phase. If neurovascular coupling is a factor in the study, it would be beneficial to increase the time of the hyperventilation period to overcome this increase in CBF that may be apparent towards the start of the breathing task. A longer hyperventilation period would also account for any time lag that may be present between the drop in $EtCO_2$ and the reduction in Bulk BTP Amplitude.

Our results suggest that levels of mild hypocapnia often seen in clinical practice are unlikely to have a strong impact on Bulk BTP Amplitude. However, further work needs to be carried out to better understand how the severity and duration of hypocapnia affects BTPs. We were also unable to alter $EtCO_2$ without simultaneously altering other physiological variables, such as PP, MAP, and HR.

To further investigate the impact that specific variables had on Bulk BTP Amplitude a linear mixed effects model was developed. Univariable analysis suggested that Age, Phase, PP, and MAP had an association with Bulk BTP Amplitude, whereas $EtCO_2$, HR and Sex showed no significant impact. The final model included Phase and Age as explanatory variables, with the inclu-

sion of Age being consistent with the previous model developed in chapter 3, however, unlike the model in chapter 3, PP was not found to be significant when Phase was introduced into the model. Therefore, it is suggested that the changes seen in Bulk BTP Amplitude are due to other physiological mechanisms, rather than changes in CO_2 levels.

The previous linear regression model in chapter 3 suggested that an increase in PP causes an increase in Bulk BTP Amplitude. PP only exhibited a slight increase during the hyperventilation phase in this study, which may explain why only a slight increase in Bulk BTP Amplitude was observed during this time. However, the significant decrease in Bulk BTP Amplitude during the recovery phase cannot be explained by the insignificant decrease in PP, suggesting there may be other variables affecting Bulk BTP Amplitude that are currently unaccounted for in the study. The relationship between PP and hypocapnia has not been directly explored in previous research, however, a study investigating orthostatic intolerance during hyperventilation also suggests an increase in PP during hypocapnia [43]. The relationship between PP and hypocapnia should be investigated further to aid interpretation of results.

MAP was found to decrease during hyperventilation, which has been established in previous studies [37], [38], [44]. The univariable analysis for the linear mixed effects model developed in this study suggests that Bulk BTP Amplitude increases with decreasing MAP, further suggesting that an increase in Bulk BTP Amplitude should be observed during hyperventilation. However, the addition of the Phase terms in the model causes the inclusion of MAP and PP to be insignificant. This also suggests that there may be additional factors causing a decrease in Bulk BTP Amplitude during the recovery phase. From these results, it is clear that the relationship between hypocapnia and BTPs needs to be explored more thoroughly.

5.5 Conclusions

This study has aided investigation into the impact of factors that may affect Bulk BTP Amplitude that are often experienced by patients in a clinical environment, such as changes in $EtCO_2$ and PP [45]. Determining the effects that these variables have on BTPs is of clinical importance, to understand how BTPs may be affected in a clinical setting. The Brain TV system is being developed to aid diagnosis of brain injury, such as stroke, and it has been previously found that patients with acute stroke often demonstrate mild hypocapnia [46], therefore, it is important to understand how hypocapnia impacts measured BTPs. The results from our study suggest that such mild hypocapnic changes would not be responsible for major changes in BTPs. Therefore, it can be suggested that any observed changes in Bulk BTP Amplitude are due to other cerebral haemodynamic factors, or disruption to the tissue structure (as seen with haemorrhages).

6 Implementing a Systemic State-space Model to Investigate the Relationship Between Blood Pressure and Brain Tissue Pulsations

6.1 Introduction

Results from the previous studies presented in this thesis have suggested that the physiological variable which has the greatest effect on BTP amplitude is pulse pressure (PP). However, in many of these studies we are unable to isolate the effect of PP. The studies involving human subjects often induce significant changes in numerous physiological variables, including BTP amplitude and PP, making it difficult to distinguish which variables are of interest. While the previous phantom study was able to control the variables, there were limitations regarding the simplicity of the phantom model, with only the flow through the major cerebral arteries being accounted for. To gain further understanding on the impact of PP on BTPs, a theoretical approach was taken, in the form of a mathematical model. Implementing a mathematical model of intracranial pressure dynamics enables us to directly alter pressures and determine the effect that this has on brain volume (a surrogate for BTPs).

There has been extensive research into simulating intracranial (IC) dynamics, with the first computational simulation of IC dynamics introduced in 1973 by Marmarou [47]. This model focused on the dynamics of cerebrospinal fluid (CSF), and it was not until 1987 that cerebral blood flow was introduced into computational models of IC dynamics, Hoffman [48]. A well-validated model by Ursino [49] includes detailed cerebral autoregulation mechanisms, and has been adapted in many subsequent models. Wakeland *et al.* carried out a review of computational models of intracranial pressure (ICP) dynamics, discussing 59 articles from 1973 to 2007 [50].

Understanding ICP dynamics poses many beneficial clinical outcomes, with the majority of research aiming to develop a non-invasive method of estimating ICP, Zhang *et al.* [51]. However, despite the considerable amount of research covering this topic within the last 5 decades, a model that can be used with ease within a clinical environment is yet to be established. This can often be

due to a variety of factors, including the complexity of the models, and the need to calibrate some models to each patient.

The majority of previous research into modelling IC dynamics assumes that the intracranial region is of constant volume and strictly enclosed within the rigid skull (the Kellie-Monroe doctrine), for example in the model by Ursino *et al.* [52]. However, this assumption makes it difficult to incorporate important processes affecting pressure dynamics outside of the intracranial vault, such as venting of CSF through the spinal cord. One particular paper develops a whole-body mathematical model which revokes the Kellie-Monroe doctrine, Lakin *et al.* [53]. This chapter will describe the dynamics of the model proposed by Lakin *et al.*, give details of the technique used to implement this as a state-space model in Simulink (The Mathworks, Inc., USA), and simulate an increase in pulse pressure. The results showing the relationship between pulse pressure and brain volume will then be presented. The preliminary coding for a simplified version of the Simulink model was carried out by Noemie Barillot during her 3 month internship at University of Leicester [54].

6.2 Compartmental Model

The model presented in Lakin *et al.* [53] divides the body into sixteen compartments, with the surrounding atmosphere treated as an additional compartment, Figure 28. Eleven compartments are vascular, two represent tissue matter (G and B), a further two contain CSF (F and T), and one is a composite compartment comprising the pulmonary circulation, organs, tissue matter and interstitial fluid (Y). Each compartment has a spatially averaged pressure assigned to it, listed in [53], and compartmental pressures are determined by their constituents (either blood, interstitial fluid, or CSF). The 17th compartment (representing the atmosphere) is constant at a reference pressure of 0 mmHg, with all other compartmental pressures being relative to this value.

The flow of either blood, interstitial fluid, or CSF between adjacent compartments is given by the equation:

$$Q_{ij} = Z_{ij}(P_i - P_j) \tag{3}$$

where Q_{ij} is the flow from compartment i into compartment j, P_i and P_j are

the spatially-averaged pressures of compartments i and j respectively, and Z_{ij} is the fluidity of the flow (which is the inverse of resistance). Out of the 29 flows in the model, 7 values are well-known and taken from literature [55] - [60]. The remaining flows can be estimated using these values. Pressures relating to each compartment are given by Lakin *et al.* [53], and are shown in Table 7. From these average pressure values and the estimated values for flow, the fluidities associated with each flow can be calculated using equation (3).

These flows represent either direct flows between adjacent compartments, such as the flow from arteries to capillaries, or the transfer of fluid between vasculature and tissue via filtration. When adjacent compartments experience a change in pressure difference, this induces a deformation of the membrane between these compartments, given by:

$$\frac{dV_{ij}}{dt} = C_{ij}\frac{dP_{ij}}{dt} \tag{4}$$

where V_{ij} is the difference in volume between two compartments i and j, and C_{ij} is the compliance between these two compartments. Extracranial compliances are constant and are calculated by multiplying the distensibility by the compartment volume, values for both distensibility and volume are well-known and can be found in the literature [55], [60] - [63]. Values of intracranial compliance are estimated by relating values for compliance given by Stevens *et al.* [64], to the current model. The compliances calculated in [64] are part of a simple model with only 4 intracranial compartments, therefore, specific percentages of these compliances are distributed between the intracranial compartments in the model presented in this chapter.

The rate of change in volume of a single compartment takes into account all flows that pass through the compartment, and is governed by the following equation:

$$\frac{dV_i}{dt} = Q_{in} - Q_{out} \tag{5}$$

Figure 28 shows a diagram produced by Lakin *et al.* [53]. It illustrates all 17 compartments in the whole-body model, and how flow moves throughout the

body. The flow to and from each compartment is depicted by the arrows, each of which have a related resistance. Indirect flows (e.g. from tissue to veins) are also shown. Certain adjacent compartments can experience deformations due to the volume changes, compartments that experience this are shown in Figure 28 by compliances depicted at the compartment membrane. The intracranial region is shown enclosed in the bold border, it should be noted that the Extra-Ventricular compartment exists both inside and outside the intracranial region.

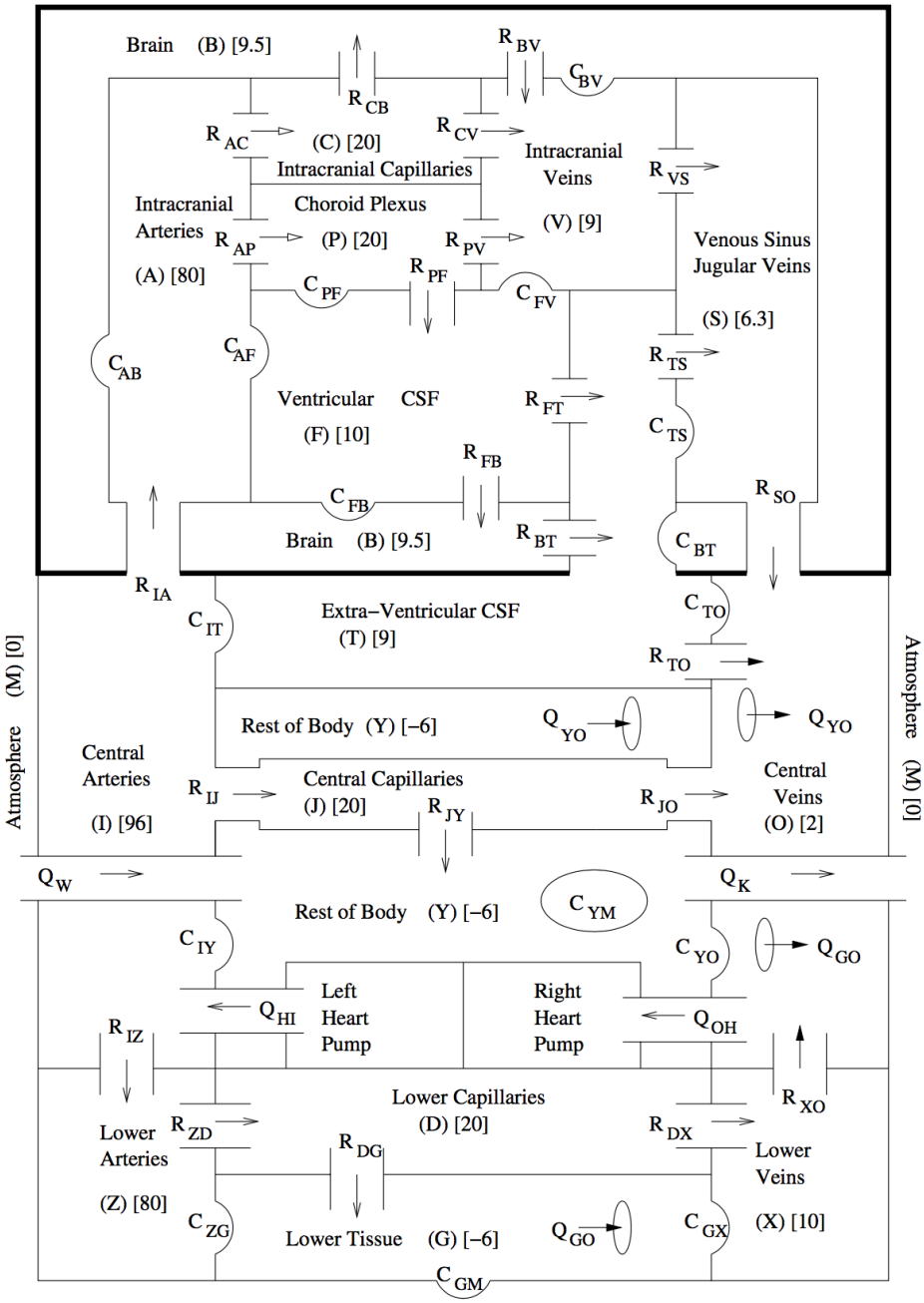

Figure 28: A diagram by Lakin *et al.* [47] showing a representation of the mathematical model, including all 16 compartments and related spatially-averaged pressures for each compartment (shown in square brackets). The flow between compartments can also be seen, as well as the compliances between adjacent compartments. Permission to use this image was granted by Springer Nature (Holtzbrinck Publishing Group, Germany).

There are 4 inputs in the mathematical model, which are as follows:

- Cardiac output (Q_{HI}): the flow of oxygenated blood from the heart into the central arteries, set at 5000 ml/min for the simulations. This value was taken from previous literature, Guyton [55].
- Cardiac input (Q_{OH}): the flow of deoxygenated blood from the central veins back to the heart, this is set to be equal to Q_{HI} in the simulations, as it is assumed that the amount of blood leaving the heart also returns to the heart, which would be the case for the healthy individuals being investigated.
- Fluid intake (Q_W): this input takes into account any fluids that may be added to the body, for example from the patient ingesting a drink. This is set to 0 ml/min in the following simulations.
- Fluid expulsion (Q_K): this takes into account any fluids being expelled from the body. This is also set to 0 ml/min for the purpose of this study.

The mathematical model also includes the effects of autoregulation, with regulation processes enforced, and the performance of each mechanism simulated and analysed in [53]. The role of autoregulation is to ensure that adequate blood flow is maintained (particularly cerebral blood flow) despite certain changes within the body, for example changes in blood pressure or cardiac output, Chillon *et al.* [65]. The mechanisms employed in this model are: lymphatic autoregulation, intracranial autoregulation, and sympathetic nervous system regulation.

Regulation systems are implemented into the state-space model in the form of feedback loops and alterations to the existing set of 16 equations. Implementation of autoregulation requires additional inputs to be included in the state-space model, as certain flows within the autoregulatory mechanisms have an exponential dependence on pressure. The addition of these flows increases the number of inputs from 4 (as described above) to 11. These inputs are represented in the state-space model by vector u. The inclusion of the regulatory flows into input vector u will be described in the following subsections, and the structure of the entire state-space model will be described later in section 6.3.3.

6.2.1 Lymphatic Autoregulation

The lymphatic system drains lymph from tissue into the blood, and lymphatic flows are governed by the interstitial fluid pressure. These flows have an exponential dependence on pressure, with flows increasing at a large rate between -6 and 4 mmHg, and reaching a plateau above 4 mmHg. There are 2 lymphatic flows between compartments in this model, they are Q_{GO} and Q_{YO}. The expressions for these flows are shown below:

$$Q_{GO}(t) = \frac{P_{lymph}(P_G)\bar{Q}_{GO}}{P_{lymph}(\bar{P}_G)} \tag{6}$$

$$Q_{YO}(t) = \frac{P_{lymph}(P_Y)\bar{Q}_{YO}}{P_{lymph}(\bar{P}_Y)} \tag{7}$$

where

$$P_{lymph}(x) = \frac{M}{1 + (M-1)e^{-r(x+6)}} \tag{8}$$

with $M = 20$ and $r = 1$.

P_{lymph} defines the relative lymph flow in terms of interstitial pressure. The two flows Q_{YO} and Q_{GO} are treated as inputs into the model and are therefore shown in vector u to represent the lymphatic system. The relationship between Q_{GO} and P_G, along with Q_{YO} and P_Y is shown in Figure 29. Figure 30 illustrates how lymphatic autoregulation is included in the model. These diagrams are heavily simplified and only include the inputs and outputs involved with lymphatic autoregulation.

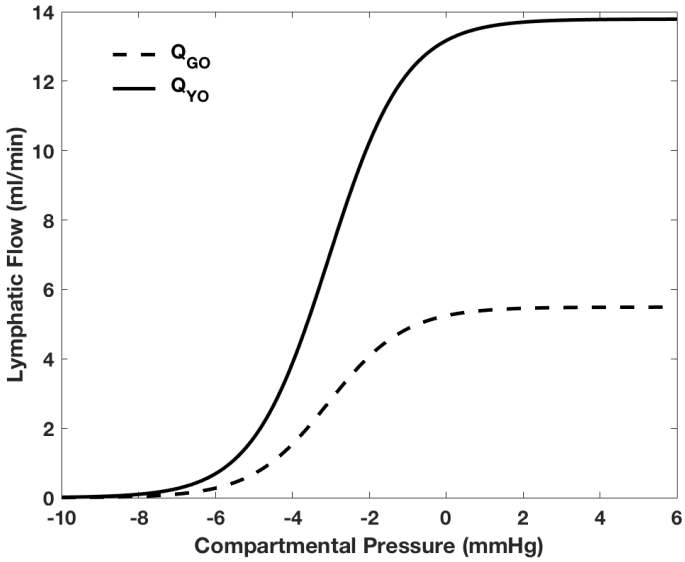

Figure 29: Lymphatic flows Q_{GO} and Q_{YO} both have an exponential dependence on pressure, with Q_{GO} changing with P_G, and Q_{YO} changing with P_Y.

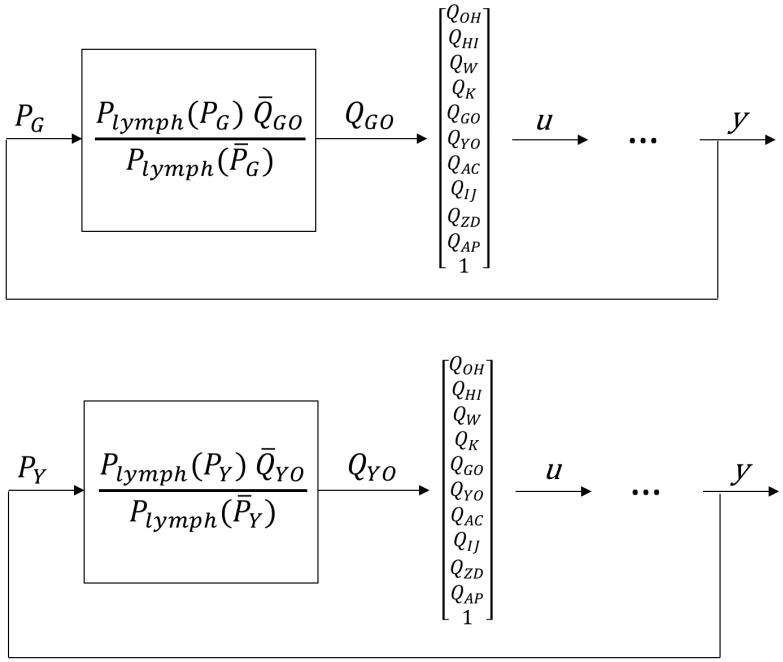

Figure 30: Regulation of lymphatic flows Q_{GO} and Q_{YO} depend on P_G and P_Y respectively. P_{lymph} is defined in equation (8). Both flows are used in the input vector u, which has a total of 11 inputs. This input vector is then used in the state-space model as shown in Figure 38. N.B. the output vector y is made up of 17 pressures, but only P_G and P_Y are used in these feedback loops.

6.2.2 Intracranial Autoregulation

Blood supply to the brain can be affected by a variety of factors, such as posture and cognition. However, it is very important that the cerebral blood flow (CBF) is maintained above a certain level to ensure that the brain is being supplied with enough oxygen. Therefore, regulation systems are in place to ensure that cerebral oxygen consumption remains constant. This regulation occurs due to a dilation or constriction of the blood vessels: when the blood supply is too low, vessels expand to increase blood flow, whereas if the blood supply is too high, the vessels contract to reduce blood flow.

As shown in Figure 28, flow from the intrancranial arteries (A) is split between the intracranial capillaries (C) and the choroid plexus (P). Thus, if the intracranial artery pressure is too high or too low, this can be regulated by modifying blood flow into the intracranial capillaries or the choroid plexus using pressure dependent fluidities, as shown below:

Regulation of blood flow into the intracranial capillaries:

$$Z_{AC} = \frac{F(P_A)}{P_A - P_C} \tag{9}$$

where

$$F(P_A) = \bar{Q}_{AC} \frac{M}{1 + (M-1)e^{r(\bar{P}_A - P_A)}} \tag{10}$$

As shown above, $F(P_A)$ and therefore Z_{AC}, increase with respect to intracranial artery pressure, P_A. From this, the blood flow into the intracranial capillaries (C) is increased, which then reduces the intracranial artery pressure, P_A. This exponential dependence on P_A is included in the model due to the fact that Q_{AC} is maintained at all pressures above 50 mmHg, however, when P_A falls below 50 mmHg this causes a significant decrease in Q_{AC}, the relationship between Q_{AC} and P_A is shown in Figure 31. The inclusion of this autoregulatory mechanism is illustrated in Figure 32.

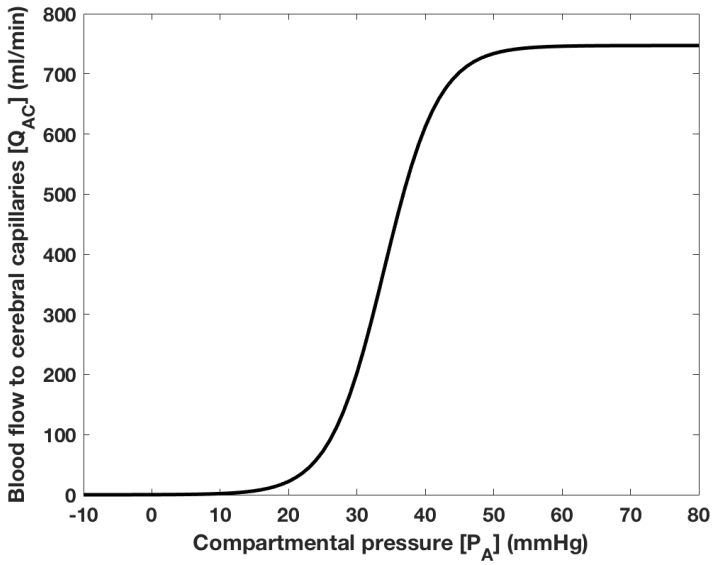

Figure 31: Blood flow to the cerebral arteries has an exponential dependence on compartmental pressure P_A, with blood flow experiencing a plateau at pressures above 50 mmHg.

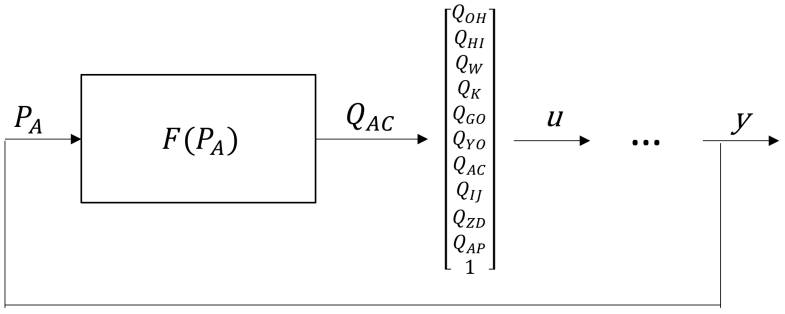

Figure 32: Regulation of intracranial blood flow to the capillaries Q_{AC} depends on P_A. $F(P_A)$ is defined in equation (10). This flow is used in the input vector u, which has a total of 11 inputs. This input vector is then used in the state-space model as shown in Figure 38. N.B. the output vector y is made up of 17 pressures, but only P_A is used in this feedback loop.

Regulation of blood flow into the choroid plexus:

$$Z_{AP} = \frac{\bar{Q}_{AP}}{P_A - P_P} G(P_{perf}) \tag{11}$$

where $P_{perf} = P_A - P_B$ and $G(P_{perf}) = 1$ if P_{perf} is greater than 55 mmHg, but decreases linearly to zero once P_{perf} drops below 55 mmHg, modelling the

fact that CSF production in the choroid plexus (P) scales with blood flow, and the relationship between Q_{AP} and P_{perf} is shown in Figure 33. The inclusion of this autoregulatory mechanism is illustrated in Figure 34.

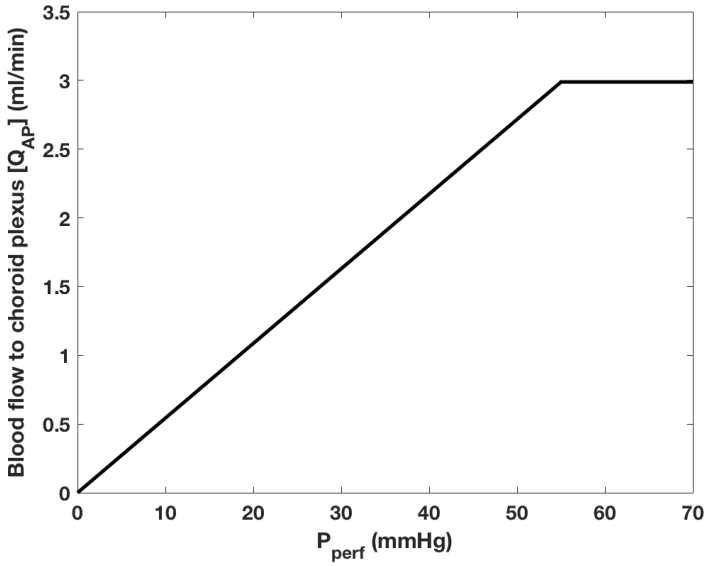

Figure 33: Blood flow to the choroid plexus is directly related to perfusion pressure ($P_A - P_B$), with a constant rate of blood flow maintained at perfusion pressures above 55 mmHg, and linearly decreasing below this point.

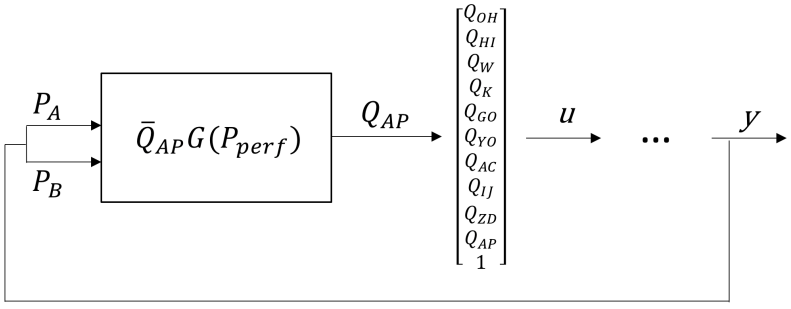

Figure 34: Regulation of intracranial blood flow to the choroid plexus Q_{AP} depends on P_A and P_B. $G(P_{perf})$ is defined in the text. This flow is used in the input vector u, which has a total of 11 inputs. This input vector is then used in the state-space model as shown in Figure 38. N.B. the output vector y is made up of 17 pressures, but only P_A and P_B are used in these feedback loops.

CSF production regulation is expressed through the pressure dependent fluidity Z_{PV}:

$$Z_{PV} = \frac{\bar{Q}_{AP} G(P_{Perf}) - Z_{PF}(P_P - P_F)}{P_P - P_V} \tag{12}$$

When P_{perf} is greater than 55 mmHg, a constant pressure difference is maintained, therefore, for normal pressures, the governing equation for the choroid plexus (P) becomes:

$$\frac{dP_{PF}}{dt} = 0 \tag{13}$$

6.2.3 Large Vessel Constrictive Response (SNSc)

When arterial pressure falls, the large vessels in the body strongly constrict to generate a rapid increase in arterial pressure. This is represented in the volume variation of V_{YO} and V_{YI} which is added using a forcing term, included as the derivative of P_I multiplied by a negative coefficient:

$$\frac{dV_{YO}}{dt} = C_{YO}\frac{dP_{YO}}{dt} - 24\frac{dP_I}{dt} \tag{14}$$

and

$$\frac{dV_{YI}}{dt} = C_{YI}\frac{dP_{YI}}{dt} - 8\frac{dP_I}{dt} \tag{15}$$

These forcing terms mean that there is a decrease in the volume of the central arteries (I) and central veins (O) depending on the central artery pressure, this decrease in pressure will therefore increase the blood flow circulating the body. As C_{YO} is considerably smaller than C_{YI}, the forcing term is larger, to ensure constriction of the veins. The integers in the forcing terms are provided by Lakin *et al.* [53], and are estimated to ensure adequate constriction of the blood vessels when arterial pressure falls.

6.2.4 Large Arteriole Constrictive Response (SNSz)

When the drop in central artery pressure is extreme this can compromise blood flow to the brain, therefore a more important system than the large vessel response (SNSc) is introduced. The large arteriole constrictive response (SNSz) generates an increase in the total peripheral resistance, which will lead to an increase in arterial pressure.

$$Total\ Peripheral\ Resistance = \frac{Mean\ Arterial\ Pressure}{Cardiac\ output} \tag{16}$$

This is represented in the model by including two multipliers in the expressions for the fluidities from the central arteries to the central capillaries (Z_{IJ}), and from the lower arteries to the lower capillaries (Z_{ZD}):

$$Z_{IJ} = \frac{\bar{Q_{IJ}}}{\bar{P_I} - \bar{P_J}} SNS_{z1}(P_I) SNS_z(Q_{AC}) \tag{17}$$

and

$$Z_{ZD} = \frac{\bar{Q_{ZD}}}{\bar{P_Z} - \bar{P_D}} SNS_{z1}(P_I) SNS_z(Q_{AC}) \tag{18}$$

where

$$SNS_{z1}(P_I) = \frac{P_I}{\bar{P_I}} \tag{19}$$

and

$$SNS_z(Q_{AC}) = \frac{M}{1 + (M-1)e^{r(\bar{Q}_{AC} - Q_{AC})}} \tag{20}$$

where $M = 1.1$ and $r = 0.02$

The first multiplier, $SNS_{z1}(P_I) < 1$ when P_I drops below its average value. Therefore, when the central artery pressure falls below its average level, the resistance increases. The second multiplier, $SNS_z(Q_{AC})$ represents the regulation system in place for when cerebral blood flow is significantly reduced. SNS_z increases the resistance when the blood flow Q_{AC} falls. When Q_{AC} is

at a normal level, SNS_z is approximately equal to 1 and does not affect the fluidity coefficients, the relationships between Q_{IJ}, Q_{ZD} and Q_{AC} are shown in Figure 35. The inclusion of these autoregulatory responses in the state-space model is illustrated in Figure 36.

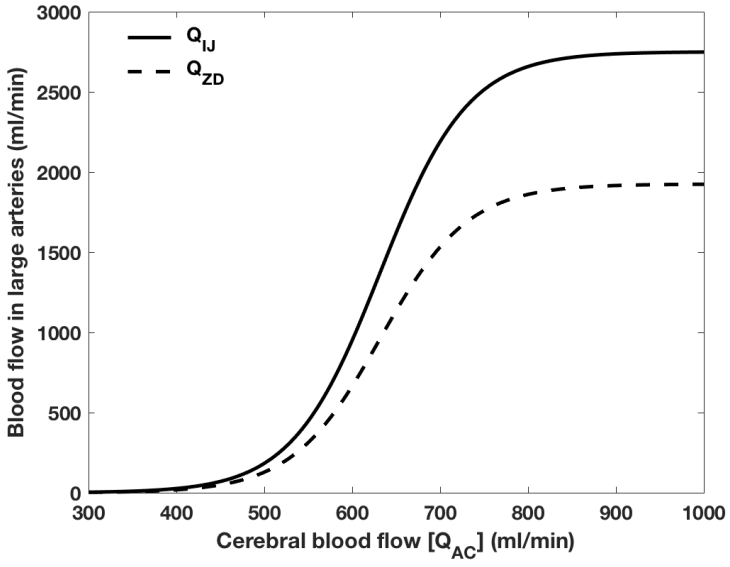

Figure 35: Blood flow in the central and lower arteries have an exponential relationship with cerebral blood flow, with the large arteries constricting and dilating in response to CBF values.

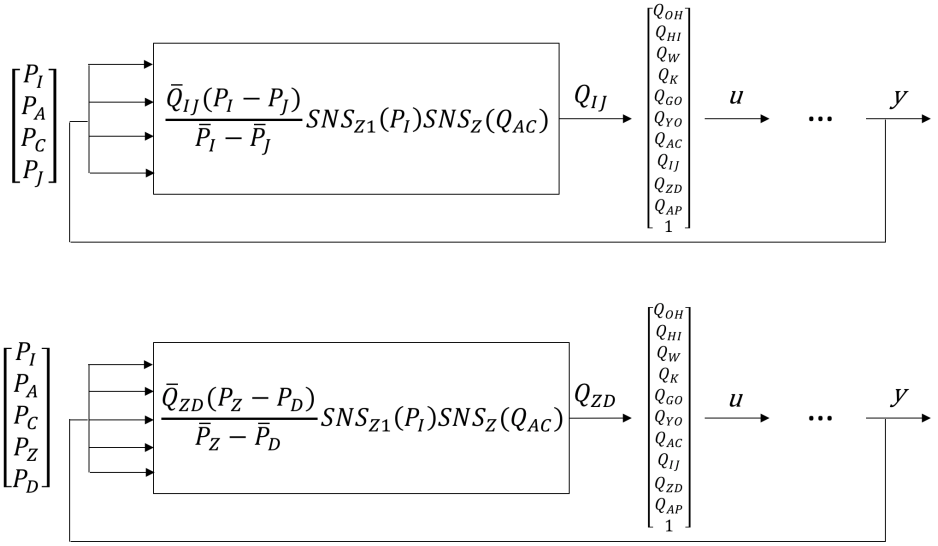

Figure 36: The large arteriole constrictive response regulates Q_{IJ} and Q_{ZD}. As shown in equations (17) - (20), the pressures that are used in this response are P_I, P_A, P_C, P_J, P_Z, and P_D. These flows are used in the input vector u, which has a total of 11 inputs. This input vector is then used in the state-space model as shown in Figure 38. N.B. the output vector y is made up of 17 pressures, but only P_I, P_A, P_C, P_J, P_Z, and P_D are used in these feedback loops.

6.2.5 Variable Intracranial Compliances

The compartments within the intracranial region are enclosed within the skull, meaning that the volume changes of such compartments are restricted by the cranial wall. Therefore, certain intracranial compliances must be variable and depend on compartmental pressure. A total of nine compliances in the model are pressure dependent, and they all lie within the intracranial region. In extracranial regions, compliances remain constant, approximating a linear relationship between pressure differences and volume adjustments.

6.3 Methods

6.3.1 Implementing a Pulsatile Cardiac Output

A realistic pulsatile cardiac output was implemented using a function proposed by Stevens *et al.* [66]. This function was derived based on a measured cardiac output waveform. The shape of the waveform is generated by multiplying the envelope function, $\sin^n(\omega t)$, by another function with the same frequency as the heart pulse, $\cos(\omega t - \phi)$, where n is an odd number, ω is half of the heart pulse frequency, and ϕ is the phase angle.

The flow waveform is then normalised and calibrated using the following variables:

- Mean cardiac output, $\bar{Q} = 5000$ ml
- Heart rate, b = 72 bpm
- Peak-to-mean flow ratio, $\sigma = 5.95$
- Output per stroke, $v = \frac{\bar{Q}}{b}$
- Period, $p = \frac{1}{b}$
- Frequency, $\omega = \frac{\pi}{p}$

Therefore, the flow waveform is given as:

$$Q(t, n, \phi) = \frac{v}{A(n, \phi)} sin^n(\omega t) cos(\omega t - \phi) \tag{21}$$

where

$$A(n, \phi) = \frac{\sqrt{\pi}\Gamma(1 + \frac{n}{2}) sin(\phi)}{\omega\Gamma(\frac{3+n}{2})} \tag{22}$$

The values for n and ϕ were chosen based on values provided for simulations in [53], and [66]. For the simulations displayed in the results section, $n = 11$ and $\phi = \frac{\pi}{10}$. The pulsatile flow waveform generated and used in the state-space model is shown in Figure 37.

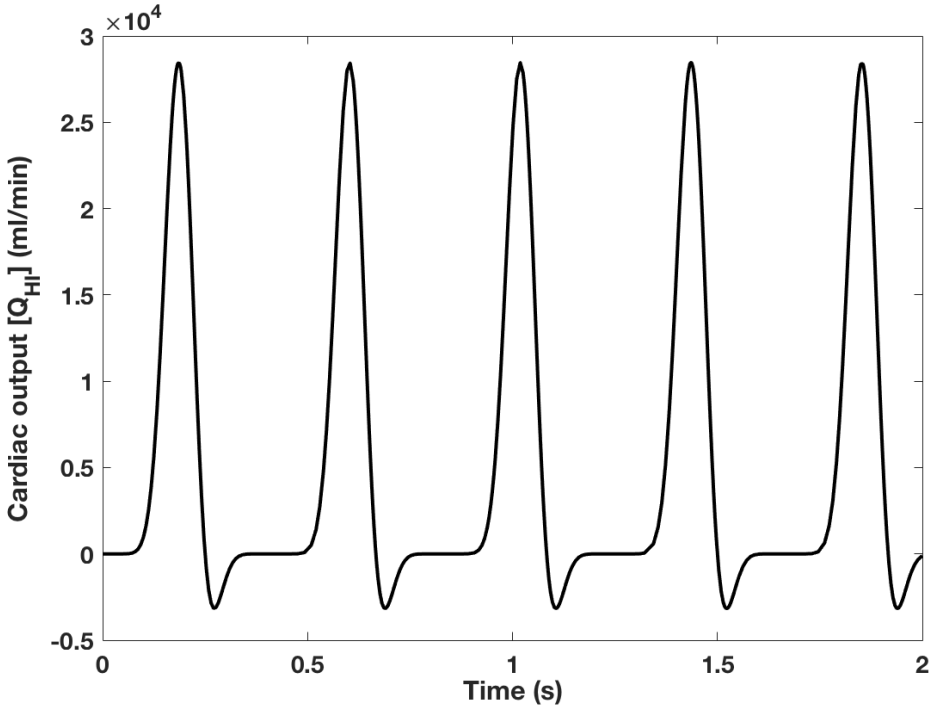

Figure 37: The realistic pulsatile cardiac output waveform (Q_{HI}) implemented as an input in the state-space model.

6.3.2 State-space Model

The mathematical model by Lakin *et al.* [53] was implemented in Simulink as a state-space model. A state-space model was chosen as they can be simplified with ease, and information about the controllability, stability, and observability of the model can be determined. The form of the state-space model is shown below:

$$E(x(t))\dot{x}(t) = Ax(t) + Bu(x(t))$$

$$y(t) = Cx(t) + Du(x(t))$$

Where E, A, B, C, and D are matrices, x is a vector containing the states, u is a vector containing the inputs into the model, and y is a vector containing the outputs from the model. For a standard state-space model the rank deficient E matrix is not included, however, due to the structure of the original mathematical model, this could not be directly represented in standard state-space form. The presence of the rank deficient E matrix determines that this is a descriptor system, making implementing and simulating the model more

complex, as E cannot simply be inverted. Methods for converting descriptor systems into state-space form have been researched, and a well-validated method called the shuffle algorithm, first described by Luenberger *et al.* [67], will be employed in this instance.

There are 17 states in the state-space model, which comprise the 16 compartmental pressures and the constant atmospheric pressure. These states are the spatially averaged pressures relating to the constituent flow through each compartment, for example, the state relating to the intracranial arteries compartment is the spatially averaged arterial blood pressure within the intracranial arteries. The initial values of the pressures used in the model are taken from [53] and are given in Table 7.

Compartment	**Initial pressure value (mmHg)**
Central Arteries (P_I)	96
Intracranial Arteries (P_A)	80
Intracranial Capillaries (P_C)	20
Choroid Plexus (P_P)	20
Ventricular CSF (P_F)	10
Brain (P_B)	9.5
Extra-Ventricular CSF (P_T)	9
Intracranial Veins (P_V)	9
Venous Sinus & Jugular Veins (P_S)	6.3
Central Veins (P_O)	2
Central Capillaries (P_J)	20
Rest of Body (P_Y)	-6
Lower Veins (P_X)	10
Lower Capillaries (P_D)	20
Lower Arteries (P_Z)	80
Lower Tissue (P_G)	-6
Atmosphere (P_M)	0

Table 7: Each compartment in the lumped-parameter model [47] has a spatially averaged pressure related to it. These 17 pressures are used as the initial values for the 17 states in the state-space model.

6.3.3 Implementing Descriptor Systems

The mathematical model in Lakin *et al.* [53] was represented as a state-space model by converting the 16 equations into the 2 equations shown in section 6.3.2, after including an additional governing equation to represent the atmospheric pressure. The vector x consists of the 17 compartmental pressures, u is a vector showing the inputs into the model. For the output equation, C is an identity matrix with dimensions $[17 \times 17]$, and D is equal to 0. For the state equation, E is a matrix consisting of compliances (some of which are pressure-dependent, see Figure 39), A is a matrix consisting of fluidities and filtration coefficients, all of which are constant, and B shows the input coefficients, which are also constant. All matrices are shown in Appendix C. Due to the dependence on pressure in the E matrix, this system is non-linear. To transform this system from descriptor form into standard state-space form for implementation and simulation, the shuffle algorithm is used. The first step of the shuffle algorithm is to display the state equation (shown in section 6.3.2) in the form shown below:

$$\begin{bmatrix} E_1(x(t)) \\ 0_{(N-n)\times N} \end{bmatrix} \dot{x}(t) = \begin{bmatrix} A_1 \\ A_2 \end{bmatrix} x(t) + \begin{bmatrix} B_1 \\ B_2 \end{bmatrix} u(t) \tag{23}$$

From this equation, it can be shown that:

$$A_2\ x(t) = -B_2\ u(t) \tag{24}$$

Using equation (24) and introducing state vector $z(t)$, the following equation can be reached:

$$\begin{bmatrix} E_1(x(t)) \\ A_2 \end{bmatrix} x(t) = \begin{bmatrix} z(t) \\ -B_2 u(t) \end{bmatrix} \tag{25}$$

where

$$z(t) = E_1(x(t))x(t) \tag{26}$$

and using the product rule, as E_1 also depends on x, we can differentiate to give:

$$\dot{z}(t) = \dot{E}_1(x(t))x(t) + A_1x(t) + B_1u(t) \tag{27}$$

From equation (25) an expression for $x(t)$ can be obtained:

$$x(t) = Q(x(t))z(t) - R(x(t))B_2u(t) \tag{28}$$

where

$$\begin{bmatrix} Q(x(t)) & R(x(t)) \end{bmatrix} = \begin{bmatrix} E_1(x(t)) \\ A_2 \end{bmatrix}^{-1} \tag{29}$$

assuming that $\begin{bmatrix} E_1(x(t)) \\ A_2 \end{bmatrix}$ is always invertible.

By relating equation (27) and (28) a state equation for $z(t)$ can be obtained:

$$\dot{z}(t) = F(x(t))z(t) + G(x(t))u(t) \tag{30}$$

where $F(x(t)) = (\dot{E}_1(x(t)) + A_1)Q(x(t))$ and $G(x(t)) = B_1 - (\dot{E}_1(x(t)) + A_1)R(x(t))B_2$.

The output equation for this system is shown below:

$$y(t) = H(x(t))z(t) + L(x(t))u(t) \tag{31}$$

Where $H(x(t)) = CQ(x(t))$, and $L(x(t)) = D - CR(x(t))B_2$, with the values for C and D described previously in this section.

Figure 38 depicts the structure of the state-space model as a block diagram. The feedback loop from the output to the input includes the pressures that are included in the autoregulation systems described previously, and the pressure dependent compliances, which are present in all 4 blocks, see Figure 39.

Due to the feedback loops within the system, a time delay of 0.05 seconds is introduced prior to calculation of $\dot{E}_1$ and $\begin{bmatrix} E_1(x(t)) \\ A_2 \end{bmatrix}^{-1}$.

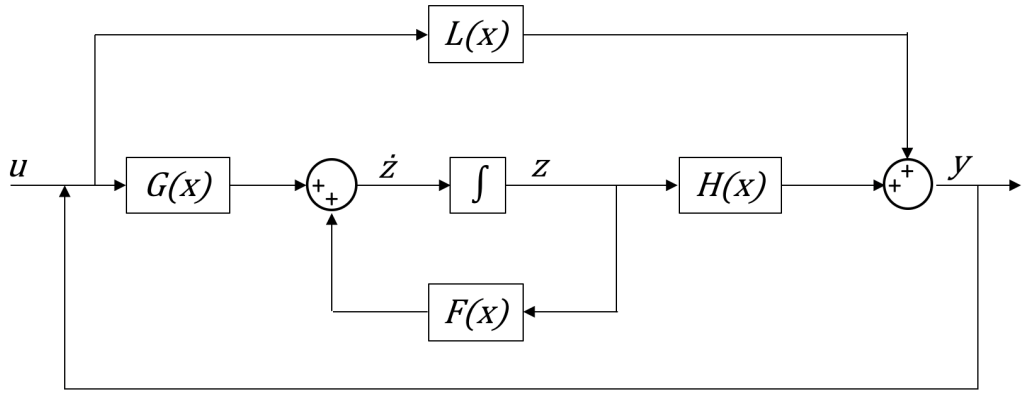

Figure 38: A block diagram showing the structure of the state-space model. N.B. u is a vector of 11 inputs, y is a vector of 17 outputs. All blocks have a pressure dependence, see Figure 39.

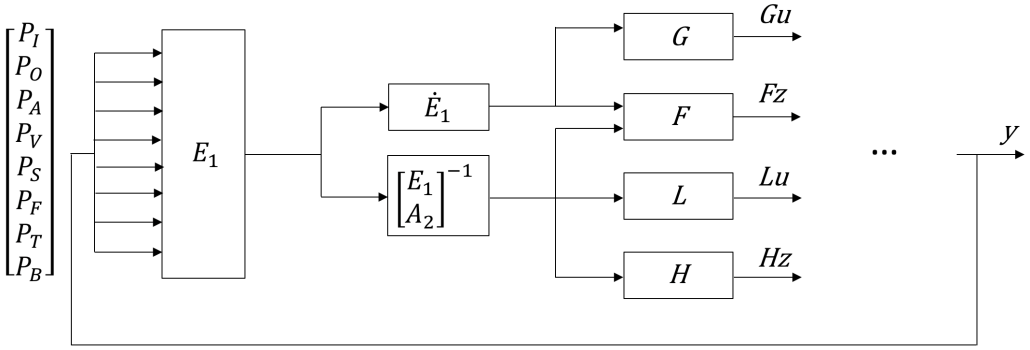

Figure 39: Variable compliances present in the E matrix depend on pressures, which are introduced into the matrix using a feedback loop. The E matrix is then used to calculate all 4 final matrices present within the state-space model. See Figure 38 for an illustration of how the final 4 matrices (F, G, H, and L) interact in the model. N.B. y is a vector of 17 outputs, only 8 of these pressures are used in the feedback loop.

6.4 Results

6.4.1 Pressure Outputs

Initial model simulations were carried out with blood flow from the heart equalling 5000 ml and the heart rate equalling 72 bpm (frequency in model = 7.54 rad/s). These simulations take approximately 4.4 seconds to run. Figure 40 shows the pressures of the central artery (P_I), intracranial artery (P_A), intracranial capillary (P_C), and brain (P_B) compartments. As blood moves from the heart and through each compartment, the pressure can be seen to decrease in each consequent compartment. The initial pressure values for each compartment can be found in Table 7.

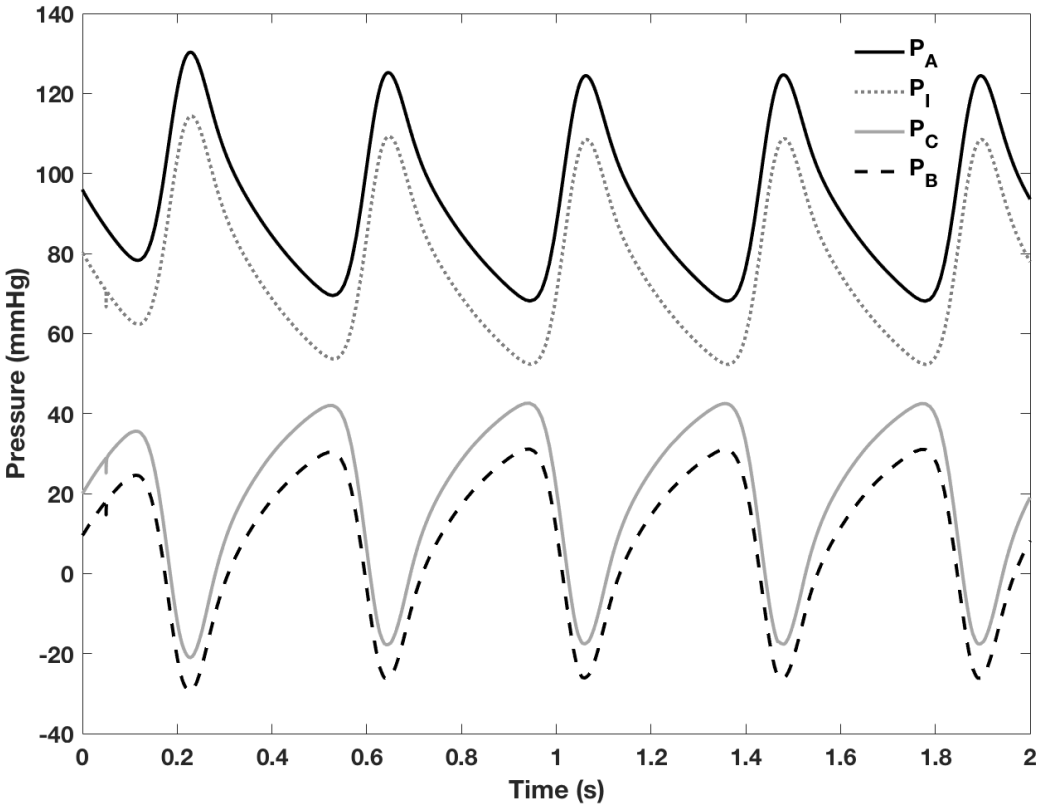

Figure 40: The pressure waveforms produced as outputs from the state-space model for the central artery (P_I), intracranial artery (P_A), intracranial capillary (P_C), and brain (P_B) compartments.

6.4.2 The Effect of Varying Pulse Pressure on Brain Volume

A decrease in pulse pressure was achieved by lowering the heart rate, and therefore, increasing the stroke volume. The cardiac output remained at 5000 ml, however, the heart rate was lowered from 72 bpm to 50 bpm (frequency in model = 5.24 rad/s). Figure 41 shows the difference in the waveforms of the central artery pressure (P_I), brain pressure (P_B), and the rate of change of brain volume (dV_B/dt). The initial pressures remained the same as in previous simulations, and are displayed in Table 7.

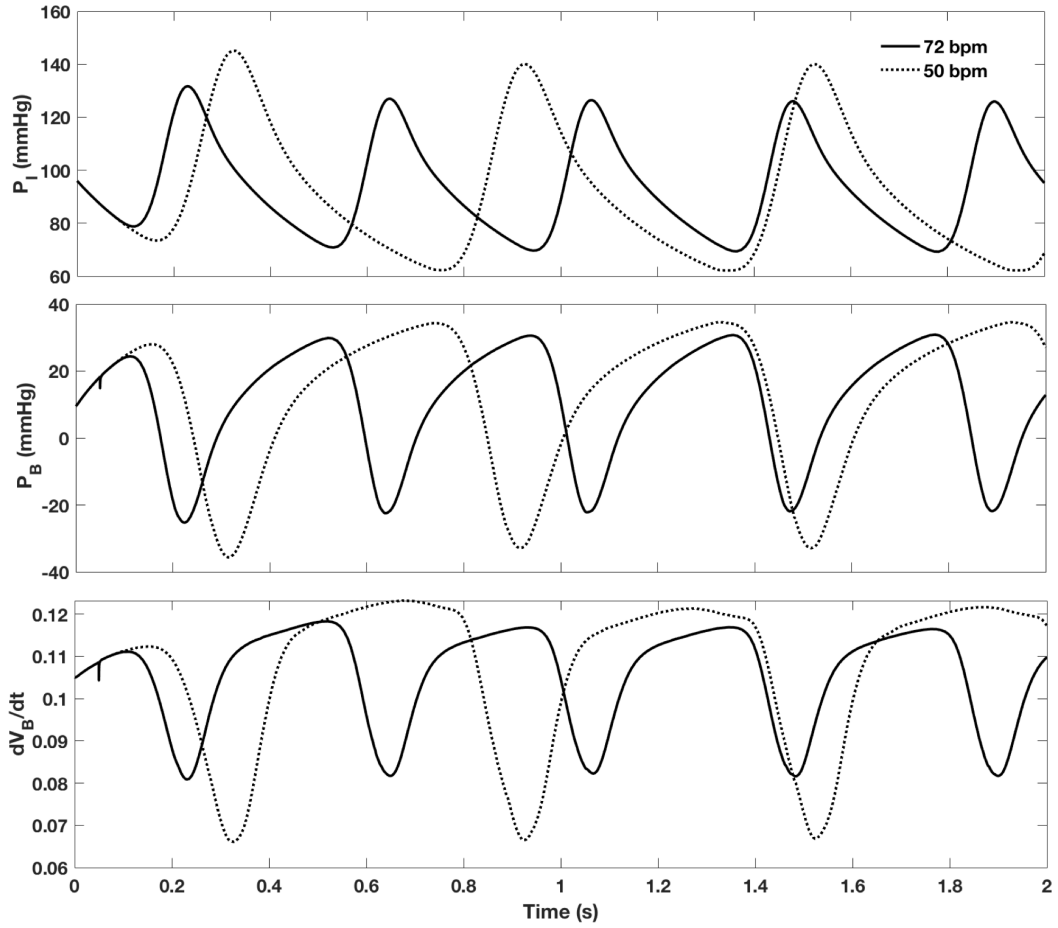

Figure 41: The waveforms produced from the state-space model for the central artery pressure (P_I), brain pressure (P_B), and the rate of change of brain volume (dV_B/dt). The waveforms are shown for a cardiac output of 5000 ml at 72 bpm (solid line), and an output of 5000 ml at 50 bpm (dashed line). It is clear that both the pulse pressure for the central arteries and the brain increases when HR decreases. It is also clear that the rate of change of brain volume increases as pulse pressure increases.

Average values for PP were calculated from the waveforms displayed in Figure 41. PP for the central arteries increased as heart rate decreased, from a value of 58.1 (1.9) mmHg at 72 bpm, to 79.3 (3.0) mmHg at 50 bpm. Similarly, PP in the brain increased as HR decreased, from a value of 52.0 (1.4) mmHg at 72 bpm, to 66.0 (2.2) mmHg at 50 bpm. These increases in PP correspond to an increase in the change in brain volume, which was calculated from the amplitude of the waveforms displayed in Figure 41. The amplitude of the rate of change of V_B waveform starts at a value of 0.035 (0.001) ml/min at 72 bpm, and increases to 0.052 (0.006) ml/min at 50 bpm.

The estimated values for the rate of change of V_B can be used to approximate the change in the radius of the brain. Assuming that the brain is spherical, the known equation for the volume of a sphere can be differentiated with respect to the radius to give the relationship shown below:

$$\frac{dV_B}{dt} = 4\pi r^2 \frac{dr_B}{dt} \tag{32}$$

The value of 0.035 ml can be substituted for the rate of change of V_B, along with an estimate of the average radius of a brain, which is assumed from the average radius of the skull being $\sim$ 9 cm, Bushby *et al.* [68]. By substituting these values into equation 32, this gives the rate of change of brain radius to be 0.3 μm/min. The values for the rate of change of radius are in the same order of magnitude as those of measured BTP Amplitudes. Although the measured values for Bulk BTP Amplitude are slightly larger, with the average Bulk BTP Amplitude measured through the forehead being 17.0 μm [IQR: 11.3, 25.4], it should be noted that these calculations are preliminary estimations based on a number of assumptions.

6.5 Discussion

In this chapter, the implementation of a state-space model was described, and the model was used to investigate the impact of pulse pressure (PP) on brain volume. All aspects of the model were successfully implemented. A significant change in PP was induced by decreasing HR from 72 to 50 bpm, and therefore, increasing the stroke volume. The central artery compartment experienced an increase in PP from 58.1 (1.9) mmHg to 79.3 (3.0) mmHg. A relative increase in PP was then observed in all pressure outputs from the model, excluding the atmosphere compartment (set at a constant reference value of 0 mmHg). The increase in PP throughout the body was accompanied by a significant increase in the rate of change of brain volume, see Figure 41.

In the results from this chapter the change in brain volume acts as a surrogate for BTPs. From this we can assume that an increase in BTP amplitude is induced by an increase in PP, which agrees with previous work in this thesis. Results from the healthy volunteer study in chapter 3 suggest a significant positive relationship between BTPs and PP in both the forehead and temporal positions, with an increase of 3.2 μm associated with a 10 mmHg increase in PP for the forehead, and an increase of 1.1 μm associated with a 10 mmHg increase in the temporal position (where amplitudes are generally smaller). Results from the phantom study in chapter 4 also support these findings, with an increase of 3.4 μm associated with an increase of 10 mmHg in PP through the forehead position. The model presented in this chapter is currently unable to quantitatively compare the results to the work in previous chapters, however, a positive relationship between BTPs and PP is clearly suggested.

The model developed by Lakin *et al.* [53] implemented in state-space form in this chapter is a very detailed model. It is the only mathematical model of ICP dynamics that takes the whole body into account, and therefore, has a greater number of compartments than any previous model [50]. This model was chosen as it does not assume that the intracranial space is an enclosed region, and accounts for venting of CSF through the spinal canal. This is achieved by the inclusion of the Extra-Ventricular CSF compartment, which exists both within and outside of the intracranial region. The venting of CSF through the spinal canal lessens the impact of fluctuations in CSF pressures

within the intracranial region, and is therefore, an important factor when considering the measurement of BTPs.

The extensive nature of this model can have limitations. For example, as the model includes 16 body compartments, this means that there are a large number of parameters that are not well-known and need to be estimated, which may lead to inaccuracy within the model. However, these parameters can be optimised by updating the model using more data as it becomes available, and future work should focus on validating the model by linking Brain TV measurements with the intracranial states in the model. Also, the size of the model leads to longer computation time. As this model was implemented to qualitatively investigate the impact of PP on BTPs, this is not an issue, however, in future work the state-space model should be simplified to improve efficiency.

The state-space model implemented in this chapter has potential to advance the understanding of BTPs and how they are affected by different factors, such as posture changes or pathology. Future work with the model should focus on quantifying BTPs to allow for direct comparison with previous studies, and validating the model using physiological data investigated in this thesis.

Ultrasound measurements of CBF in the middle cerebral artery (MCA) are often used as an input in mathematical models aiming to non-invasively estimate ICP, Ursino *et al.* [69], Kashif *et al.* [70]. As discussed previously in this thesis, CBF measurements can be difficult to obtain in many subjects as a skilled operator is required, and measurements are not possible in approximately 10-15 % of the population, due to the skull, Boespflug *et al.* [71], Marinoni *et al.* [72]. Alternative MRI techniques have also been developed to non-invasively estimate ICP, with a well validated technique involving the calculation of an intracranial elastance index using MRI measurements of CBF and CSF flows, and relating these values with ICP, Alperin *et al.* [73]. However, as previously mentioned, MRI measurements are not suitable for continuous monitoring, and availability of MRI is relatively low. Therefore, understanding how BTPs are affected by ICP through the use of this model may prove to be beneficial in future research, and by using BTPs as a variable, rather than CBF, TCTD may prove to be a more feasible method for non-invasively estimating ICP.

6.6 Conclusions

The model implemented in this chapter has enabled us to isolate the effects of BP on BTPs. A significant increase in the change in brain volume was observed when a significant increase in PP was simulated, supporting results from previous studies presented in chapters 3 and 4. With further work, the state-space model implemented in this chapter has the potential to further understanding on the relationship between BTPs and ICP, and be of great clinical importance when incorporated into the Brain TV system.

7 Discussion

The research presented in this thesis had 2 main aims: firstly, to understand healthy brain tissue pulsations (BTPs) and the factors that affect them, and secondly, to investigate the feasibility of using the Brain TV system as a clinical tool to monitor and aid diagnosis of brain injury. To do this, a number of studies were carried out, including healthy volunteer studies, and a phantom study. Intracranial pressure dynamics were also investigated using a state-space model to relate blood pressure (BP) alterations to the change in brain volume.

7.1 Key findings

7.1.1 Characterising and Quantifying Healthy BTPs

In chapter 3, 107 healthy volunteers were studied, with measurements of BTP amplitude, BP, heart rate (HR), and demographical information such as age and sex being recorded. This study introduced the technique of transcranial tissue Doppler (TCTD) ultrasound as an alternative, inexpensive, portable method of measuring BTPs, that does not require an expert user. This study has the largest healthy population sample size of all previous research, with the next largest sample of healthy volunteers being n = 39. This enabled variations between individuals to be investigated.

It was found that BTP signals could be obtained in all participants, at numerous positions on the skull. This is a very beneficial finding, as all previous ultrasound techniques have needed to obtain measurements through acoustic windows in the skull, such as the occipital or temporal window, which can often be difficult to locate. The ability to measure BTPs through the forehead supports the feasibility of this technique being used clinically, especially in emergency situations. BTP measurements can be obtained easily by anybody with appropriate training, therefore, a specialist operator is not required.

The findings of this study support previous MRI research into BTPs [2], [3], [6], with results suggesting that tissue pulsations are weakest closer to the skull and increase with depth into the brain. Regional tissue pulsations are also indicated by the significantly larger BTP amplitudes observed from the

forehead compared to the temporal position, with a median Bulk BTP Amplitude of 17.0 μm [IQR: 11.3, 25.4] through the forehead position, compared to 9.2 μm [IQR: 6.0, 12.9] through the temporal position. BTP amplitudes were extremely variable and differed greatly between volunteers, with amplitudes skewed towards lower values.

A multivariate regression model was developed to determine which of the measured variables had a significant impact on Bulk BTP Amplitude measured through the temporal and forehead positions. It was found that pulse pressure (PP) had the most significant impact, with an increase in PP corresponding to an increase in Bulk BTP Amplitude for both probe positions. An increase of 1% in PP resulted in an increase in Bulk BTP Amplitude of 0.8% for the forehead position, and an increase of 0.6% for the temporal position. Pulse pressure gives a representation of the force that is generated by the heart contracting, therefore, higher levels of PP correspond to greater force being exerted by the heart. PP depends on stroke volume ejected through the left ventricle of the heart and arterial compliance, with a decrease in arterial compliance leading to increased PP, Homan *et al.* [74]. PP is also an important predictor of mortality in patients, and in some cases is deemed to be the most important BP parameter for predicting outcomes of illness, Malone and Reddan [75]. Therefore, it is important to understand the impact of PP on BTPs for use of BTP measurement as a diagnostic tool.

Age was found to be significant in the multivariate regression model when Bulk BTP Amplitude was measured through the forehead, with an increase in Age corresponding to a decrease in Bulk BTP Amplitude. A 1 year increase in Age, above the age of 20 years, results in a decrease in Bulk BTP Amplitude of 0.9%. This dependence on age is consistent with previous research [14]. However, Age was not a significant factor in Bulk BTP Amplitude variability when measured through the temporal position, where amplitudes were lower. Conversely, Sex was found to be a significant factor through the temporal position, but not through the forehead position, with Bulk BTP Amplitude found to be 29% greater in males than in females. This may be explained by PP as a confounding variable, as males had significantly higher PP than females ($p < 0.0001$). The relationship between BTPs and sex was previously unexplored.

7.1.2 The Impact of Blood Pressure on BTPs

Chapter 4 presents the first study to use the Brain TV system, which was still under development in the previous healthy volunteer study. The Brain TV system allowed for changes in BP within individuals to be investigated using continuous measurements. BTP signals were successfully obtained for all 20 volunteers and for the ultrasound phantom. The Brain TV system was well tolerated by all volunteers.

In the healthy volunteer study, both PP and MAP were successfully increased using a leg raise manoeuvre, with PP increasing by 6.3 mmHg [95% CI: 3.5, 9.1, p = 0.0002], and MAP increasing by 4.1 mmHg [95% CI: 1.5, 6.7, p = 0.004]. These increases in PP and MAP were accompanied by a significant increase in median Bulk BTP Amplitude from a baseline value of 12.5 μm [IQR: 10.0, 18.1], to 15.5 μm [IQR: 13.3, 20.3] during the leg raise manoeuvre. These results support previous research into BTPs in patients with orthostatic hypotension [19]. However, the leg raise manoeuvre used in this study also caused an increase in all other measured variables (HR and $EtCO_2$). Because of this, the increase in BP could not be isolated and the cause for the increase in Bulk BTP Amplitude could not be determined. Therefore, a phantom experiment was carried out, where all additional variables could be controlled, and only BP was altered.

The first phantom experiment successfully raised MAP whilst keeping PP relatively constant. The results from this study suggested only a slight change in Bulk BTP Amplitude with MAP. However, the second experiment, focusing on altering PP rather than MAP, resulted in a large change in Bulk BTP Amplitude, with increases in Bulk BTP Amplitude appearing to mirror increases in PP. The linear relationship between Bulk BTP Amplitude and PP suggests an increase in Bulk BTP Amplitude of 3.4 μm with every 10 mmHg increase in PP. This closely agrees with the results from the healthy volunteer study in chapter 3, with a 10 mmHg increase from 40 to 50 mmHg resulting in an increase in Bulk BTP Amplitude of 3.2 μm, when measured through the forehead.

7.1.3 The Impact of End-tidal CO_2 on BTPs

In chapter 5, the impact of CO_2 levels was investigated, to fully understand how all measured variables in the Brain TV system contribute to Bulk BTP Amplitude. Once again, the Brain TV system was tolerated well by all 30 participants, and BTP signals were successfully obtained for all volunteers.

The period of hyperventilation used in the study successfully lowered $EtCO_2$ by -4.7 mmHg [95% CI: -5.8, -3.6, $p < 0.0001$], and this change was accompanied by the expected changes in other variables, such as a decrease in MAP. It was found that Bulk BTP Amplitude increased slightly during hyperventilation by < 2 μm, but was followed by a significant decrease in Bulk BTP Amplitude for the right hemisphere, from a value of 14.5 μm [IQR: 8.5, 19.5] during hyperventilation, to a value of 10.2 μm [IQR: 6.6, 18.2] during the recovery phase. These results contrast to previous findings into the effects of CO_2 on BTPs by Kucewicz *et al.* who found that BTP Amplitude significantly decreased during hyperventilation [12]. However, the study presented in chapter 5 of this thesis aimed to induce mild hypocapnia for a much shorter period of time. Therefore, it is possible that a time lag occurred between the period of hyperventilation and the effect becoming evident in BTP Amplitudes. To further understand the relationship between hypocapnia and BTP Amplitude it would be useful to repeat this study using a longer period of hyperventilation to account for any potential time lag, and to account for the possible impact of neurovascular coupling.

To further understand which of the measured variables caused the change in Bulk BTP Amplitude, a linear mixed effects model was developed. This model allowed for multiple observations from each participant to be included. Univariable analysis suggested that Age, PP, MAP, and Recovery Phase were significant factors in Bulk BTP Amplitude. However, after analysing the relationship between these factors in all possible model structures, only Age and Recovery Phase were significant factors ($p = 0.042$ and $p = 0.004$ respectively). A increase of 1 year in Age results in a 2.7% decrease in Bulk BTP Amplitude, which is a larger decrease than reported in the previous multivariate model in chapter 3 (0.9%). The results from the model support previous results from the study, suggesting a slight increase in Bulk BTP Amplitude of 3.3% during

the hyperventilation phase, followed by a significant decrease of 16% during the recovery phase. The change in Bulk BTP Amplitude during the recovery phase suggests that there may be other variables that are not currently accounted for that affect BTPs.

7.1.4 Implementing a State-space Model of Intracranial Pressure Dynamics to Understand the Impact of Pulse Pressure on BTPs

In chapter 6, an existing mathematical model was converted into state-space form and implemented in Simulink (MATLAB, The MathWorks). The only variables in the model are compartmental pressures and volumes. Therefore, the relationship between blood pressure and intracranial dynamics could be investigated theoretically, without the need to account for other variables, such as CO_2 levels.

The state-space model was implemented successfully, and was used to simulate a change in PP by decreasing HR, and observing the resulting change in brain volume. The simulations resulted in a significant increase in central artery PP from 58.1 (1.9) mmHg to 79.3 (3.0) mmHg, and this increase in PP was observed throughout the remaining body compartments. The rate of change of brain volume was also shown to significantly increase following this increase in PP. In this model, the change in brain volume is used as a surrogate for BTP measurements, which therefore, suggests that BTP amplitude is dependent on PP. These preliminary results support previous findings, however, the model should be adapted to enable direct comparison with BTP measurements obtained in previous research.

7.2 Limitations

Although the Brain TV system and the TCTD technique was well tolerated by volunteers, and gave measurements that were consistent with previous research, there are some limitations that need to be addressed in future research.

The main limitation regarding this technique is that it is not possible to accurately determine which brain structures are being measured without additional imaging information. As previously mentioned, the generated ultrasound beam

will be distorted by the skull, and the level of distortion may vary between individuals due to different skull shape and thickness. The beam plot shown in Figure 4 shows the ultrasound beam profile with no obstruction or attenuation of the beam. It would be useful to plot the beam profile through a piece of human skull to have an idea of the level of distortion that may occur. However, it is encouraging that we have obtained measurements that agree closely with previous MRI studies, such as Weaver *et al.* [6], suggesting that the assumed depth that the ultrasound beam reaches within the brain is accurate.

Another limitation that became apparent throughout the thesis is the decline in visualisation depth. For the first healthy volunteer study in chapter 3, a commercially available TCD system was modified to obtain BTP measurements. In this study, clear BTP signals were visualised up to a depth of 8 cm into the brain. However, when using the Brain TV system in all subsequent studies, the visualisation depth decreases to only 6 cm into the brain. As this is a newly developed system, this could be due to a number of factors, and it is important that the cause of this is determined so that the system can be improved. The original TCD system is often used on patients in a clinical environment, therefore, all protective tests have been carried out to ensure that interference between medical devices is limited. For the Brain TV system, it was ensured that there was shielding to prevent the system causing interference to surrounding medical equipment, however, it is possible that the system may be experiencing interference from other devices.

The lack of visualisation depth may also be due to lower output power in the Brain TV system, compared to the Spencer Technologies TCD system. A decrease in power may result in decreased penetration of the ultrasound beam. It should also be noted that the visualisation depth also seemed to decrease when 2 ultrasound probes were used simultaneously, further suggesting that a lack of power could be causing the decreased visualisation. This requires further investigation through ultrasound beam plots and output power measurements.

The intensity of the received ultrasound echoes is currently being investigated. It is possible that the large signals as seen in Figure 7(d) could be due to the ultrasound beam entering the ventricles, which are filled with fluid rather than tissue, resulting in a lack of signal. However, this does not explain why this

was not witnessed in the 107 volunteers measured with the conventional TCD machine. It should also be noted that the visualisation depth remained largely consistent between recordings for individuals, i.e. if visualisation depth was poor for a recording, it is likely that all of the recordings related to that participant will have poor visualisation depth. This may suggest that differences between participants may cause differing visualisation depths, for instance, different skull thicknesses between volunteers coupled with a lack of power may account for this issue. The most likely explanation is that ultrasound echoes were weak, providing poor signal to noise beyond $\sim$6 cm.

7.3 Future Work

The analysis in this thesis focused on BTP amplitude to describe healthy brain tissue motion. However, there are many other aspects of BTP signals that can be investigated, such as waveform shape and morphology. A full list of the features calculated from the BTP signals is given in the Brain TV analysis GUI user instruction manual, shown in Appendix A. Preliminary work has been carried out at the University of Leicester investigating the differences between waveform shape of healthy volunteers and stroke patients, suggesting a possible difference between the two. The results from this study are published in an article, on which I am listed as a coauthor, Ince *et al.* [76]. A difference between healthy and pathological waveform shapes may prove to be a clinically useful tool to quickly identify brain pathology, as opposed to relying on the amplitude of pulsations. Therefore, future work should also focus on additional features that are available from the received TCTD signals.

Although we have identified particular factors affecting BTPs, such as pulse pressure, some aspects of how BTPs relate to cerebral haemodynamics remain unclear. It would be useful to investigate the relationship between BTPs and cerebral blood flow (CBF), which can be measured simultaneously using the Brain TV system. This will aid interpretation of how BTPs may be affected in pathology. This can also be investigated using the model, with the added benefit of being able to investigate venous and CSF outflow, which also affect intracranial pulsatility, Wagshul *et al.* [1]. Changes in venous and CSF pulsatility have previously been associated with increased WMH development, Blair *et al.* [77], and previous research has suggested strong negative correla-

tion between BTPs and WMH volume, Ternifi *et al.* [13]. The impact of the blockage of outflow pathways on BTPs has also been investigated by Terem *et al.* [9], with a difference in BTPs between a patient with a Chiari I malformation and a healthy volunteer being reported. Therefore, an understanding on how CBF, including venous outflow and CSF pathways, affect BTPs will give an understanding on how BTP measurement can be used as a potential marker for brain pathology.

As the Brain TV system is being developed as a tool for use in the diagnosis and monitoring of brain injury, it is important to understand how well the system can be used in a clinical setting. For example, it needs to be determined how well the equipment is tolerated by patients, and also the quality of patient data needs to be assessed. Therefore, future work should focus on obtaining measurements from patients with brain injury, which can then be compared to the healthy data presented in this thesis.

Another important area of future work arising from this thesis is the adaptation of the state-space model. Currently the model is used to distinguish the relationship between blood pressure and the change in brain volume, however, the model has the potential to be used as a method of non-invasively estimating intracranial pressure (ICP) using BTP measurements. Therefore, future work should focus on simplifying the model for clinical use, and validating the ICP estimates using ICP data from patients.

The relationship between ICP and BTPs also has the potential to be investigated using the phantom, as previous phantom work has investigated the relationship between CSF dynamics and invasive ICP measurements, Bottan *et al.* [78]. Research suggests that an increase in ICP is linked to decreased intracranial compliance [79], and due to the Windkessel effect, this decreased intracranial compliance would also lead to greater intracranial pulsatility. The Windkessel effect is the damping of fluctuations in BP over the cardiac cycle, due to elastic arterial properties. Arterial stiffness can occur with age and pathology, therefore, the arteries become less elastic which causes an increase in pulsatility, due to the lack of damping [80]. Previous research also suggests that increased intracranial pulsatility is present in brain pathologies such as cerebral small vessel disease, Shi *et al.* [81]. The previously unknown relation-

ship between BTPs and PP presented in this thesis may suggest that BTP measurement could be used as a surrogate for measuring brain PP, which is often altered in pathologies such as hydrocephalus and traumatic brain injury, Wagshul *et al.* [82]. Therefore, future work should look into investigating BTPs in pathological cases in which intracranial PP is altered, to determine if BTP measurements can be used as a marker for these pathologies.

Conclusions

In this thesis I have introduced a technique for measuring brain tissue pulsations, and visualising pulsations in real-time, using a novel prototype device. The Brain TV system gives BTP measurements that are comparable to results obtained from previous MRI and ultrasound studies, with the benefit of the system being portable, low-cost, and optimised for continuous transcranial measurements. BTP signals were successfully obtained in all volunteers studied, due to the ability of TCTD to obtain measurements through any part of the skull. The Brain TV system has great potential for use in diagnosis and monitoring of brain injury in a clinical environment, due to the ease at which measurements are taken, particularly through the forehead, and the portable nature of the system.

Throughout this thesis I have investigated factors that affect healthy brain tissue motion, while aiming to highlight areas for further research. I did this by carrying out an initial healthy volunteer study, investigating 107 volunteers, to understand variability in healthy BTPs across the population, finding that pulsations varied greatly between individuals. The results from this study also suggested a strong association between Bulk BTP Amplitude and both Age, and PP when measured through the forehead. The mixed effects model in chapter 5 validated the initial finding that Bulk BTP Amplitude decreases with increasing age, which has been suggested in one previous BTP study. The findings related to PP were also validated in subsequent healthy volunteer and phantom studies, and through the implementation of a state-space model describing ICP dynamics. All of which suggested a positive relationship between Bulk BTP Amplitude and PP, which is a relationship that was previously unexplored. Studies also suggested no effect of MAP, $EtCO_2$, or HR, the relationship between these variables and BTPs had not been directly explored in previous research.

The main outputs from my PhD work include the generation of a large database of healthy BTP data, which can be used in future clinical research to determine differences between healthy and pathological brain tissue motion. The impact of PP on BTPs is a novel finding, which can be used to further understanding on how BTPs may vary between individuals, and in pathology. The

implementation of the state-space model describing ICP dynamics will be of great use in future research. The model can be used to further investigate the generation of BTPs, and simulate specific pathologies to determine how BTPs may be affected in these situations. Future adaptations of this model may also provide a method to estimate ICP non-invasively using BTP measurements, which would be of great clinical significance.

Throughout my PhD I have gained knowledge on cerebral dynamics, state-space control systems, and statistics for use in clinical research. I have also gained experience in programming using MATLAB, model implementation using Simulink, and statistical analysis using Stata. I have gained opportunities to develop my research and presentation skills throughout my PhD, by presenting my work at national and international conferences, for which I previously received an award for Best Poster Presentation at IPEM's Medical Physics and Engineering Conference, 2017. I have also had the opportunity to develop my teaching and communication skills by supervising a number of Medical Physics, Engineering, and Biosciences MSc and BSc projects. I have gained experience in all aspects of clinical research, from the conception of a hypothesis to data collection and analysis. I hope that the work that I have carried out in my PhD will continue to be developed and applied to the investigation of brain motion, which has the potential to have great impact on patients with brain injury.

Appendix A - Brain TV GUI User Manual

University Hospitals of Leicester NHS
NHS Trust
Caring at its best

UNIVERSITY OF LEICESTER

Brain TV Graphical User Interface (GUI)

User Instructions

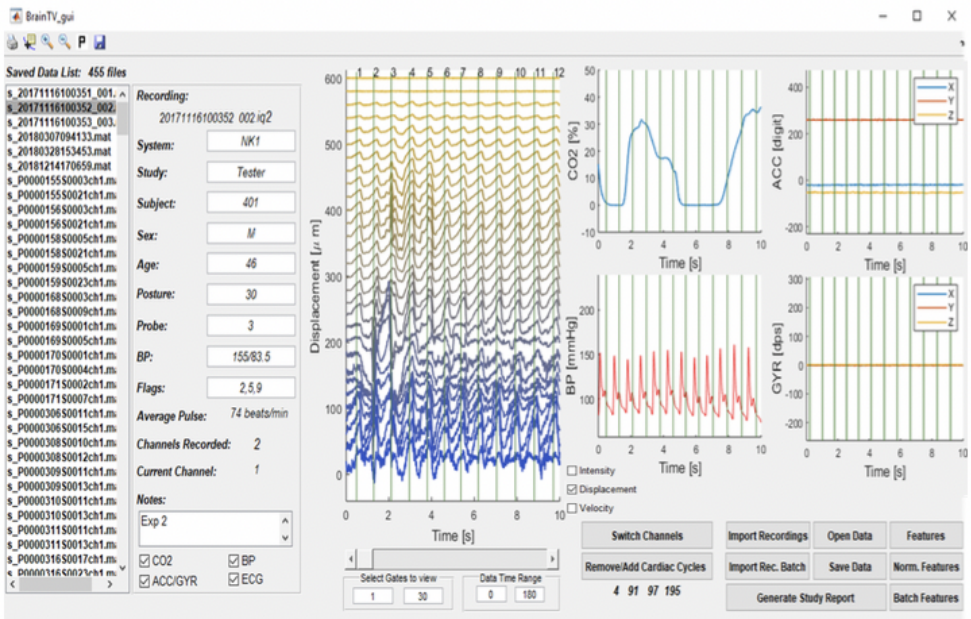

Table of Contents

Opening the GUI in MATLAB

- Copy the Brain TV GUI file path from windows explorer

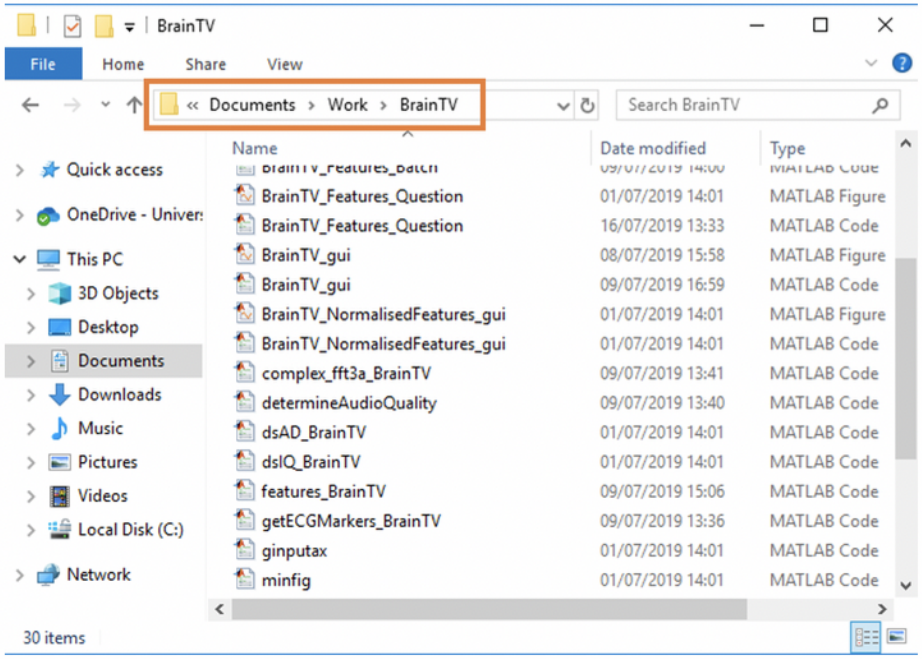

Figure 1

- Open MATLAB, paste copied file path, and press 'Enter' on your keyboard to set the correct directory for running the GUI

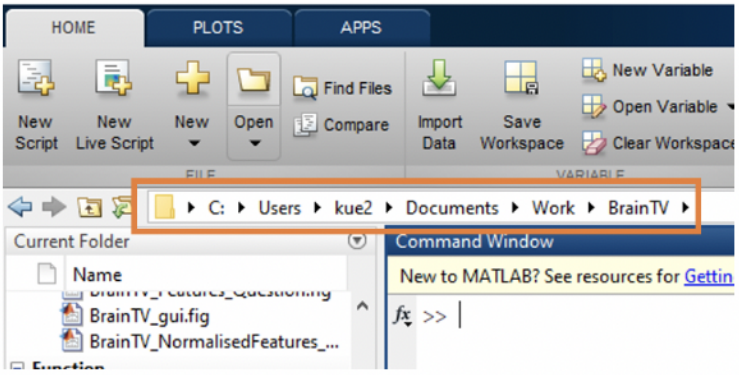

Figure 2

Running the GUI

To run the GUI, you can either:

1. Double click on the 'BrainTV_gui' script file under the function heading.
2. This will open up the code in Editor.
3. Click on the 'Run' button or press 'F5' on the keyboard.

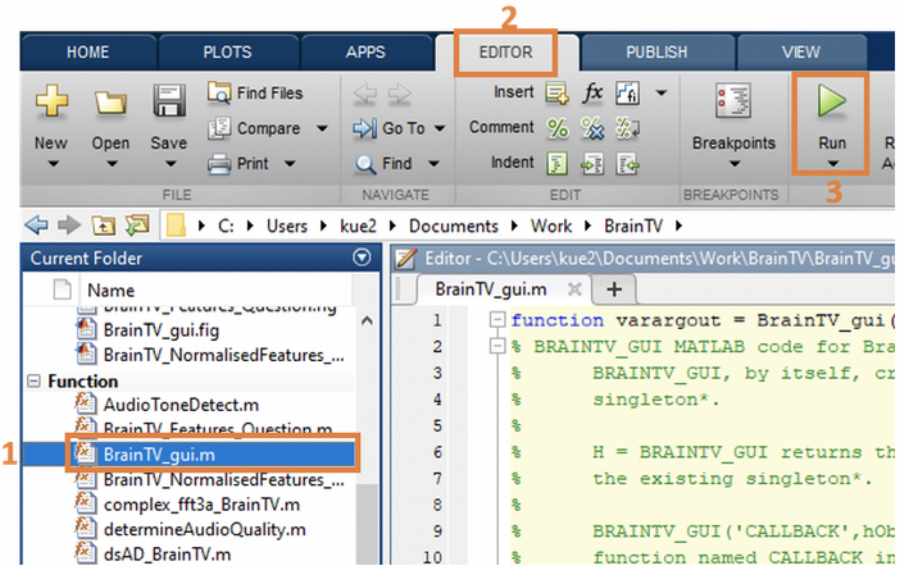

Figure 3

OR

1. Type 'BrainTV_gui' into the command window and press 'Enter' on the keyboard.

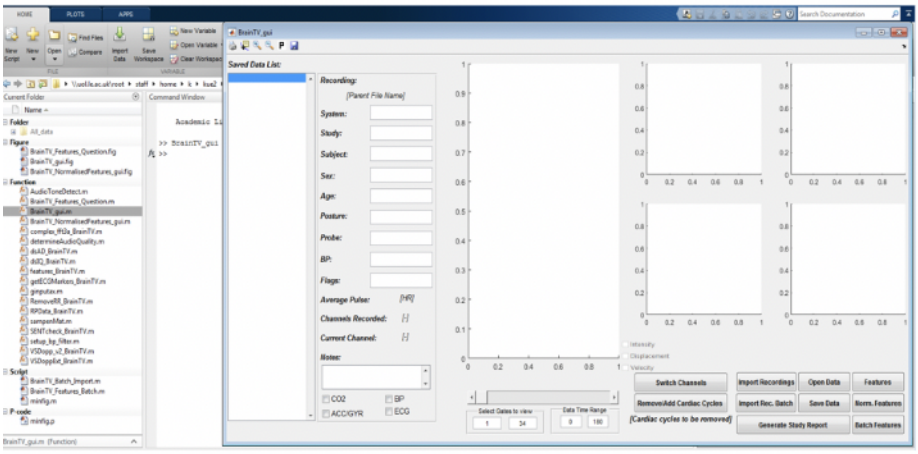

Figure 4

GUI Description

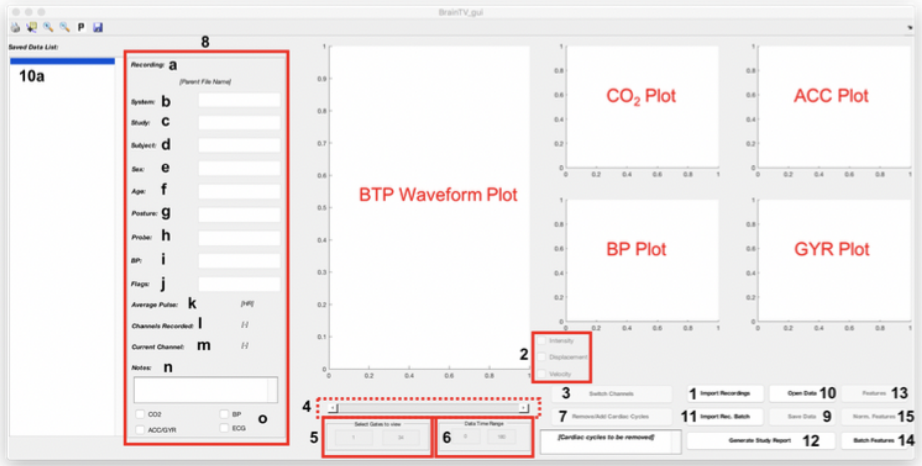

Figure 5

1. **Import Recordings:** This pushbutton is used to select a relevant Brain TV recording file in any folder which the GUI reads and displays. When such recording has a separate file containing time variables and/or cardiac cycle points, they both **must** be in the same folder.
2. **Waveform Plot Choice:** The waveform plot uses the displacement data as its default plot but the user may choose to switch data by clicking on "Velocity", "Displacement", or "Intensity" checkboxes. These checkboxes are disabled on default and are enabled once there is a waveform plot. If there are large velocity/displacement signals from a particular gate the intensity of the ultrasound echo at that gate can be viewed using the "Intensity" checkbox.
3. **Switch Channels:** This pushbutton is disabled on default. It is enabled only if imported recording contains more than one channel. It is then used to switch between waveform data in different channels.
4. **Slider:** This is used to scroll through data on all active plots. It is disabled on default and is only enabled if the range of the x-axis data time exceeds 10.
5. **Gates:** This shows the Doppler gates on display on the waveform plot and can be modified by user to view specific gates. It is disabled on default and only enabled when there is a waveform plot. This auto-corrects to default gates if user enters a wrong input. If a specific number of gates is entered prior to "Features" analysis then the features will only be calculated using the number of gates input.
6. **Time:** This shows the start and end time of recording. It is disabled on default and only enabled when there is a waveform plot. It is also used to calculate the average pulse from the data. The average pulse is updated if the user modifies the start and end times based on the cardiac cycles within the new time range. This auto-corrects to default times if user enters a wrong input. If a specific time range is entered prior to "Features" analysis, then the features will only be calculated using the time range that is input.

7. **Remove/Add Cardiac Cycles:** This pushbutton is disabled on default and is only enabled if imported recording has cardiac cycles within. The user must click on this pushbutton before clicking on any cardiac cycle in the waveform plot either to add to the list below the pushbutton or to remove from it. When all desired cardiac cycles have been added/removed, the pushbutton should be clicked again to enable "Features" calculation.
8. **Recording Profile:** This part contains unique details of the recording on display on the GUI. They may be entered automatically or manually by the user. The details are as follows:
    a. **Recording:** This shows the original file name of the recording and cannot be edited
    b. **System:** This shows the name of the system used for the recording and may vary, this can be edited
    c. **Study:** This shows the name of the Study being carried out for which current recording is a part of, this can be edited
    d. **Subject:** This shows a numeric unique identifier of the subject – the individual on whom the ultrasound probe was used, this is usually determined at the time of recording and may vary depending on the study.
    e. **Sex:** This shows the gender of subject, currently denoted as either 'M' or 'F'
    f. **Age:** This shows the age of subject in numerical form i.e. '56'
    g. **Posture:** This shows the posture of subject at the time when the recording was taken, denoted numerically in angular degrees, from '0' [as in a supine position] to '90' [as in a sitting up position]
    h. **Probe:** This shows the position where the probe was placed on subject when the recording was taken. It is denoted numerically and may differ between studies; an example is as follows:
        - 1 – forehead right
        - 2 – temporal right
        - 3 – forehead left
        - 4 – temporal left
    i. **BP:** This shows the Blood Pressure (BP) of subject. This may be entered manually even when there is no BP data in the recording. However, if BP data is included in subject's recording, the processes below occur:

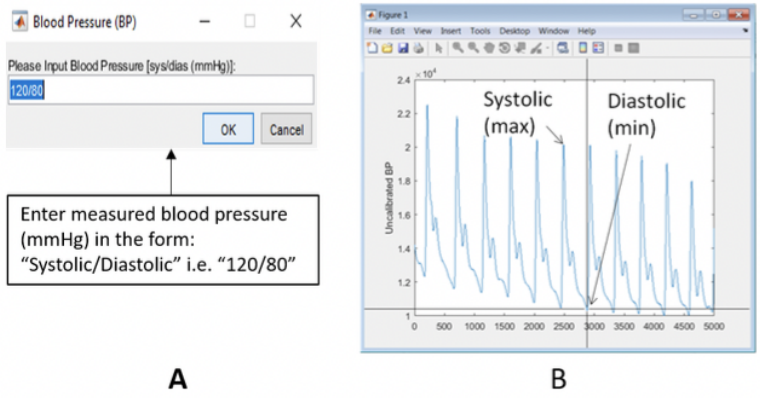

Figure 6

When an imported or saved recording contains BP data, the 'A' part of figure above is displayed in front of the GUI:

1) Enter the measured BP values from the cuff to calibrate the finapres recording e.g. 120/80 and click 'OK'. Entered BP values automatically fills in the BP in 8i.
2) User may also choose to click 'Cancel' to stop the processing of BP data.

Following from 1) above, the GUI is minimised and part 'B' follows:

3) A graph appears displaying the blood pressure recording for the first 10 seconds with cross-hairs over it for the user to select the peak of one of the blood pressure waveforms and then the minimum point (as in figure 'B'). This selection leads to the calibration of the BP data in the recording.

The figure in 3) above closes thereafter and the GUI is maximised again, showing the BP plot. If the user clicks on the 'Cancel' button, the process continues without processing BP reading (and BP is ticked) along with an input box for you to write the measured systolic and diastolic blood pressure readings from the arm cuff.

j. **Flags**: This shows flagged points in recordings numerically denoted.
k. **Average Pulse:** This shows the Average Pulse calculated based on the time range selected and the cardiac cycles within it. Firstly, the mean RR interval is calculated for the recording to give the Mean Cardiac Cycle Length, then the average pulse for the recording is calculated using the following equation:

$$Average\ Pulse\ (bpm) = \frac{60}{Mean\ Cardiac\ Cycle\ Length}$$

The value is rounded to the nearest integer and updated if the time range is modified.

l. **Channels Recorded:** This shows the number of channels in the recording i.e. '2'.
m. **Current Channel:** This shows the current channel of recording being displayed on the GUI i.e. '1'
n. **Notes:** This shows extra information unique to subject and recording.
o. **Ticks:** CO2, Blood Pressure (BP), Accelerometer and Gyroscope (ACC/GYR) and ECG are automatically ticked if the recording on display contains data particular to them respectively i.e. BP will be automatically ticked if BP data is in the recording on display in GUI.

9. **Save Data:** Click this button to save the imported data. This will save any removed cardiac cycles that have been selected, and will save any participant information that has been input. This will then be stored in a folder called 'Saved Data' which can be found on the left-hand side of the MATLAB window.
10. **Open Data:** Once this button is clicked, any data in the 'Saved Data' folder will be displayed on the left-hand side of the Brain TV GUI. These files can be viewed in the GUI by selecting them from this list.
11. **Import Recordings Batch:** This is similar to '1.' above but reads an excel sheet containing information regarding Brain TV recordings (such as file name, and participant information). The format of the excel sheet is shown in Figure 7, below:

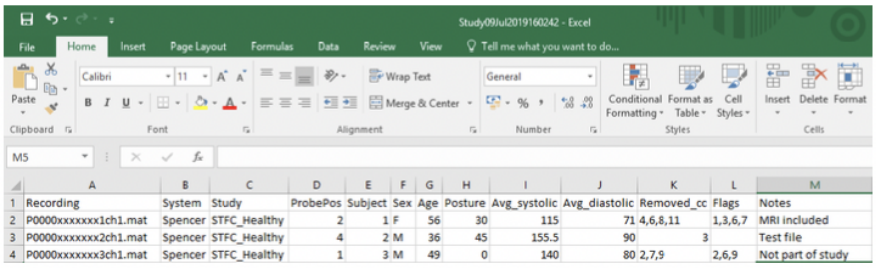

	A	B	C	D	E	F	G	H	I	J	K	L	M
1	Recording	System	Study	ProbePos	Subject	Sex	Age	Posture	Avg_systolic	Avg_diastolic	Removed_cc	Flags	Notes
2	P0000xxxxxxx1ch1.mat	Spencer	STFC_Healthy	2	1	F	56	30	115	71	4,6,8,11	1,3,6,7	MRI included
3	P0000xxxxxxx2ch1.mat	Spencer	STFC_Healthy	4	2	M	36	45	155.5	90	3		Test file
4	P0000xxxxxxx3ch1.mat	Spencer	STFC_Healthy	1	3	M	49	0	140	80	2,7,9	2,6,9	Not part of study

Figure 7

By clicking 'Import Rec. Batch' you will then be asked to select an Excel sheet to read (the Excel sheet should list all of the files names you want to import, as shown in the template above). Once you have selected an Excel sheet, the MATLAB code will begin importing the files. However, the excel sheet **must** be stored in the same folder as the recordings that are to be imported, along with their corresponding time variable and/or cardiac cycle files, if this is not the case an error will appear in the MATLAB command window. Once all files have been imported a message box will appear on the screen to say the Batch Import is complete. You will then be able to view the data using the 'Open Data' button.

12. **Generate Study Report:** After recordings have been imported it is possible to generate an Excel sheet in the form of the template shown in Figure 7 using the saved data. This will include all of the information input into the GUI for each recording, including selected cardiac cycles to remove. This is done by clicking the 'Generate Study Report' button and selecting all of the files from the 'Saved Data' folder that you wish to include in the Study Report Excel sheet.
13. **Features:** By clicking the 'Features' button, the MATLAB code will be used to calculate the features of the data that is currently open and displayed on the GUI. Once the features have been calculated, a window will appear which will allow you to save the features file. This window gives you the option to save as a new file by typing the desired file name into the text box (also a default name is provided), and clicking 'New'. There is also the option to append the newly calculated features to an existing features file, by clicking 'Append to existing' and then selecting the features file that you want to add to. The features can be viewed in MATLAB, the method for doing this is outlined in the following section titled 'Study file'.
14. **Batch Features:** Batch features is similar to features; however, this calculates the features for a batch of data, rather than individual recordings. To do this, click the 'Batch Features' button and then select all of the files that you want to calculate the features for. A box then appears which allows you to name the Batch features file that will be saved once the calculations are complete, it also allows you to select the number of gates, and time range that you would like to calculate the features for. These features can then be viewed using the method described in the following section.
15. **Normalised Features:** Clicking this pushbutton opens a separate window (shown in Figure 8) in which you can compare the normalised features for the recroding that is being displayed in the GUI when the pushbutton is pressed. Numerous features can be compared to see how they change over each cardiac cycle, for the duration of the recording. BTP features from single gates can be viewed using the tick boxes on the left hand side, while the features can

be viewed using the tick boxes on the right hand side of the window. If a recording has 2 channels then these can be viewed using the tick boxes at the bottom of the window.

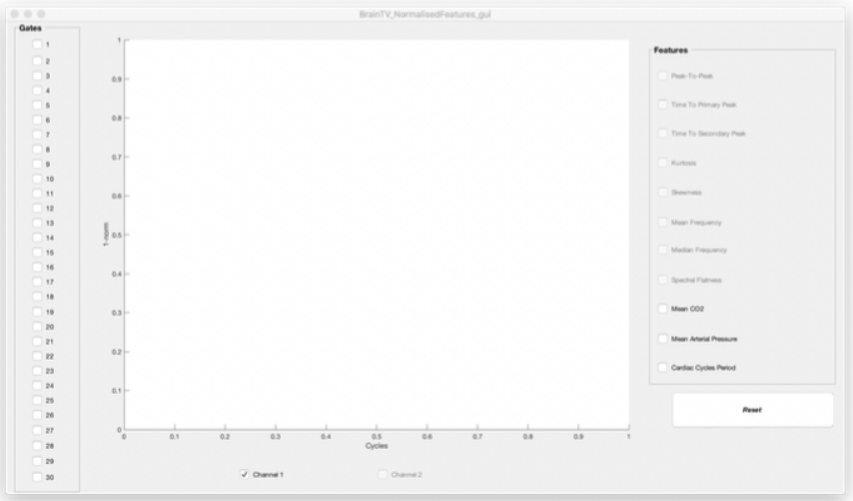

Figure 8

Study file

After calculating the features of the recordings, either using the "Features" or "Batch Features" pushbuttons described above, it is possible to view these calculated features in MATLAB. The features file will be saved in the "Batch Features" folder which can be found in the "Current folder" section of the MATLAB window (on the left hand side), this is labelled using an arrow in Figure 9. Once the features file has been located in this folder it should be double-clicked to load the data into the current workspace in MATLAB. Once this has been done a file called "Study" should appear in the Workspace section of the MATLAB window (on the right hand side), this is also labelled in Figure 9.

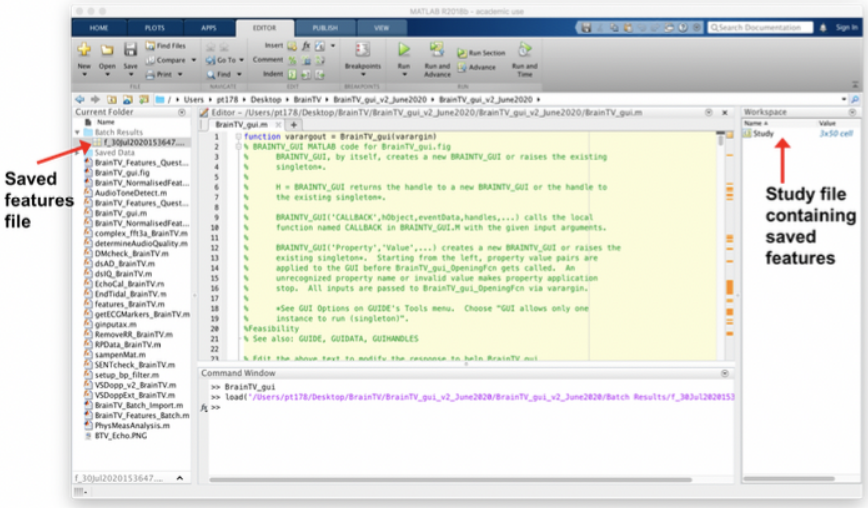

Figure 9

This Study file can be double-clicked to open the file in a new tab in the MATLAB window. The headings for each column are in the last row of the file. The first 10 columns give the recording information that can be seen in the GUI (section 8 highlighted in Figure 5). The remaining column headings are explained below:

11. Intensity: There are 3 parts to this cell, the first gives the gate number, the second gives the intensity of the ultrasound echo at each gate for the first channel, the third give the intensity of the ultrasound echo for the second channel (if 2 channels were used).

12. Displacement: This gives the displacement data used to plot the BTP signal waterfall plot, this is the displacement of the brain tissue before the features have been calculated.

13. First gate: This indicates the first gate that was included in the features calculations, e.g. if gates 1 – 30 were analysed, the first gate would be 1.

14. Last gate: This indicates the last gate that was included in the features calculations, e.g. if gates 1 – 30 were analysed, the last gate would be 30.

15. Time: This gives the time at which each ultrasound echo was received, this is used to plot the BTP signals in the waterfall plot.

16. Start time: This indicates the start of the time range that was analysed for this particular recording, e.g. if seconds 1- 15 were analysed, the start time would be 1.

17. End time: This indicates the end of the time range that was analysed for this particular recording, e.g. if seconds 1- 15 were analysed, the end time would be 15.

18. RR: This gives the time of each R wave.

19. RR_Mid: This gives the time of the midpoint between each RR interval.

20. BadRR: This indicates the cardiac cycles that were removed prior to features analysis.

21. Flags: These are the numerical flags that are input directly into the GUI, or in the Excel sheet used to import a batch of recordings.

22. BP: This gives the BP data used to plot the BP waveform in the GUI.

23. Co2: This gives the CO_2 data used to plot the CO_2 waveform in the GUI.

24. End-tidal CO2: This gives the end-tidal CO_2 value and the time at which it occurs, the end-tidal CO_2 is also indicated by the red stars on the CO_2 plot in the GUI.

25. Gyr: This gives the gyroscope data used to plot the gyroscope waveform in the GUI.

26. Acc: This gives the accelerometer data used to plot the accelerometer waveform in the GUI.

27. PTPG_Av_CV: This gives the peak-to-peak BTP amplitude values for each gate (with the first gate in the first row), averaged over the length of the recording. The peak-to-peak amplitude is the distance between the peak and the trough of the BTP signal. The second column gives the covariance on this result. N.B. standard deviation can be calculated by multiplying the mean value by the covariance.

28. Peak Direction: This gives an indication of the whether the peak or trough of the BTP waveform occurs first after the start of the R-R interval. A positive value indicates that the peak occurs before the trough, whereas a negative value indicates that the trough occurs first.

29. TTPPG_Av_CV: This gives the time-to-primary-peak for each gate (starting with the first gate), averaged over the length of the recording. The primary peak is the first peak in the BTP signal after the start of the R wave. The covariance for each is given in the second column.

30. TTSPG_Av_CV: This gives the time-to-secondary-peak for each gate (starting with the first gate), averaged over the length of the recording. The secondary peak is the second peak in the BTP signal after the start of the R wave. The covariance for each is given in the second column.

31. KUG_Av_CV: This gives the kurtosis of the BTP signal for each gate, averaged over the length of the recording. The covariance of each is given in the second column.

32. SKG_Av_CV: This gives the skewness of the BTP signal for each gate, averaged over the length of the recording. The covariance of each is given in the second column.

33. MEFG_Av_CV: This gives the mean frequency of the BTP signal for each gate, averaged over the length of the recording. The covariance of each is given in the second column.

34. MDFG_Av_CV: This gives the median frequency of the BTP signal for each gate, averaged over the length of the recording. The covariance of each is given in the second column.

35. SFG_Av_CV: This gives the sample frequency of the BTP signal for each gate, averaged over the length of the recording. The covariance of each is given in the second column.

36. Sample Entropy: This gives the sample entropy at each gate for the BTP signal.

37: [SPP, ED]: This gives the values for 'samples per period' and 'embedded dimensions' that are input before the features calculation is made.

38: Instantaneous Frequency: This gives the instantaneous heart rate for each cardiac cycle, this depends on the length of the cardiac cycle.

39: MAP_CC: This gives the mean arterial pressure for each cardiac cycle, calculated using the systolic and diastolic blood pressure.

40: Ave_CO2_CC: This gives the average value of the CO2 waveform for each cardiac cycle.

41: PTP_CC: This gives the peak-to-peak BTP amplitude for each cardiac cycle and each gate, starting with the first gate in the first row. The last row gives the Bulk BTP Amplitude for each cardiac cycle (the Bulk BTP Amplitude is calculated after averaging the BTP waveforms of each gate).

42. TTPP_CC: This gives the time-to-primary-peak for each cardiac cycle and each gate, starting with the first gate. The last row gives the TTPP of the Bulk signal for each cardiac cycle.

43. TTSP_CC: This gives the time-to-secondary-peak for each cardiac cycle and each gate, starting with the first gate. The last row gives the TTSP of the Bulk signal for each cardiac cycle.

44. KU_CC: This gives the kurtosis for each cardiac cycle and each gate, starting with the first gate. The last row gives the kurtosis of the Bulk signal for each cardiac cycle.

45. SK_CC: This gives the skewness for each cardiac cycle and each gate, starting with the first gate. The last row gives the skewness of the Bulk signal for each cardiac cycle.

46. MEF_CC: This gives the mean frequency for each cardiac cycle and each gate, starting with the first gate. The last row gives the skewness of the Bulk signal for each cardiac cycle.

47. MDF_CC: This gives the median frequency for each cardiac cycle and each gate, starting with the first gate. The last row gives the skewness of the Bulk signal for each cardiac cycle.

48. SF_CC: This gives the sample frequency for each cardiac cycle and each gate, starting with the first gate. The last row gives the skewness of the Bulk signal for each cardiac cycle.

49. PP_CC: This gives the pulse pressure of each cardiac cycle, this is calculated using the systolic and diastolic blood pressure.

50. Max_CO2_CC: This gives the maximum value of the CO_2 waveform for each cardiac cycle.

N.B. For all of the features associated with the BTP signal shows the features calculated for each gate (e.g. results from each gate in separate rows), with the value associated with the Bulk BTP waveform given in the last row. Therefore, if 30 gates are analysed, there should be 31 rows of values.

Troubleshooting & bugs

1. The prototype software developed by Nihon Kohden outputs the recording as one large file and also breaks the file down into 3 minute subsections. This helps with processing the data (especially on slow/old PCs). This will be an issue for BP calibration as normally a cuff measurement is made at the start of the recording. The code currently doesn't have an option to take the calibration from the first recording. **This definitely needs to be addressed**

Appendix B - Healthy Volunteer Study Documents

Chapter 3 study, participant information sheet:

PARTICIPANT INFORMATION SHEET (21/2/17, version 1)

Title: Brain tissue pulsation in healthy volunteers

Principal Investigator: Dr Emma Chung (emlc1@le.ac.uk, 0116 2525839)

Investigators: E. Chung[1,2], J. Nath[1], S. Berger[1], A Lecchini-Visintini[3], C. Banahan[1,2], S. Venturini[1]

1 Department of Cardiovascular Sciences, University of Leicester
2 University Hospitals of Leicester NHS Trust
3 Department of Engineering, University of Leicester

Invitation
You have been invited to take part in a research study. Before deciding if you wish to take part it is important for you to understand why the research is being done and what it will involve. Please take time to read the following information carefully and discuss it with others if you wish. Ask us if anything is not clear to you, or if you would like more information. Take time to decide whether or not you wish to take part.

What is the purpose of this study?
In a previous study we showed that pulsatile motion of brain tissue can be detected using ultrasound. Analysis of these measurements suggests that the magnitude of brain tissue pulsations varies with Age, Sex, Blood Pressure and Heart Rate, where young men exhibited the largest magnitude pulsations and elderly females the lowest. We now want to expand our preliminary study to investigate variations in Brain Tissue Pulsation in a much larger population of 160 healthy volunteers. Data gathered as part of this project will be statistically modelled to quantify how Age, Sex, Blood Pressure and Heart Rate influence brain tissue pulsations in healthy subjects.

Am I eligible to take part in this study?
If you are an adult over 18 years of Age and have no known brain injuries or heart problems you will be eligible to participate in this study.

What will be involved if I take part in the study?
We will briefly discuss involvement in the study and invite you to provide written informed consent. Following consent we will ask you to answer the following questions:

- Age?
- Male or female?
- Do you suffer from Migraine, high blood pressure, diabetes, or kidney problems?
- Are you taking any Blood Pressure altering medication

As part of our measurements, we will take your Blood Pressure using an arm-cuff device and will ask you to attach three stickers to your torso for monitoring heart rate using an ECG machine. For ultrasound examination, you will be asked to wear an elastic headband, which will be used to hold a small gel-covered ultrasound probe against the forehead. Our team will then record ultrasound signals along two different directions on both the left and right sides of the forehead. During the recordings we will ask you to close your eyes and remain as still as possible. Each measurement takes approximately one minute and may be repeated by up to two different observers. Setting up the measurement and obtaining the recordings should take no longer than 10-20 mins.

Do I have to take part?
It is up to you to decide whether or not to take part. If you do decide to take part you will be asked to sign a consent form. Even if you have given your consent, you are still free to withdraw at any time without giving a reason and no further data will be collected.

What are the possible disadvantages and risks of taking part?
The monitoring techniques we will be using are non-invasive and are not known to be harmful. As we are monitoring heart rate we may notice an irregular heartbeat. This is usually nothing to worry about, but if irregularities are observed we will let you know straight away and recommend you go to your GP for a check-up. As we are scientists, not doctors, we are unable to offer any medical advice. If the elasticated headband used to hold the ultrasound probe feels uncomfortable please let us know.

What are the benefits of taking part?
The information we get from the study will improve our understanding of pulsations of the brain in health and disease. As a 'thank you' we are offering each participant a £5 voucher.

Will the information obtained in the study be confidential?
If you wish to take part in this study your signed consent form will be kept in a secure Study Site File held by the Principal Investigator. Storage of data will conform to University of Leicester data governance policies: http://www2.le.ac.uk/offices/ias/dp/data-protection. If you would like a summary of the results of our research at the end of the study and/or would be interested in receiving information about future research studies please provide your contact details. All information and recordings from the study will be separated from your personal data so that you cannot be recognised. Only these anonymised data will be shared externally.

What if I am harmed by the study?
It is highly unlikely that you will be harmed during this study and there are no special compensation arrangements. If you are harmed due to someone's negligence, then you may have grounds for a legal action against the University of Leicester but you could have to pay for it.

What if I have a complaint?
If you have a concern about any aspect of this study, you should ask to speak with the researchers, who will do their best to answer your questions, or contact the Principal Investigator, Dr Emma Chung, **Tel**. 0116 2525839. You may also utilise complaints procedures regarding the conduct of this research through the University grievance procedures.

What will happen to the results of the research study?
The results of the study may be shared with external organisations, presented at medical conferences, and published in journals. All published data will be completely anonymous and your identity will not be revealed in any publication or presentation of these results.

Who has reviewed the study?
All research involving human subjects must receive approval from the College of Medicine Biological Sciences and Psychology Committee for Research Ethics Concerning Human Subjects (Non-NHS) before it can go ahead. Approval does not guarantee that you will not come to any harm if you take part. However, approval means that the committee is satisfied that your rights will be respected, that the study carries no more than minimal risk, and that you have been given sufficient information on which to make an informed decision.

Contact for further information
If you have any questions or queries about this research project please contact Emma Chung.
(**Tel:** 0116 2525839 **Email:** emlc1@le.ac.uk)

Thank you for reading this. This information leaflet is for you to keep.

Chapter 3 study, ethical approval letter:

University Ethics Sub-Committee for Medicine and Biological Sciences

09/03/2017

Ethics Reference: 10583-emlc1-cardiovascularsciences

TO:
Name of Researcher Applicant: Emma Chung
Department: Cardiovascular Studies
Research Project Title: Brain tissue pulsation measurements in healthy volunteers

Dear Emma Chung,

RE: Ethics review of Research Study application

The University Ethics Sub-Committee for Medicine and Biological Sciences has reviewed and discussed the above application.

1. Ethical opinion

The Sub-Committee grants ethical approval to the above research project on the basis described in the application form and supporting documentation, subject to the conditions specified below.

2. Summary of ethics review discussion

The Committee noted the following issues:
Hi Emma,
Thank you for addressing all those points raised and making relevant amendments. This looks really good now and Iâ€™m happy to approve the study.
Good Luck.
John

3. General conditions of the ethical approval

The ethics approval is subject to the following general conditions being met prior to the start of the project:

As the Principal Investigator, you are expected to deliver the research project in accordance with the University's policies and procedures, which includes the University's Research Code of Conduct and the University's Research Ethics Policy.

If relevant, management permission or approval (gate keeper role) must be obtained from host organisation prior to the start of the study at the site concerned.

4. Reporting requirements after ethical approval

You are expected to notify the Sub-Committee about:

- Significant amendments to the project
- Serious breaches of the protocol
- Annual progress reports
- Notifying the end of the study

5. Use of application information

Details from your ethics application will be stored on the University Ethics Online System. With your permission, the Sub-Committee may wish to use parts of the application in an anonymised format for training or sharing best practice. Please let me know if you do not want the application details to be used in this manner.

Best wishes for the success of this research project.

Yours sincerely,

Dr. Chris Talbot
Chair

Chapter 5 study, participant information sheet:

UNIVERSITY OF LEICESTER

PARTICIPANT INFORMATION SHEET (12/02/2019, version 1.2)

Title: Brain Tissue Pulsation in Healthy Volunteers with Different Variables

Principal Investigator: Dr Emma Chung (emlc1@leicester.ac.uk)

Investigators: M. Alharbi[1], J. Ince[1], P. Turner[1], J. Minhas[1,2], E. Chung[1,2]

[1] Department of Cardiovascular Sciences, University of Leicester

[2] University Hospitals of Leicester NHS Trust

Invitation
You have been invited to take part in a research study. Before deciding if you wish to take part it is important for you to understand why the research is being done and what it will involve. Please take time to read the following information carefully and discuss it with others if you wish. Ask us if anything is not clear to you, or if you would like more information. Take time to decide whether or not you wish to take part.

What is the purpose of this study?
Recently we showed that movement of the brain can be detected in healthy volunteers over a range of depths. This was done by placing a small ultrasound probe on the forehead and analysing the generated waveform to measure brain tissue movement.

In this study, we would like to obtain measurements from the forehead to assess the reproducibility of measuring brain tissue movement at different time points in the same individual and also to assess whether different observes can obtain the same measurements (protocol one).

Also in this study, we would like to investigate whether changing some variables could alter brain tissue movement. These variables are asking the participant to have higher levels of carbon dioxide (hypercapnia) (protocol two), change their posture (protocol three), and breath fast (hyperventilation) (protocol four).

All of these variables could be different in a clinical patient, so investigation of their effects with this study will improve our understanding of brain tissue movements.

What will be involved if I take part in the study?
We will discuss involvement in the study and you will have at least 24 hours to decide if you want to take part. If you are keen to participate, please contact us and we will invite you to visit our lab to complete the consent process and perform the measurements.

For the ultrasound measurements, you will be asked to wear an elastic headband, which will be used to hold a small gel-covered ultrasound probe against your forehead. During ultrasound monitoring you will receive ECG (heart rate) monitoring using 3 self-

adhesive leads attached to your chest; this will allow us to calibrate brain tissue movements with your heart rate.

You will also receive blood pressure monitoring before and after each measurement using a cuff around your arm. Also, you will have continuous blood pressure monitoring by small cuff around your middle finger. CO2 monitoring using a nasal adapter (which has 2 plastic prongs which sit in either nostril) will also be used.

This study includes four different recordings, you can choose to participate in any of the protocols as you wish.

Firstly, the first researcher will take two different recordings in two different probe positions on your forehead as described in Table 1. Then, the second researcher will repeat these readings for these probe positions.

Following this, you will be asked to breathe a carbon dioxide and oxygen mixture through a face mask to measure whether increased CO2 levels cause any measurement alterations (Table 2). You will then have a rest period and the process will be repeated. Additional carbon dioxide has been used in numerous previous research studies and is deemed to be safe.

Next, you will be asked to change position, as described in Table 3, to check the effect of different postures on brain tissue movements.

Afterwards, the second researcher will ask you to hyperventilate for 90 seconds as shown in Table 4. This will lead to lowering of the CO2 level in your body. You will then be given a rest period and you will then be asked to repeat this.

The total time for the recordings should be around an hour. We may ask your permission to take photos or videos of part of the measurements to record the position of the probe. These would be accessed by our research team only.

Table 1 - Protocol One

First Researcher Readings	- 30 second recording taken with the probe holder 1cm above each eyebrow. - 30 second reading taken with the probe holder directly above the middle of the eyebrow.
Second Researcher Readings	- 30 second reading taken with the probe holder 1cm above each eyebrow. - 3 minute recording taken with the probe holder directly above the middle of the eyebrow.

Table 2 - Protocol Two

Baseline Reading	1 minute recording taken as a baseline level.
CO_2 Administration	Recording with 5% CO_2 administration using a face mask for 90 seconds. After CO_2 administration, a 1 minute recording is taken to monitor recovery. A baseline recording of 1 minute is then taken. The participant then will have 1 minute of rest.
Repeated CO_2 Administration	Repeat the CO_2 administration step.

Table 3 - Protocol Three

Baseline Reading	1 minute recording taken as a baseline level.
Sitting at 90^0	The participant will be asked to sit upright and then a 1 minute recording will be taken.
Reclined 30^0	The participant will be asked to lie reclined at 30º and then a 1 minute recording will be taken.
Supine	The participant will be asked to lie flat and then a 1 minute recording will be taken.
Reclined 30^0	The participant will be asked to lie reclined at 30º and then a 1 minute recording will be taken.

Table 4 - Protocol Four

Baseline Reading	1 minute recording taken as a baseline level.
Hyperventilation	The participant will be asked to hyperventilate in time with a metronome for 90 seconds. This will be followed with a 1 minute recovery recording and a 1 minute baseline recording. The participant will then have a 1 minute rest.
Repeated CO_2 Administration	Repeat the hyperventilation step at a slightly higher rate.

If any unexpected findings are found during the protocol, the researcher will advise you to visit your GP.

Do I have to take part?
It is up to you whether to take part. If you do decide to take part you will be asked to sign a consent form. Even if you have given your consent, you are still free to withdraw at any time without giving a reason. No further data will be collected, but any data collected so far will still be included in our analysis, unless you request otherwise.

What are the possible disadvantages and risks of taking part?
All of the monitoring techniques we will be using are non-invasive and are not known to be harmful. Although some of the monitoring equipment many feel uncomfortable, physiological monitoring using transcranial Doppler ultrasound and ECG measurements have been used clinically for many years and are generally well tolerated.

As mentioned above, supplementary carbon dioxide has been used in many other research studies and is deemed to be safe. In the event of any side effects, the carbon dioxide nasal prongs can be easily removed.

What are the benefits of taking part?
Participants receive a £5 gift voucher. Also, by giving your time towards this research study, we can further our knowledge about brain tissue motion, which could guide future clinical advancements.

Will the information obtained in the study be confidential?
If you wish to take part in this study, your signed consent form will be kept in a secure Study Site File held by the principal investigator. Any identifiable information will remain confidentially stored in a secure location. All other information and physiological measurements collected about you during the course of the research will be anonymised so that you cannot be recognised. The data may be shared with

external researchers, but all information that leaves the university will have your name, address, and other personal data removed.

What if I have a complaint?
If you have any concerns about the way you have been approached or treated in connection with the study, you should ask to speak to Dr Emma Chung on 0116 2525839 who will do her best to answer your questions and address your concerns. If you are not satisfied with the response you receive from the principle investigator, there is also a formal university complaints procedure. In the first instance write to the Chair of the College of Life Sciences Research Ethics Committee, currently Dr. Chris Talbot (cjt14@le.ac.uk).

What will happen to the results of the research study?
The results of this research study will be used to further our knowledge on brain tissue motion. The results may also be presented at medical conferences and published in a specialised medical journal. All published data will be anonymous, and your identity will not be revealed in any publication or presentation of the results.

Who has reviewed the study?
Our research project will receive approval from the College of Life Sciences Committee for Research Ethics Concerning Human Subjects before it goes ahead. Approval does not guarantee that you will not come to any harm if you take part. However, approval means that the committee is satisfied that your rights will be respected, that the study carries no more than minimal risk, and that you have been given sufficient information on which to make an informed decision.

Contact for further information
If you have any questions or queries about this research project, please contact Dr Emma Chung; email emlc1@le.ac.uk, Tel: 0116 2525839.

Thank you for reading this. This information leaflet is for you to keep.

Chapter 5 study, ethical approval letter:

Medicine and Biological Sciences Research Ethics Committee

03/01/2019

Ethics Reference: 18110-ji46-ls:medicine,schoolof

TO:
Name of Researcher Applicant: Jonathan Ince
Department: Cardiovascular Studies
Research Project Title: Brain Tissue Pulsation in Healthy Volunteers with Different Variables
Module Name or Course: Intercalated Masters in Medical Research
Supervisor's or Module Leader's Name: Emma Chung

Dear Jonathan Ince,

RE: Ethics review of Research Study application

The Medicine and Biological Sciences Research Ethics Committee has reviewed and discussed the above application.

1. Ethical opinion

The Committee grants ethical approval to the above research project on the basis described in the application form and supporting documentation, subject to the conditions specified below.

2. Summary of ethics review discussion

The Committee noted the following issues:
Minor amendment approved.

3. General conditions of the ethical approval

The ethics approval is subject to the following general conditions being met prior to the start of the project:

As the Principal Investigator, you are expected to deliver the research project in accordance with the University's policies and procedures, which includes the University's Research Code of Conduct and the University's Research Ethics Policy.

If relevant, management permission or approval (gate keeper role) must be obtained from host organisation prior to the start of the study at the site concerned.

4. Reporting requirements after ethical approval

You are expected to notify the Committee about:

- Significant amendments to the project
- Serious breaches of the protocol
- Annual progress reports
- Notifying the end of the study

5. Use of application information

Details from your ethics application will be stored on the University Ethics Online System. With your permission, the Committee may wish to use parts of the application in an anonymised format for training or sharing best practice. Please let me know if you do not want the application details to be used in this manner.

Best wishes for the success of this research project.

Yours sincerely,

Dr. Chris Talbot
Chair

Appendix C - State-space Model Matrices

The descriptor matrix E consists of compliances between adjacent compartments, some of which are pressure dependent.

```
E = [Cit+Cyi+24 0  -Cyi  0  0  0  0  0  0  0  0  0  0  -Cit  0  0;
-Cyi-8-24  0  Cym+Cyi+Cyo -Cyo  0  0  0  0  0  0  0  0  0  0  0  -Cym;
24  0  -Cyo  Cto+Cyo  0  0  0  0  0  0  0  0  0  0  -Cto  0  0;
0  0  0  0  Czg  0  -Czg  0  0  0  0  0  0  0  0  0  0;
0  0  0  0  -Czg  0  Czg+Cgx+Cgm  -Cgx  0  0  0  0  0  0  0  0  -Cgm;
0  0  0  0  0  0  -Cgx  Cgx  0  0  0  0  0  0  0  0  0;
0  0  0  0  0  0  0  0  Cab+Caf  0  0  0  0  -Caf  0  -Cab  0;
0  0  0  0  0  0  0  0  0  0  1  0  0  -1  0  0  0;
0  0  0  0  0  0  0  0  0  0  0  Cbv+Cfv  0  -Cfv  0  -Cbv  0;
0  0  0  0  0  0  0  0  0  0  0  0  Cts  0  -Cts  0  0;
0  0  0  0  0  0  0  0  -Caf  0  0  -Cfv  0  Caf+Cfb+Cfv  0  -Cfb  0;
-Cit  0  0  -Cto  0  0  0  0  0  0  0  0  -Cts  0  Cts+Cbt+Cto+Cit  -Cbt  0;
0  0  0  0  0  0  0  0  -Cab  0  0  -Cbv  0  -Cfb  -Cbt  Cab+Cbv+Cfb+Cbt  0;
0  0  0  0  0  0  0  0  0  0  0  0  0  0  0  0  1;
0  0  0  0  0  0  0  0  0  0  0  0  0  0  0  0  0;
0  0  0  0  0  0  0  0  0  0  0  0  0  0  0  0  0;
0  0  0  0  0  0  0  0  0  0  0  0  0  0  0  0  0];
```

The A matrix consists of fluidities describing the flows between compartments, all of which are constant in the model. K_{JY} and K_{DG} are the fluidities of the filtration flow between tissue compartments and vessels, there are both constant.

```
A = [-Ziz-Zia  0  0  0  Ziz  0  0  0  Zia  0  0  0  0  0  0  0  0;
0  Kjy -Kjy  0  0  0  0  0  0  0  0  0  0  0  0  0  0;
0  Zjo  0  -Zjo-Zxo-Zso-Zto  0  0  0  Zxo  0  0  0  0  Zso  0  Zto  0  0;
Ziz 0  0  0  -Ziz  0  0  0  0  0  0  0  0  0  0  0  0;
0  0  0  0  0  Kdg -Kdg  0  0  0  0  0  0  0  0  0  0;
0  0  0  Zxo  0  Zdx  0  -Zdx-Zxo  0  0  0  0  0  0  0  0  0;
Zia 0  0  0  0  0  0  0  -Zia  0  0  0  0  0  0  0  0;
0  0  0  0  0  0  0  0  0  0  0  0  0  0  0  0  0;
0  0  0  0  0  0  0  0  0  Zcv  0  -Zcv-Zbv-Zvs  Zvs  0  0  Zbv  0;
0  0  0  Zso  0  0  0  0  0  0  0  0  Zvs  -Zvs-Zts-Zso  0  Zts  0  0;
0  0  0  0  0  0  0  0  0  0  0  0  0  -Zfb-Zft  Zft  Zfb  0;
0  0  0  Zto  0  0  0  0  0  0  0  0  0  Zts  Zft  -Zft-Zbt-Zts-Zto  Zbt  0;
0  0  0  0  0  0  0  0  0  Zcb  0  Zbv  0  Zfb  Zbt  -Zcb-Zfb-Zbv-Zbt  0;
0  0  0  0  0  0  0  0  0  0  0  0  0  0  0  0  0;
0  -Zjo-Kjy  Kjy Zjo  0  0  0  0  0  0  0  0  0  0  0  0  0;
0  0  0  0  0  -Zdx-Kdg  Kdg  Zdx  0  0  0  0  0  0  0  0  0;
0  0  0  0  0  0  0  0  0  -Zcb-Zcv  0  Zcv  0  0  0  Zcb  0];
```

The B matrix consists of the coefficients relating to the inputs in the model. The terms containing K_{JY} and K_{DG} are constant terms relating to filtration. $Q_{PF}m$ is the mean flow from the choroid plexus to the intracranial CSF compartment, which is constant in the model.

```
B = [0 1  0  0  0  0  0  -1  0  0;
0  0  1  -1  -Kjy*Sigmajy*Pijy  0  -1  0  0  0  0;
-1 0  0  0  0  1  1  0  0  0  0;
0  0  0  0  0  0  0  0  0  -1  0;
0  0  0  0  -Kdg*Sigmadg*Pidg  -1  0  0  0  0  0;
0  0  0  0  0  0  0  0  0  0  0;
0  0  0  0  0  0  0  -1  0  0  -1;
0  0  0  0  0  0  0  0  0  0  0;
0  0  0  0  -Qpfm 0  0  0  0  0  0;
0  0  0  0  0  0  0  0  0  0  0;
0  0  0  0  Qpfm  0  0  0  0  0  0;
0  0  0  0  0  0  0  0  0  0  0;
0  0  0  0  0  0  0  0  0  0  1;
0  0  0  0  0  0  0  0  0  0  0;
0  0  0  0  Kjy*Sigmajy*Pijy  0  0  0  1  0  0;
0  0  0  0  Kdg*Sigmadg*Pidg  0  0  0  0  1  0;
0  0  0  0  0  0  0  1  0  0  0];
```

References

[1] ME. Wagshul, PK. Eide, and JR. Madsen. The pulsating brain: A review of experimental and clinical studies of intracranial pulsatility. *Fluids and Barriers of the CNS*, 8(5), 2011.

[2] X. Zhong, CH. Meyer, DJ. Schlesinger, JP. Sheehan, FH. Epstein, JM. Larner, SH. Benedict, PW. Read, K. Sheng, and J. Cai. Tracking brain motion during the cardiac cycle using spiral cine-DENSE MRI. *Medical Physics*, 36(8):3413–3419, July 2009.

[3] D. Greitz, R. Wirestam, A. Franck, B. Nordell, C. Thomsen, and F. Ståhlberg. Pulsatile brain movement and associated hydrodynamics studied by magnetic resonance phase imaging. *Neuroradiology*, 34:370–380, 1992.

[4] O Balédent, MC. Henry-Feugeas, and I. Idy-Peretti. Cerebrospinal fluid dynamics and relation with blood flow: A magnetic resonance study with semiautomated cerebrospinal fluid segmentation. *Investigative Radiology*, 37:368–377, 2001.

[5] DE. Strandness and DS. Sumner. *Hemodynamics for Surgeons*. Grune and Stratton, 1975.

[6] JB Weaver, AJ. Pattison, MD. McGarry, IM. Perreard, JG. Swienckowski, CJ. Eskey, SS. Lollis, and KD. Paulsen. Brain mechanical property measurement using MRE with intrinsic activation. *Physics in Medicine and Biology*, 57(22):7275–7287, October 2012.

[7] V. Kiviniemi, X. Wang, V. Korhonen, T. Keinanen, T. Tuovinen, J. Autio, P. LeVan, S. Keilholz, YF. Zang, J. Hennig, and M. Nedergaard. Ultra-fast magnetic resonance encephalography of physiological brain activity - glymphatic pulsation mechanisms? *Journal of Cerebral Blood Flow and Metabolism*, 36(6):1033–1045, 2016.

[8] S. Atwi, AD. Robertson, AE. Theyers, J. Ramirez, RH. Swartz, S. Marzolini, and BJ. MacIntosh. Cardiac-related pulsatility in the insula is directly associated with middle cerebral artery pulsatility index. *J Magn Reson Imaging*, 51:1454–1462, 2020.

[9] I. Terem, WW. Ni, M. Goubran, M. Salmani Rahimi, G. Zaharchuk, KW. Yeom, ME. Moseley, M. Kurt, and SJ. Holdsworth. Revealing subvoxel motions of brain tissue using phase-based amplfied MRI (aMRI). *Magnetic Resonance in Medicine*, pages 2549–2559, 2018.

[10] SR. Ommen, RA. Nishimura, CP. Appleton, FA. Miller, JK. Oh, MM. Redfield, and AJ. Tajik. Clinical utility of Doppler echocardiography and tissue Doppler imaging in the estimation of left ventricular filling pressures: A comparative simultaneous Doppler-catheterization study. *Circulation*, 102:1788–1794, 2000.

[11] JC. Kucewicz, B. Dunmire, DF. Leotta, H. Panagiotides, M. Paun, and KW. Beach. Functional tissue pulsatility imaging of the brain during visual stimulation. *Ultrasound in Medicine and Biology*, 33:681–690, 2007.

[12] JC. Kucewicz, B. Dunmire, ND. Giardino, DF. Leotta, M. Paun, SR. Dager, and KW. Beach. Tissue pulsatility imaging of cerebral vasoreactivity during hyperventilation. *Ultrasound in Medicine and Biology*, 34(8):1200–1208, 2008.

[13] R. Ternifi, X. Cazals, T. Desmidt, F. Andersson, V. Camus, J-P. Cottier, and et al. Ultrasound measurements of brain tissue pulsatility correlate with the volume of MRI white-matter hyperintensity. *Journal of Cerebral Blood Flow and Metabolism*, 34:942–944, 2014.

[14] L. Angel, B. Bouazzaoui, M. Isingrini, S. Fay, L. Taconnat, and S. Vanneste. Brain tissue pulsatility mediates cognitive and electrophysiological changes in normal aging: Evidence from ultrasound tissue pulsatility imaging (TPI). *Brain Cogn*, 123:74–80, 2018.

[15] T. Desmidt, F. Andersson, B. Brizard, PA. Dujardin, J-P. Cottier, and F. Patat. Ultrasound measures of brain pulsatility correlate with subcortical brain volumes in healthy young adults. *Ultrasound in Medicine and Biology*, 44(11):2307–13, 2018.

[16] MA. Siragusa, B. Brizard, P-A. Dujardin, JP. Remenieras, F. Patat, V. Gissot, V. Camus, C. Belzung, W. El-Hage, T. Wosch, and T. Desmidt. When classical music relaxes the brain: An experimental study using ultrasound brain tissue pulsatility imaging. *International Journal of Psychophysiology*, 150:29–36, 2020.

[17] T. Desmidt, ME. Hachemi, JP. Remenieras, P. Lecomte, N. Ferreira-Maldent, F. Patat, and V. Camus. Ultrasound brain tissue pulsatility is decreased in middle aged and elderly type 2 diabetic patients with depression. *Psychiatry Research Neuroimaging*, 193(1):63–64, July 2011.

[18] T. Desmidt, B. Brizard, PA. Dujardin, R. Ternifi, JP. Remenieras, F. Patat, F. Andersson, JP. Cottier, E. Vierron, V. Gissot, K. Kim, H. Aizenstein, W. El-Hage, and V. Camus. Brain tissue pulsatility is increased in midlife depression: a comparative study using ultrasound pulsatility imaging. *Neuropsychopharmacology*, 42:2575–2582, June 2017.

[19] J. Biogeau, T. Desmidt, PA. Dujardin, R. Ternifi, C. Eudo, E. Vierron, JP. Remenieras, F. Patat, V. Camus, and T. Constans. Ultrasound tissue pulsatility imagine suggests impairment in global brain pulsatility and small vessels in elderly patients with orthostatic hypotension. *Journal of Stroke and Cerebrovascular Diseases*, 26(2):246–251, February 2017.

[20] R. Jurkonis, M. Makunaite, M. Baranauskas, A. Lukosevicius, A. Sakalauskas, V. Matijosaitis, and D. Rastenyte. Quantificantion of endogenous brain tissue displacement imaging by radiofrequency ultrasound. *Diagnostics*, 10:57, 2020.

[21] M. Baranauskas, R. Jurkonis, A. Lukosevicius, M. Makunaite, V. Matijosaitis, R. Gleizniene, and D. Rastenyte. Ultrasonic assessment of the medial temporal lobe tissue displacements in Alzheimer's disease. *Diagnostics*, 10(2):57, 2020.

[22] J. Ince, M. Alharbi, JS. Minhas, and EM. Chung. Ultrasound measurement of brain tissue movement in humans: a systematic review. *Ultrasound*, 28(2):70–81, 2020.

[23] M. Soellinger, AK. Rutz, S. Kozerke, and P. Boesiger. 3D cine displacement-encoded MRI of pulsatile brain motion. *Magnetic Resonance in Medicine*, 61:153–162, 2009.

[24] APG. Hoeks, PJ. Brands, TGJ. Arts, and RS. Reneman. Subsample volume processing of Doppler ultrasound signals. *Ultrasound in Medicine and Biology*, 20(9):953–965, 1994.

[25] P. Turner, C. Banahan, M. Alharbi, J. Ince, S. Venturini, S. Berger, I. Bnini, J. Campbell, KW. Beach, M. Horsfield, M. Oura, A. Lecchini-Visintini, and EML. Chung. Brain tissue pulsation in healthy volunteers. *Ultrasound in Medicine and Biology*, 46(12):3268–3278, December 2020.

[26] JL. Peixoto. Hierarchical variable selection in polynomial regression models. *The American Statistician*, 41(4):311–313, 1987.

[27] R. Aaslid, TM. Markwalder, and H. Nornes and. Noninvasive transcranial Doppler ultrasound recording of flow velocity in basal cerebral arteries. *Journal of Neurosurgery*, 57(6):769–774, December 1982.

[28] J. Naqvi, KH. Yap, G. Ahmad, and J. Ghosh. Transcranial Doppler ultrasound: A review of the physical principles and major applications in critical care. *International Journal of Vascular Medicine*, 2013:13 pages, 2013.

[29] DH. Evans and J. Gittins. Limits of uncertainty in measured values of embolus-to-blood ratios in dual-frequency TCD recordings due to non-identical sample volume shapes. *Ultrasound in Medicine and Biology*, 31(2):233 – 242, 2005.

[30] B. Brekke, LCL. Nilsen, J. Lund, H. Torp, T. Bjastad, BH. Amundsen, A. Stoylen, and SA. Aase. Ultra-high frame rate tissue Doppler imaging. *Ultrasound in Medicine and Biology*, 40(1):222–231, 2014.

[31] MO. Culjat, D. Goldenberg, P. Tewari, and RS. Singh. A review of tissue substitutes for ultrasound imaging. *Ultrasound in Medicine and Biology*, 36(6):861–873, 2010.

[32] I. Reinertsen and DL. Collins. A realistic phantom for brain-shift simulations. *Medical Physics*, 33(9):3234–3240, 2006.

[33] KJM. Surry, HJB. Austin, A. Fenster, and TM. Peters. Poly (vinyl alcohol) cryogel phantoms for use in ultrasound and MR imaging. *Physics in Medicine and Biology*, 49:5529–5546, 2004.

[34] P. Scheel, C. Ruge, and M. Schöning. Flow velocity and flow volume measurements in the extracranial carotid and vertebral arteries in healthy adults: reference data and the effects of age. *Ultrasound in Medicine and Biology*, 26(8):1261–1266, 2000.

[35] J. Alastruey, KH. Parker, J. Peiró, SM. Byrd, and SJ. Sherwin. Modelling the circle of Willis to assess the effects of anatomical variations and occlusions on cerebral flows. *Journal of Biomechanics*, 40:1794–1805, 2007.

[36] JS. Minhas, T. Robinson, and R. Panerai. $PaCO_2$ measurement in cerbral haemodynamics: face mask or nasal cannulae? *Physiological measurement*, 38(7), 2017.

[37] JS. Minhas, RB. Panerai, and TG. Robinson. Modelling the cerebral haemodynamic response in the physiological range of $PaCO_2$. *Physiological measurement*, 39(6):65001–065001, 2018.

[38] JS. Minhas, RB. Panerai, D. Swienton, and TG. Robinson. Feasibility of improving cerebral autoregulation in acute intracerebral hemorrhage (BREATHE-ICH) study: Results from an experimental interventional study. *International Journal of Stroke*, pages 174749301987369–1747493019873690, 2019.

[39] J. Donnelly, KP. Budohoski, P. Smielewski, and M. Czosnyka. Regulation of the cerebral circulation: bedside assessment and clinical applications. *Critical care (London, England)*, 20(1):129, 2016.

[40] P. Liu, JB. DeVis, and H. Lu. Cerebrovascular reactivity (cvr) mri with co_2 challenge: A technical review. *Neuroimage*, 187:104–115, 2019.

[41] M. Alharbi, P. Turner, J. Ince, M. Oura, KU. Ebirim, A. Almudayni, A Lecchini-Visintini, JS. Minhas, and EML. Chung. The effects of hypocapnia on brain tissue pulsations. *Brain Sciences*, 10(9):614, September 2020.

[42] J. Minhas, V. Haunton, T. Robinson, and R. Panerai. Determining differences between critical closing pressure and resistance-area product: responses of the healthy young and old to hypocapnia. *Pflugers Arch - Eur J Physiol.*, 471(8):1117–1126, 2019.

[43] V. Novak, JM. Spies, P. Novak, BR. McPhee, TA. Rummans, and PA. Low. Hypocapnia and cerebral hypoperfusion in orthostatic intolerance. *Stroke*, 29(9):1876–1881, 1998.

[44] JF. Burnum, JB. Hickam, and HD. Mcintosh. The effect of hypocapnia on arterial blood pressure. *Circulation*, 9(1):89–95, 1954.

[45] CJ. Avezaat, JH. van Eijndhoven, and DJ. Wyper. Effects of hypercapnia and arterial hypotension on cerebrospinal fluid pulse pressure and intracranial volume-pressure relationships. *Journal of Neurology, Neurosurgery and Psychiatry*, 43(3):222–234, 1980.

[46] ASM. Salinet, JS. Minhas, RB. Panerai, E. Bor-Seng-Shu, and TG. Robinson. Do acute stroke patients develop hypocapnia? A systematic review and meta-analysis. *Journal of the Neurological Sciences*, 402:30–39, 2019.

[47] A. Marmarou. *A Theoretical Model and Experimental Evaluation of the Cerebrospinal Fluid System*. PhD thesis, Drexel University, Philadelphia, 1973.

[48] O. Hoffman. Biomathematics of intracranial CSF and haemodynamics. simulation and analysis with the aid of a mathematical model. *Acta Neurochirurgica Supplement*, 40:117–130, 1987.

[49] M. Ursino. A mathematical model of overall cerebral blood flow circulation in the rat. *IEEE Trans Biomed Eng*, 1991.

[50] W. Wakeland and B. Goldstein. A review of physiological simulation models of intracranial pressure dynamics. *Computers in Biology and Medicine*, 38:1024–1041, 2008.

[51] X. Zhang, JE. Medow, BJ. Iskandar, F. Wang, M. Shokoueinejad, J. Koueik, and JG. Webster. Invasive and noninvasive means of measuring intracranial pressure: A review. *Physiological measurement*, 38(8), 2017.

[52] M. Ursino. A mathematical study of human intracranial hydrodynamics part 1 - the cerebrospinal fluid pulse pressure. *Annals of Biomedical Engineering*, 16(4):379–401, July 1988.

[53] WD. Lakin, SA. Stevens, BI. Tranmer, and PL. Penar. A whole-body mathematical model for intracranial pressure dynamics. *Journal of Mathematical Biology*, 46:347–383, 2003.

[54] N. Barillot. Modelling of intracranial pressure. University of Leicester Project Report, April 2019.

[55] AC. Guyton. *Textbook of Medical Physiology.* W.B. Saunders Company, Philadelphia, PA, tenth edition edition, 2000.

[56] SI. Rapaport. *Blood-brain barrier in physiology and medicine.* New York: Raven Press, 1976.

[57] Z. Karni, J. Bear, S. Sorek, and Z. Pinczewki. A quasi-steady state compartmental model of intracranial fluid dynamics. *Med Biol Engng Comput.*, 25:167–172, 1987.

[58] WW. Tourtellotte and RJ. Shorr. *Cerebrospinal Fluid. Neurological Surgery.* Philadelphia: W.B. Saunders, 1982.

[59] SA. Stevens. Mean pressures and flows of the human intracranial system as determined by mathematical simulations of a steady state infusion test. *Neurological research*, 22:809–814, 2000.

[60] WR. Milnor. *Hemodynamics (Second Edition).* Baltimore: Williams and Wilkins, 1989.

[61] G. Nylin, S. Hedlun, and O. Regnstrom. Studies of the cerebral circulation with labeled erythrocytes in healthy man. *Circulation Research*, 9:664–674, 1961.

[62] WW. Nichols and MF. O'Rourke. *McDonald's Blood Flow in Arteries: Theoretical, experimental and clinical principles.* New York: Arnold, fourth edition, 1998.

[63] S. Sorek, J. Bear, and Z. Karni. A non-steady compartmental flow model of the cerebrovascular system. *J. Biomechanics*, 21:695–704, 1988.

[64] SA. Stevens and WD. Lakin. Local compliance effects on the global CSF pressure-volume relationship in models of intracranial pressure dynamics. *Mathematical and Computer Modelling of Dynamical Systems*, 6(4):445–465, 2000.

[65] JM. Chillon and GL. Baumbach. Autoregulation of cerebral blood flow. *Primer on Cerebrovasular Diseases*, pages 51–54, 1997.

[66] SA. Stevens, WD. Lakin, and W. Goetz. A differentiable, periodic function for pulsatile cardiac output based on heart rate and stroke volume. *Mathematical Biosciences*, 182(2):201–211, April 2003.

[67] DG. Luenberger. Time-invariant descriptor systems. *Automatica*, 14(5):473–480, September 1978.

[68] KM. Bushby, T. Cole, JN. Matthews, and JA. Goodship. Centiles for adult head circumference. *Arch Dis Child*, 67(10):1286–7, October 1992.

[69] M. Ursino, M. Giulioni, and CA. Lodi. Relationships among cerebral perfusion pressure, autoregulation, and transcranial Doppler waveform: a modeling study. *Journal of Neurosurgery*, 89(2):255–266, 1998.

[70] FM. Kashif, GC. Verghese, V. Novak, M. Czosnyka, and T. Heldt. Model-based noninvasive estimation of intracranial pressure from cerebral blood flow velocity and arterial pressure. *Science Translational Medicine*, 4:129–144, 2012.

[71] O. Boespflug and L. Chun Feng. Transcranial pulsed Doppler. problems posed by the temporal window (834 patients). *J Mal Vasc*, 17:112–115, 1992.

[72] M. Marinoni, A. Ginanneschi, P. Forleo, and L. Amaducci. Technical limits in transcranial Doppler recording: inadequate acoustic windows. *Ultrasound in Medicine and Biology*, 23:1275–1277, 1997.

[73] N. Aplerin, S. Lee, F. Loth, P. Raksin, and T. Lichtor. Mr-intracranial pressure (ICP): a method to measure intracranial elastance and pressure non-invasively by means of MR imaging: baboon and human study. *Radiology*, 217:877–885, 2000.

[74] TD. Homan, S. Bordes, and E. Cichowski. *Physiology, Pulse Pressure*. Treasure Island (FL): Stats Pearl Publishing, 2020.

[75] AF. Malone and DN. Reddan. Pulse pressure. Why is it important? *Peritoneal Dialysis International*, 30(3):265–268, 2010.

[76] J. Ince, C. Banahan, S. Venturini, M. Alharbi, P. Turner, M. Oura, KW. Beach, TG. Robinson, AK. Mistri, A. Lecchini-Visintini, JS. Minhas, and

EML. Chung. Acute ischemic stroke diagnosis using brain tissue pulsations. *Journal of the Neurological Sciences*, 419:117164, December 2020.

[77] GW. Blair, MJ. Thrippleton, Y. Shi, I. Hamilton, M. Stringer, F. Chappell, DA. Dickie, P. Andrews, I. Marshall, FN. Doubal, and JM. Wardlaw. Intracranial hemodynamic relationships in patients with cerebral small vessel disease. *Neurology*, 94(21):e2258–e2269, 2020.

[78] S. Bottan, D. Poulikakos, and V. Kurtcuoglu. Phantom model of physiologic intracranial pressure and cerebrospinal fluid dynamics. *IEEE Trans Biomed Eng*, 59(6), 2012.

[79] A. Marmarou, K. Shulman, and RM. Rosende. A non-linear analysis of the cerebrospinal fluid system and intracranial pressure dynamics. *Neurosurgery*, 48:332–344, 1978.

[80] K. Sagawa, RK. Lie, and J. Schaefer. Translation of Otto Frank's paper "Die Grundform des Arteriellen Pulses" Zeitschrift fur Biologie. 37:483-526 (1899). *J Mol Cell Cardiol*, 22:253–277, 1990.

[81] Y. Shi, MJ. Thrippleton, I. Marshall, and JM. Wardlaw. Intracranial pulsatility in patients with cerebral small vessel disease: A systematic review. *Clinical Science*, 132:157–171, 2018.

[82] ME. Wagshul, EJ. Kelly, H. Jing Yu, B. Garlick, T. Zimmerman, and MR. Egnor. Resonant and notch behaviour in intracranial pressure dynamics. *Journal of Neurosurgery: Pediatrics*, 3(5), 2009.